

UNIVERSITY OF WARMIA AND MAZURY IN OLSZTYN

Technical Sciences

19(3) 2016



PUBLISHER UWM

Editorial Board

Ceslovas Aksamitauskas (Vilnius Gediminas Technical University, Lithuania), Olivier Bock (Institut National de L'Information Géographique et Forestière, France), Stefan Cenkowski (University of Manitoba, Canada), Adam Chrzanowski (University of New Brunswick, Canada), Davide Ciucci (University of Milan-Bicocca, Italy), Sakamon Devahastin (King Mongkut's University of Technology Thonburi in Bangkok, Thailand), German Efremov (Moscow Open State University, Russia), Mariusz Figurski (Military University of Technology, Poland), Maorong Ge (Helmholtz-Zentrum Potsdam Deutsches GeoForschungsZentrum, Germany), Dorota Grejner-Brzezinska (The Ohio State University, USA), Janusz Laskowski (University of Life Sciences in Lublin, Poland), Arnold Norkus (Vilnius Gediminas Technical University, Lithuania), Stanisław Pabis (Warsaw University of Life Sciences-SGGW, Poland), Lech Tadeusz Polkowski (Polish-Japanese Institute of Information Technology, Poland), Arris Tijsseling (Technische Universiteit Eindhoven, Netherlands), Vladimir Tilipalov (Kaliningrad State Technical University, Russia), Alojzy Wasilewski (Koszalin University of Technology, Poland)

Editorial Committee

Marek Markowski (Editor-in-Chief), Piotr Artiemjew, Kamil Kowalczyk, Wojciech Sobieski, Piotr Srokosz, Magdalena Zielińska (Assistant Editor), Marcin Zieliński

Features Editors

Piotr Artiemjew (Information Technology), Marcin Dębowski (Environmental Engineering), Zdzisław Kaliniewicz (Biosystems Engineering), Marek Mróz (Geodesy and Cartography), Ryszard Myhan (Safety Engineering), Wojciech Sobieski (Mechanical Engineering), Piotr Srokosz (Civil Engineering), Jędrzej Trajer (Production Engineering)

Statistical Editor

Paweł Drozda

Executive Editor

Mariola Jezierska

The Technical Sciences is indexed and abstracted in BazTech (<http://baztech.icm.edu.pl>) and in IC Journal Master List (<http://journals.indexcopernicus.com>)

The Journal is available in electronic form on the web sites
<http://www.uwm.edu.pl/techsci> (subpage Issues)
<http://wydawnictwo.uwm.edu.pl> (subpage Czytelnia)

The electronic edition is the primary version of the Journal

PL ISSN 1505-4675

e-ISSN 2083-4527

© Copyright by Wydawnictwo UWM • Olsztyn 2016

Address

ul. Jana Heweliusza 14
10-718 Olsztyn-Kortowo, Poland
tel.: +48 89 523 36 61
fax: +48 89 523 34 38
e-mail: wydawca@uwm.edu.pl

Contents

S. RAY, R. SAHA, U. RAYCHAUDHURI, R. CHAKRABORTY – <i>Different Quality Characteristics of Tomato (<i>Solanum lycopersicum</i>) as a Fortifying Ingredient in Food Products: A Review</i>	199
A. NIEDŹWIEDZKA, W. SOBIESKI – <i>Analytical Analysis of Cavitating Flow in Venturi Tube on the Basis of Experimental Data</i>	215
Y. POVSTENKO, J. KLEKOT – <i>The Cauchy Problem for the Time-Fractional Advection Diffusion Equation in a Layer</i>	271
L. DZYUBA, V. BARYLIAK – <i>Dynamics of Electromechanical Drive of Suspended Timbertransporting Rope System</i>	245
M. GWOŹDZIK – <i>Structure Studies of Porous Oxide Layers Formed on 13crmo4-5 Steels Long-Term Operated in the Power Industry</i>	257
D. JANECKI, G. BARTELMUS, A. BURGHARDT – <i>Modelling of the Hydrodynamics of Concurrent Gas and Liquid Flow Through Packed Bed</i>	267



Quarterly peer-reviewed scientific journal

ISSN 1505-4675
e-ISSN 2083-4527

TECHNICAL SCIENCES

Homepage: www.uwm.edu.pl/techsci/



DIFFERENT QUALITY CHARACTERISTICS OF TOMATO (*SOLANUM LYCOPERSICUM*) AS A FORTIFYING INGREDIENT IN FOOD PRODUCTS: A REVIEW

***Sohini Ray, Rumki Saha, Utpal Raychaudhuri,
Runu Chakraborty***

Dept. of Food Technology and Biochemical Engineering,
Jadavpur University, Kolkata-700032, India

Received 8 February 2016; accepted 27 June 2016; available online 14 July 2016

Key words: Tomato, nutritional benefit, bioactive component, lycopene, application, preservation.

Abstract

Tomato (*Solanum lycopersicum*) is an economically important vegetable crop grown in tropical and sub-tropical parts of the world. The objective of this paper is to review nutritional benefits of tomato, its different bioactive components and their application in food products. Tomato and tomato products are very beneficial to our health as they decrease the risk of many diseases, such as cancer, asthma, heart disease etc. The whole fruit of tomato i.e pomace, seed and tomato solids have many nutraceutical benefits and is extensively used in food processing industry either as raw or in powder form. Many bioactive components are present in tomato, such as lycopene, oleoresin, carotenoids etc. Tomato is very popular for high content of antioxidant compounds and antioxidant activity. It is preserved mainly by drying (tray drying, freeze drying) and encapsulation process. We have tried to focus on to get the answer, which one is better in food application, lycopene supplementation or direct tomato powder fortification in food products.

Introduction

Tomatoes (*Solanum lycopersicum*) are one of the most widely used and versatile vegetable crops. They are consumed fresh and are also used to manufacture a wide range of processed products (MADHAVI and SALUNKHE

Correspondence: Runu Chakraborty, Professor, Department of Food Technology and Biochemical Engineering, Jadavpur University, Kolkata – 700032, India. Tel./fax: +91 (033) 24 146 822, e-mail: crunu@hotmail.com

1998). Tomatoes and tomato products are rich in health-related food components. United States, Turkey, Italy, and Spain are the leading tomato growing countries (JUMAH et al. 2004). The advantages of using tomato by-products as food ingredients are noticeable both to reduce environmental pollution and to provide an extra-income for producers (LAVELLI and SCARAFONI 2012). Tomato can be consumed as raw or as an ingredient in many dishes, sauces, salads, and drinks. Factors influencing the considerable increase in tomato consumption include consumer awareness of benefits such as preventing cancer and chronic diseases (LANA and TIJSKENS 2006). This beneficial effect is due to the action of antioxidant compounds, which reduce oxidative damage in the body (BEECHER 1998). Tomatoes are rich in lycopene (87%) and other carotenoids such as carotene, phytoene, phytofluene, lutein and L-ascorbic acid (SOMA 2013). Lycopene is a carotenoid that can be incorporated into foods with the purposes of conferring both color and functional characteristics (NUNES and MERCADANTE 2007). Lycopene has attracted attention due to its biological and physicochemical properties, especially related to its effects as a natural antioxidant. Lycopene does exhibit a physical quenching rate constant with singlet oxygen almost twice as high as that of beta-carotene (SHI and LE MAGUER 2000). Several food technology studies have been carried out to optimize the processing and storage of the tomato products by preventing the heat and oxidative damage on the antioxidants (SHI et al. 1999). Tomatoes are not as sweet due to its lower sugar content than other edible fruits. Tomatoes are low in calories and a good source of vitamins A and C, the flavor, texture, and cooking characteristics of tomatoes depend on the variety, growing method, local environment, and handling techniques used during and after harvest (PARNELL et al. 2004). Most of the tomatoes are processed for its juice, ketchup, sauce, paste, puree and powder. Flavor characteristics of tomatoes are an important purchasing criterion (KRUMBEIN et al. 2004). Researchers have reported that lack of flavor of tomato is associated with various storage treatments, e.g., modified atmosphere (HO 1996, HOBSON 1988, MAUL et al. 2000). Dried tomato products (i.e., tomato halves, slices and powders) are in high consumption as compared to other tomato products due to their excellent properties (ARSLAN and OZCAN 2011). Tomato solids in powder form have many advantages, including ease of packing, transportation and mixing, and no drum-clinging loss (GIOVANELLI et al. 2000).

Nutritional benefits of tomato derivatives

Skin

The by-products of tomato processing (skin) contain a very high amount of lycopene. In particular, tomato skin has 2.5 times higher lycopene level than the pulp (SHI et al. 1999). Tomato skin contains more than 20 ppm lycopene, protected within the chromoplasts in the cells. Besides serving as a micronutrient with important health benefits, lycopene is an excellent natural food colorant (LAVELLI and TORRESANI 2011). Tomato skin contains more than 70% (w/w, db) of dietary fibre. Tomato skin fibre is mainly insoluble (ZEINAB et al. 2010). The use of dried tomato skin in powder form are proposed as an addition to refined oils for carotenoid solubilization in view of upgrading low quality oils, in the formulation of ketchup, in dry fermented sausages, and in beef hamburgers (BENAKMOUM et al. 2008, CALVO et al. 2008, FARAHAKEY et al. 2008, GARCÍA et al. 2009). The skin powder also provides proteins, cellulose and pectins, thus representing a good candidate to be used to modulate water sorption and rheological properties of food. Indeed the use of skin powders in the formulation of ketchup, improves its textural properties (FARAHAKEY et al. 2008). Approximately one-third of the total weight of tomatoes in the form of skin and seeds is discarded during processing of tomatoes into paste (TOOR and SAVAGE 2005).

Seed

Seeds are the major part of the pomace, and they are, 34% protein and 30% lipid (weight basis). Seed proteins have been extracted to produce protein concentrate (SAVADKOOHI and FARAHAKEY 2012). Studies on nutritive value of tomato seed proteins *in vivo* could not be found, however, reports involving the use of microorganism and enzymes are available. CANELLA and CASTRIOTTA (1980) reported that the tomato-seed protein is a mixture of globulin, albumin, prolamine and glutelin components. Tomato-seed protein components are adsorbed at oil-water (o/w) interfaces and reduce the interfacial tension considerably. Furthermore, compared to isolated soy protein, tomato proteins produce emulsions with greater globule size (SAVADKOOHI and FARAHAKEY 2012). Tomato seed protein is rich in lysine (approximately 13% more lysine than soya protein) and can supplement feed that is deficient in lysine (LAVELLI and TORRESANI 2011). Tomato seed was dried and fortified in bread and has significant effect on antioxidant activity, nutritional and sensory profile analysis (RANAWANA et al. 2016). Tomato seed was used to replace corn and soyabean meal and it is healthy diet (based on protein efficiency ratio, amino acid content and digestibility) for chick (PERSIA et al. 2003).

Pomace

Tomato pomace is an inexpensive by-product of tomato manufacturing, contains almost 75% water and the cost of shipping tends to be very high (due to its weight). The conventional procedure for tomato processing generates heat-treated tomato pomace (skins and seeds); in contrast, a new plant operates the pulping/finishing steps on raw fruits at room temperature, thus producing an unheated pomace (SAVADKOOHI and FARAHNAKY 2012). Dehydrated tomato pomace as a by-product of tomato production lines can be used for animal feed or human food. Tomato pomace contains high levels of polysaccharides, such as fiber and pectin (YUANGLANG et al. 2010). It increasingly has been used as valuable feed stuff in ruminants and poultry nutrition in developing countries. Tomato pomace is the mixture of tomato peels, crushed seeds and small amounts of pulp that remains after the processing of tomato for juice, paste and ketchup (AGHAJANZADEH et al. 2010, VENTURA et al. 2009, KING and ZEIDLER 2004). It contains 5.1% moisture, 11.9% fat, 26.8% protein and 26.3% crude fiber (YITBAREK 2013) Moreover, it contains 13% more lysine than soybean protein, a good source of vitamin B, fair source of vitamin A and 2130 kcal/kg metabolizable energy (AL-BETAWI 2005). Tomatoes contain a solanine-like alkaloid (saponin) called tomatine which have medicinal properties such as antibiotic, anticancer, anti cholesterol, anti inflammatory and anti pyretic affects (CALVO et al. 2008).

Tomato solids

Tomato powder is much in demand by dehydrated soup manufacturers, and it also can be used as an ingredient in many food products, mainly soups, sauces and ketchup. The skin powder also provides proteins, cellulose and pectins, thus representing good characteristics to be used to modulate water sorption and rheological properties of food (PAPADAKIS et al. 1998). The solubility of the powder is associated with the moisture content and operational conditions of the dryer, increasing with decrease in the moisture content (GOULA and ADAMOPOULOS 2005, PAIVA and RUSSELL 1999).

Bioactive components of tomato

The main bioactive compound of tomato which lycopene is discussed below and the other bioactive components oleoresin, phenol and flavonoid, carotenoid and ascorbic acid are discussed in table 2.

Lycopene

Lycopene, a member of carotenoid family; is a lipid soluble antioxidant synthesized by many plants and microorganisms but not by animals and humans. It serves as an accessory light-gathering pigment and protects the plant against the toxic effects of oxygen and light. Tomato (lycopene, 8.8–42 µg/g W/W) and its derivative mainly represent main dietary sources of lycopene, but also watermelon, papaya, guava and pink grapes are rich sources. It is the naturally occurring compound that gives the characteristic red color to the tomato, watermelon, pink grapefruit, orange, and apricot (RAO and AGARWAL 2000). Lycopene has polynutrient, in many fruits and vegetables it consist of the potent antioxidant. Tomatoes and processed tomato products constitute the major source of dietary lycopene accounting for up to 85% of the daily intake (CHAUHAN et al. 2011).

Lycopene content of various fruits and vegetables were represented in Table 1 (NGUYEN and SCHWARTZ 1998).

Table 1

Lycopene content of various fruits and vegetables

Foods	Lycopene content (mg/100 g)
Tomato foods	
Tomatoes, raw	0.9–4.2
Tomatoes, cooked	3.7–4.4
Tomato sauce	7.3–18.0
Tomato paste	5.4–55.5
Tomato soup (condensed)	8.0–10.9
Tomato juice	5.0–11.6
Ketchup	9.9–13.4
Other fruits and vegetables	
Apricots, fresh	0.005
Watermelon, fresh	2.3–7.2
Papaya, fresh	2.0–5.3
Grapefruit, pink/red	0.2–3.4
Guava, raw	5.3–5.5
Vegetable juice	7.3–9.7

Source: NGUYEN and SCHWARTZ (1998)

The lycopene levels are lower for peeled tomatoes as the removed peel is known to have higher content. It was reported that the concentration of lycopene is two folds higher in pericarp than in locular cavity and β -carotene is four folds higher in locular cavity (CHAUHAN et al. 2011). Lycopene

Table 2
Some other bioactive components in tomato apart from lycopene

Name of the bioactive component	Oleoresin	Carotenoid	Phenol and flavonoid	Ascorbic acid
Composition	Tomato oleoresin is a semisolid mixture of a resin and essential oil (Rizk et al. 2014).	Tomato carotenoids include compounds called carotenes and xanthophylls (BRAMLEY 2002).	Phenolics include flavonoids, phenolic acids. Phenol such as- hydroxybenzoic acid and hydroxycinnamic acids, and tannins. And flavonoid such as quercetin and kaempferol, flavanols catechins, Naringerin, anthocyanidins (MARTIN and APPEL 2010).	L-ascorbic acid and dehydroascorbic acid are the main dietary forms of vitamin C, a labile molecule with reducing property. It is a water-soluble compound easily absorbed but it is not stored in the body (PADAYATTY et al. 2003).
Application and use	Oleoresins have medicinal properties, used mainly as a flavoring agent in the food processing industry such as dairy products, non alcoholic flavored drinks, cereal and cereal products, bread and baked goods because it is more economical to use and it gives a consistent quality to the food products (LUCERA et al. 2012).	The carotenoids in tomatoes are yellow, orange and red pigment that act as antioxidants to help protect cells and is a natural cancer fighting agent (BRAMLEY 2002).	Maintain of heart health neutralizes free radicals; associated with therapeutic tools in inflammatory diseases including obesity, neurodegenerative disease, diabetes, cancer and aging (RAHMAN 2007).	Vitamin C in tomato is highly bioavailable, so a regular intake of small amounts of tomato products can increase cell protection from DNA damage induced by oxidant species (PADAYATTY et al. 2003).

is a highly unsaturated straight chain hydrocarbon with a total of 13 double bonds, 11 of which are conjugated. *In vitro* studies have shown lycopene to be twice as potent as β -carotene and ten times that of α -tocopherol in terms of its singlet oxygen quenching ability (ALI et al. 2010). Lycopene in raw tomatoes is generally present as the all-*trans* geometric isomer, the most thermodynamically stable form. Lycopene, either as a pure agent or as part of tomato components, can be incorporated into semi-purified diets for studies of carcinogenesis or tumorigenesis (NGUYEN and SCHWARTZ 1998). Moreover, several studies suggested that lycopene is a more potent scavenger of oxygen radicals than other major dietary carotenoids (GAJIC et al. 2006). Lycopene in tomatoes are found in association with protein complex or membrane structure, which prevent lycopene digestion and absorption. Harsh treatments during food processing, such as mechanical texture disruption and steam, may denature the lycopene-protein complex and release lycopene from the cellular matrix (SHI et al. 2004).

Lycopene metabolism

The enzymatic metabolism of lycopene and other carotenoids is only beginning to be understood. Lycopene, like β -carotene, when metabolized by carotenoid monooxygenase 2 will generate apo lycopenals (KHACHIK et al. 1995). The major metabolite of lycopene identified in human plasma is 5,6-dihydroxy-5,6-dihydrolycopene, probably due to the oxidation of lycopene via conversion from intermediate lycopene epoxides (ERDMAN et al. 1993).

Relationship between bioavailability and bioaccessibility with lycopene

Accessibility of lycopene is mainly influenced by crystalline formation called bioavailability. The bioavailability of *cis*-isomers in food is higher than that of all *trans*-isomers. Lycopene bioavailability in processed tomato products is higher than in unprocessed fresh tomatoes (SHI et al. 2000). Lycopene absorption was found to be apparently more efficient at low dosages than at higher dosages, possibly due to the low potential to form crystals at low dosages (STAHL and SIES 1992). Ultrasound processing can cause decrease in lycopene bioaccessibility, due to lycopene entrapment in the stronger network of pectin, making it less accessible for digestion. The effects of lipids on lycopene bioaccessibility are the use of lycopene as food supplement dissolved in a lipophilic carrier, which can improve the lycopene bioavailability (BEEBY and POTTER 1992).

Preservation methods for tomato

Drying

Drying is a complex process of removal of moisture from wet material by means of thermal energy where both heat and mass transfer take place. Many physical, chemical, and nutritional changes occur in foods during the dehydration process (ROBERTS et al. 2008). Though food drying indicates the loss of volatiles and flavors, changes in color and texture, and minimally decrease in nutritional value, drying is the useful means to increase the shelf life of perishable food for further use (MARS and SCHER 1990). During processing and storage a number of changes occur in dried tomato products. It is reported that the moisture content, bulk density and solubility of tomato powder, three most commonly quoted specifications of a powder product, were all dependent on the spray drying conditions, i.e. air inlet temperature, drying air flow rate, and compressed air flow rate (CHAUHAN et al. 2011). Sousa et al observed spray drying operational condition on tomato and analysed moisture content, solubility, consistency, wettability and color index (SOUSA et al. 2008). Freeze drying was done on tomato peel and tomato peel powder effect was analyzed on physicochemical properties after incorporation of extruded snack (ZEINAB et al. 2010). Tomato was dried by solar drying and color retention and rehydration ratio was analyzed (RAJKUMAR et al. 2007). Drying kinetics and quality attributes of oven dried tomato powder were analyzed (ABANO et al. 2011). Antioxidant content, color and rehydration ratio were studied on tray dried tomato powder (SANCHEZ et al. 2012). To investigate the effect of temperature and osmotic dehydration on air drying kinetics, quality and moisture removal tomato pomace was dried by cabinet air oven (AL MUHTASEB et al. 2010). Different drying methods used for preparing various tomato products are given in Table 3.

Encapsulation

Microencapsulation is a technique by which solid, liquid or gaseous active ingredients are packaged within a second material from the surrounding environment for the purpose of shielding the active ingredient (DUBEY et al. 2009). Microencapsulation allows the creation of a physical barrier between the core and the wall materials (FAVARO-TRINDADE et al. 2008). A convenient and simple procedure for the formation of microcapsules is the method known as complex coacervation (GOUIN 2004, GÜLAY and SEDA 2014). Encapsulated natural colors such as carotenoids, anthocyanins, and chlorophylls are easier to handle and offer improved stability to oxidation and solubility

Table 3

Different drying methods of tomato

Tomato drying process	Observation	References
Tray drying	To incorporate tomato powder in place of artificial coloring and flavoring agent in the fudge and to evaluate its sensory and microbial parameters and antioxidant activity. Antioxidant content, color and rehydration ratio were analysed.	SOMA 2013 SANCHEZ et al. 2012
Spray drying	The effects of the spray dryer operational conditions on the moisture content, solubility, consistency, wettability and color index were analyzed.	SOUSA et al. 2008
Freeze drying	Physico chemical property of extruded snack with tomato peel powder was analysed. Lycopene content, product density, hardness, percentage of moisture loss and color parameters of the snacks evaluated.	ZEINAB et al. 2010
Solar drying	Color retention and rehydration ratio were analyzed.	RAJKUMAR et al. 2007
Laboratory solar drying	Effect of different drying thickness and drying kinetics of tomato slices.	BAGHERI et al. 2013
Cabinet air oven drying	To investigate the effect of temperature and osmotic dehydration on air drying kinetics and quality of tomato pomace and to assess moisture removal.	AL MUHTASEB et al. 2010
Hot air oven drying	To study drying kinetics and quality attributes of tomato slices.	ABANO et al. 2011

(DUBEY et al. 2009). Lycopene was encapsulated in powder form by spray drying and inclusion freeze drying process (NUNES and MERCADANTE 2007). Carotenoid rich extract was obtained from tomato paste and it was encapsulated by inulin in a prebiotics matrix system. Encapsulated carotenoid was used for formulation of functional foods (CLARA et al. 2011).

Application

Tomato, either as a whole or as powder form has several uses in different food industries to prepare cookies, snacks, jelly, sauce, ketch up etc.

Tomato powder vs lycopene supplement

Many researchers have suggested that tomato can be used in powder form as well as as lycopene supplement. The points below are discussion on the

application of both the tomato powder and lycopene supplement in food industry.

Tomato powder

Tomato powder has good potential as substitute of tomato paste and other tomato products; the final quality of dehydrated products is affected by the drying conditions. Among several processing methods spray drying is the efficient mode of preservation of tomato powder. The temperatures and drying conditions experienced by a droplet during the drying have an important influence on the powder properties (BENAKMOUM et al. 2008). Tomato powder is readily marketable due to ease in packaging, transportation and utilization in different ready to eat food preparations with extended storage life. The quality of dehydrated tomato depends on many parameters such as tomato variety, total soluble solid content (°Brix) of the fresh product, the air humidity, the size of the tomato segments, the air temperature and velocity and the efficiency of the drying system. The dehydrated powder was packed in polythene bags and kept in glass bottles at room temperature; here the peroxide value increases with storage period, indicating deterioration (REIHANEH and MEHDI 2010).

Uses

– The tomato powder used in soups, instant sauce premixes, ketchups, sambar and rasam mix, puddings, bakery products, health foods, sweets, biscuits, baby foods, confectioneries, snacks etc.

– They are also used in the preparation of recipes viz., tomato dosa, soup, rice and burfi and compared with fresh tomato recipes. As the powder is in the concentrated form, it gave attractive appearance, color and taste to the recipes.

– Tomato skin powder was incorporated into refined oils for carotenoid solubilisation in view of upgrading low quality oils.

The use of skin powders in the formulation of ketchup, improves its textural properties (SHU et al. 2006).

Lycopene supplement

Researchers observed that the stability of microencapsulated lycopene was significantly higher when compared to the free material such as lycopene obtained by spray drying using gelatin, sucrose and modified starch. Human

populations consume lycopene from both food and supplements (ROCHA et al. 2012). Lycopene is an important issue in nutrition due to the bioavailability of a bioactive substance. The lycopene taken as a supplement is easy to the body as a food substitute. Recent studies have suggested a protective role for lycopene, an antioxidant carotenoid, in the prevention of oxidative stress (GAJIC et al. 2006).

Uses

- Lycopene was used for preventing heart disease, (atherosclerosis) and cancer of the prostate, breast, lung, bladder, ovaries, colon, and pancreas.
 - Lycopene is also used for treating human papilloma virus (HPV) infection, which is a major cause of uterine cancer.
 - Some people also use lycopene for cataracts and asthma.
- The application of tomato in food products is represented in Table 4.

Table 4

Application of tomato in food products

Tomato by products	Use in type of food	Observation	References
Tomato powder	Cookies	Physico chemical, color, texture and sensory parameters.	CHUNG 2007
Tomato peels	Ice cream	Carotenoid content, antioxidant content and sensory parameter analysed.	RIZK et al. 2014
Tomato seed meal	Bread	Physico chemical property analysed	SOGI et al. 2005
Tomato peel, tomato powder and lycopene	Beef patties, sausages, minced meat and frankfruters	The presence of lycopene from different tomato matrices leads to a better colour in the meat products, improved nutritional quality, reduced lipid oxidation and increased stability during the shelf life period and retaining overall acceptability.	CANDOGAN 2002, CALVO et al. 2008, ØSTERLIE and LERFALL 2005, DEDA et al. 2007
Tomato skin powder	Refined oil	For carotenoid solubilisation in view of upgrading lowo quality oils	BENAKMOUM et al. 2008

Conclusion

Tomatoes are the most valuable and are the most commonly used crops in many food dishes. They are very much beneficial to our health due to their antioxidant properties. Tomato contains high concentration of lycopene, L-ascorbic acid, oleoresin, phenol, flavonoids and carotenoid. Dietary intake of tomatoes and tomato products decreases chronic diseases, cardiovascular diseases and also reduces certain risk of cancer. Various tomato products are made from tomato skin, seed, pomace and are very much useful in our diet. Now -a-days tomato in powder form are mainly used due to their excellent nutrient properties in the formulations of ketchup, soups, sauces and they can also act as a natural colorant. Tomato powder can easily be handled, preserved and stored, have low transportation cost. The shelf life of tomato powder is much more than raw tomatoes. Hence, tomato is very useful for our body due to its great antioxidant properties, health effects, and in enzymatic metabolism. It is always better to use tomato powder than only lycopene for the purpose of food fortification.

References

- ABANO E.E., MA H. and QU W. 2011. *Influence of Air Temperature on the Drying Kinetics and Quality of Tomato Slices*. *Journal of Food Processing and Technology*, 2, 5.
- AGHAJANZADEH G.A., MAHERI S.N., MIRZAEI A.A., BARADARAN H.A. 2010. *Comparison of nutritional value of tomato pomace and brewer's grain for ruminants using in vitro gas production technique*. *Asian Journal of Animal and Veterinary Advances*, 5: 43–51.
- AL-BETAWI N.A. 2005. *Preliminary Study on Tomato Pomace as Unusual Feedstuff in Broiler Diets*. *Pakistan Journal of Nutrition*, 4: 57–63.
- AL-MUHTASEB A.H., AL-HARAHSEH M., HARARAH M., MAGEE T.R.A. 2010. *Drying characteristics and quality change of unutilized-protein rich-tomato pomace with and without osmotic pre-treatment*. *Industrial Crops and Products*, 31: 171–177.
- ALI A.A., MANAL A. A.O., SAHAR A.A.S., ABDULLAH H.A.A., JUN J.Z., KAI Y. L. 2010. *Tomato powder is more protective than lycopene supplement against lipid per oxidation in rats*. *Nutrition Research*, 30: 66–73.
- ARSLAN D., ÖZCAN M. M. 2011. *Drying of tomato slices: changes in drying kinetics, mineral contents, antioxidant activity and color parameters*. *CyTA – Journal of Food*, 9(3): 229–236.
- BAGHERI H., ARABHOSSEINI A., KIANMEHR M.H., CHEGINI G.R. 2013. *Mathematical modeling of thin layer solar drying of tomato slices*. *Agricultural Engineering International: CIGR Journal*, 15(1): 146–153.
- BEEBY C., POTTER O.E. 1992. *Steam drying*, In R. Toei, A.S. Majumdar (Eds.), *Drying* (pp. 41–58). New York, Hemisphere Publication Corporation.
- BEECHER G.R. 1998. *Nutrient content of tomatoes and tomato products*. *Proceeding of the Society for Experimental Biology and Medicine*, 218: 98-100.
- BENAKMOUM A., ABBEDDOU S., AMMOUCHE A., KEFALAS P., GERASOPOULOS P.D. 2008. *Valorisation of low quality edible oil with tomato peel waste*. *Food Chemistry*, 110: 684–690.
- BRAMLEY P.M. 2002. *Regulation of carotenoid formation during tomato fruit ripening and development*. *Journal of Experimental Botany*, 53: 2107–2113.

- CALVO M.M., GARCIA M.L., SELGAS M.D. 2008. *Dry fermented sausages enriched with lycopene from tomato peel*. *Meat Science*, 80: 167–172.
- CANDOGAN K. 2002. *The effect of tomato paste on some quality characteristics of beef patties during refrigerated storage*. *European Food Research and Technology*, 215: 305–309.
- CANELLA M., CASTRIOTTA G. 1980. *Protein composition and solubility of tomato seed meal*. *Lebensmittel-Wissenschaft and Technologie*, 13(1): 18–21.
- CHAUHAN K., SHARMA S., AGARWAL N., CHAUHAN B. 2011. *Lycopene of tomato fame: its role in health and disease*. *International Journal of Pharmaceutical Sciences Review and Research*, 10(1): Article-018.
- CHUNG H.J. 2007. *Quality attributes of cookies prepared with tomato powder*. *Journal of Food Science and Nutrition*, 12: 229–233
- CLARA D., BEIRÃO-DA-COSTA S., ANA I.B., ANA C.P., SERRA A.T., MARTINS M.M., ANTÓNIO A.V., CATARINA M.M.D., BEIRÃO-DA-COSTA M.L. 2011. *Encapsulation and delivery of carotenoids-rich extract from tomato pomace in a prebiotic matrix*. ICEF11 – 11th International Congress on Engineering and Food: Food Process Engineering in a Changing World (Proceedings). Athens, Greece.
- DEDA M.S., BLOUKAS J.G., FISTA G.A. 2007. *Effect of tomato paste and nitrite level on processing and quality characteristics of frankfurters*. *Meat Science*, 76: 501–508.
- DUBEY R., SHAMI T., RAO B.K. 2009. *Microencapsulation technology and application*. *Defence Science Journal*, 59: 82–95.
- ERDMAN J.W.JR., BIERER T.L., GUGGER E.T. 1993. *Absorption and transport of carotenoids*. *Annals of the New York Academy of Sciences*, 691: 76–85.
- FAVARO-TRINDADE C.S., PINHO S.C., ROCHA G.A. 2008. *Microencapsulac4o de ingredientes alimenticio*. *Brazilian Journal of Food Technology*, 11: 103–112.
- FARAHNAMY A., ARAHNAKY A., ABBASI J., JAMALIAN J., MESBAHI G. 2008. *The use of tomato pulp powder as a thickening agent in the formulation of tomato ketchup*. *Journal of Texture Studies*, 39: 169–182.
- GAJIC M., ZARIPHEH S., SUN F., ERDMAN J.W. 2006. *Jr, Apo-8'-lycopenal and apo-12'-lycopenal are metabolic products of lycopene in rat liver*. *The Journal of Nutrition*, 136(6): 1552–1557.
- GARCIA M.L., CALVO M.M., SELGAS M.D. 2009. *Beef hamburgers enriched in lycopene using dry tomato peel as an ingredient*. *Meat Science*, 83: 45–49.
- GIOVANELLI G., ZANONI B., LAVELLI V., NANI R. 2000. *Water sorption, drying and antioxidant properties of dried tomato products*. *Journal of Food Engineering*, 52: 135–141.
- GOUIN S. 2004. *Microencapsulation: Industrial appraisal of existing technologies*. *Food Science and Technology*, 15: 330–347.
- GOULA A.M., ADAMOPOULOS K.G. 2005. *Spray drying of tomato pulp in dehumidified air: II. The effect on powder properties*. *Journal of Food Engineering*, 2005, 66: 35–42.
- GÜLAY Ö., SEDA E.B. 2014. *Microencapsulation of Natural Food Colourants*. *International Journal of Nutrition and Food Science*, 3(3): 145–156.
- HOBSON G. 1988. *How the tomato lost its taste*. *New Science*, 1632: 46–50.
- HO L. 1996. *The mechanism of assimilates partitioning and carbohydrate compartmentation in fruit in relation to the quality and yield of tomato*. *Journal of Experimental Botany*, 47: 1239–1243.
- JUMAH R., BANAT F., AL-ASHEH S., HAMMAD S. 2004. *Drying kinetics of tomato paste*. *International Journal of Food Properties*, 7: 253–259.
- KHACHIK F., BEECHER G.R., SMITH J.C. JR. 1995. *Lutein, lycopene, and their oxidative metabolites in chem. prevention of cancer*. *Journal of Cellular Biochemistry Supplement*, 1995, 22: 236–246.
- KING A.J., ZEIDLER G. 2004. *Tomato Pomace May be a Good Source of Vitamin E in Broiler Diets*. *California Agriculture*, 58(1): 59–62.
- KRUMBEIN A., PETERS P., BRUCKNER B. 2004. *Flavor compounds and a quantitative descriptive analysis of tomatoes (Lycopersicon esculentum Mill.) of different cultivars in short-term storage*. *Postharvest Biology and Technology*, 32: 15–28.
- LANA M.M., TIJSKENS L.M.M. 2006. *Effects of cutting and maturity on antioxidant activity of fresh cut tomatoes*. *Food Chemistry*, 97: 203–211.
- LAVELLI V., SCARAFONI A. 2012. *Effect of water activity on lycopene and flavonoid degradation in dehydrated tomato skins fortified with green tea extract*. *Journal of Food Engineering*, 110: 225–231.

- LAVELLI V., TORRESANI M.C. 2011. *Modelling of lycopene-rich by-products of tomato processing*. *Food Chemistry*, 125: 529–535.
- LUCERA A., COSTA C., CONTE A., NOBILE M.A.D. 2012. *Food applications of natural antimicrobial compounds*. *Frontiers in Microbiology*, 3: 287–304.
- MADHAVI D.L., SALUNKHE D.K. 1998. *Tomato*. In D.K. Salunkhe and S.S. Kadam, (Eds), *Handbook of vegetable science and technology: Production, Composition, Storage, and Processing*, chapter 7, (pp. 171–201). Marcel Dekker, New York, United States.
- MARS G.J., SCHER H.B. 1990. *Controlled delivery of crop protecting agents*. Wilkens, R.M. (Ed) Taylor and Francis, London, 65–90.
- MARTIN K.R., APPEL C.L. 2010. *Polyphenols as dietary supplements: A double-edged sword*. *Nutrition Dietary Supplement*, 2: 1–12.
- MAUL F., SARGENT S.A., SIMS C.A., BALDWIN E.A., BALABAN M.O., HUBER D.J. 2000. *Tomato flavor and aroma quality as affected by storage temperature*. *Journal of Food Science*, 65: 1228–1237.
- NGUYEN M.L., SCHWARTZ S.J. 1998. *Lycopene stability during food processing*. *Proceedings of the Society for Experimental Biology and Medicine*, 218: 101–105.
- NUNES I.L., MERCADANTE A.Z. 2007. *Encapsulation of lycopene using spray drying and molecular insulation process*. *Brazilian Archives of Biology and Technology*, 50(5): 893–900.
- ØSTERLIE M., LERFALL J. 2005. *Lycopene from tomato products added minced meat: Effect on Storage quality and color*. *Food Research International*, 38: 925–929.
- PADAYATTY S.J., KATZ A., WANG Y., ECK P., KWON O., LEE J.H. 2003. *Vitamin C as an antioxidant: evaluation of its role in disease prevention*. *Journal of the American College of Nutrition*, 22(1): 18–35.
- PAIVA S.A.R., RUSSELL R.M. 1999. *β -Carotene and Other Carotenoids as Antioxidants*. *Journal of American College of Nutrition*, 18(5): 426–433.
- PAPADAKIS S.E., GARDELI C., TZIA C. 1998. *Raizin Extract Powder: Production, Physical and Sensory Properties*. In: *Proceeding of the 11th International Drying Symposium ID's 98*, Haldiki: Ziti Editions.
- PARNELL T.L., SUSLOW T.V., HARRIS L.J. 2004. *Tomatoes: Safe Methods to Store, Preserve, and Enjoy*. University of California, Division of Agriculture and Natural Resources.
- PERSIA M.E., PARSONS C.M., SCHANG M., AZCONA J. 2003. *Nutritional evaluation of dried tomato seeds*. *Poultry Science*, 82: 141–146.
- RAHMAN K. 2007. *Studies on free radicals, antioxidants, and cofactors*. *Clin Interv Aging*, 2(2): 219–236.
- RAJKUMAR P., KULANTHAISAMI S., RAGHAVAN G.S.V., GARIEPY Y., ORSAT V. 2007. *Drying Kinetics of Tomato Slices in Vacuum Assisted Solar and Open Sun Drying Methods*. *Drying Technology*, 25: 1349–1357.
- RANAWANA V., RAIKOS V., CAMPBELL F., BESTWICK C., NICOL P., MILNE L., DUTHIE G. 2016. *Breads fortified with freeze-dried vegetables: quality and nutritional attributes. part 1: breads containing oil as an ingredient*. *Foods*, 5(19): 1–13.
- RAO A.V., AGARWAL S. 2000. *Role of antioxidant lycopene in cancer and heart disease*. *Journal of American College of Nutrition*, 19: 563–569.
- REIHANEH A.G., MEHDI G.D. 2010. *Studies on Physicochemical properties of tomato powder as affected by different dehydration methods and pretreatments*. *World Academy of Science Engineering and Technology*, 69: 117–129.
- RIZK E.M., EL-KADY A.T., EL-BIALY A.R. 2014. *Characterization of carotenoids (lyco-red) extracted from tomato peels and its uses as natural colorants and antioxidants of ice cream*. *Annals of Agricultural Science*, 59(1): 53–61.
- ROBERTS J.S., KIDD D.R., ZAKOUR O.P. 2008. *Drying kinetics of grape seeds*. *Journal of Food Engineering*, 89: 460–465.
- ROCHA G.A., F'AVARO-TRINDADE C.S., GROSSO C.R.F. 2012. *Microencapsulation of lycopene by spray drying: characterization, stability and application of microcapsules*. *Food and Bioproducts Processing*, 90(1): 37–42.
- SÁNCHEZ N.F.S., BLANCO R.V., GÓMEZ M.S.G., HERRERA A.P., CORONADO R.S. 2012. *Effect of rotating tray drying on antioxidant components, color and rehydration ratio of tomato saladette slices*. *LWT – Food Science and Technology*, 46: 298–304.

- SAVADKOOHI S., FARAHNAKY A. 2012. *Dynamic rheological and thermal study of the heat-induced gelation of tomato-seed proteins. Journal of Food Engineering*, 113 (3): 479–485.
- SHI J., LE M.M., KAKUDA Y., LIPTAY A., NIEKAMP F. 1999. *Lycopene degradation and misomerization in tomato dehydration, Food Research International*, 32: 15–25.
- SHI J., LE MAGUER M. 2000. *Lycopene in tomatoes: chemical and physical properties affected by food processing. Critical Reviews in Biotechnology*, 20(4): 293–334.
- SHI J., QU Q., KAKUDA Y., YEUNG D., JIANG Y. 2004. *Stability and synergistic effect of antioxidative properties of lycopene and other active components. Critical Review Food Science and Nutrition*, 44: 559–573.
- SHU B., YU W., ZHAO Y., LIU X. 2006. *Study on microencapsulation of lycopene by spray-drying. Journal of Food Engineering*, 76(4): 664–669.
- SOGI D.S., BHATIA R., GARG S.K., BAWA A.S. 2005. *Biological evaluation of tomato waste seed meals and protein concentrate. Food Chemistry*, 89, 53–56.
- SOMA S. 2013. *Development and evaluation of antioxidant activity of tomato based confectionary. International Food Research Journal*, 20(6): 3167–3170.
- SOUSA A.S.DE., BORGES S.V., MAGALHÃES N.F., RICARDO H.V., AZEVEDO A.D. 2008. *Spray-Dried Tomato Powder: Reconstitution Properties and Color. Brazilian Archives of Biology and Technology*, 51(4): 807–814.
- STAHL W., SIES H. 1992. *Uptake of lycopene and its geometrical isomer is greater from heat-processed than from unprocessed tomato juice in humans. Journal of Nutrition*, 122: 2161–2166.
- TOOR R.K., SAVAGE G.P. 2005. *Antioxidant activity in different fractions of tomatoes. Food Research International*, 38(5): 487–494.
- VENTURA M.R., PIELTIN M.C., CASTANON J.I.R. 2009. *Evaluation of tomato crop by-products as feed for goats. Animal Feed Science and Technology*, 154: 271–275.
- YITBAREK M.B. 2013. *The effect of feeding different levels of dried tomato pomace on the performance of Rhode Island Red (RIR) grower chicks. Global Journal of Poultry Farming and Vaccination*, 1(1): 052–058.
- YUANGLANG C., VASUPEN K., WONGSUTHAVAS S., PANYAKAEW P., ALHAIDARY A. 2010. *Growth performance in beef cattle fed rations containing dried tomato pomace. Journal of Animal and Veterinary Advances*, 9: 2261–2264.
- ZEINAB D.S., ALLAN K.H., CHARLES S.B. 2010. *The physico-chemical characteristics of extruded snacks enriched with tomato lycopene. Food Chemistry*, 123: 1117–1122.



ANALYTICAL ANALYSIS OF CAVITATING FLOW IN VENTURI TUBE ON THE BASIS OF EXPERIMENTAL DATA

Agnieszka Niedźwiedzka, Wojciech Sobieski

Department of Mechanics and Basics of Machine Construction
University of Warmia and Mazury in Olsztyn

Received 5 March 2016; Accepted 31 May 2016; Available online 1 June 2016.

Key words: cavitation, Venturi tube, mass flow rate.

Abstract

The content of this article is a direct continuation of the prior experimental works on the topic of cloud cavitation in Venturis. The results of the experimental tests were used to create a set of characteristics for three types of Venturis. The article has two aims: 1) verification of the similarity between the characteristics obtained and reported in the literature, 2) verification of the range of the obtained characteristics with respect to parallel diagrams. Both aims were achieved, which confirms that the quality of the prior results of the experimental measurements is at least sufficient to realize the main objective of the whole project: creation of numerical models of cavitating flow in Venturis. The literature overview showed that the issue has been not solved until today, even at the qualitative level. This reason was the motivation for the undertaken research, including contents of the article.

Introduction

The Venturis (Fig. 1) are devices, which have the main role of the control of mass flow rate. Their advantage is a simple rule describing the control mechanism. The mass flow rate is proportional to the throat area. Throat area is the middle part of the cavitating Venturi, between converging and diverging section. Cavitating Venturis are useful especially in devices that require a very small liquid flow rate with constant delivery. Examples of such necessities are:

Correspondence: Agnieszka Niedźwiedzka, Katedra Mechaniki i Podstaw Konstrukcji Maszyn, Uniwersytet Warmińsko-Mazurski, ul. Oczapowskiego 11, 10-736 Olsztyn, e-mail: niedzwiedzka.agnieszka@gmail.com

flow ratio about few grams per second, have e.g. lab scale monopropellants or hybrid rocket motors. To provide such small flow rate, it is necessary to use Venturis with small throat diameters. The small size of the throat may result in problems with viscous phenomena and varying downstream pressure in the performance of the Venturis (GHASEMMI, FASIH 2011, ASHRAFIZADEH, GHASEMMI 2015). The Venturis are not a common topic in the research world. There is a small amount of work, which consider this issue, so the request for such study is huge.

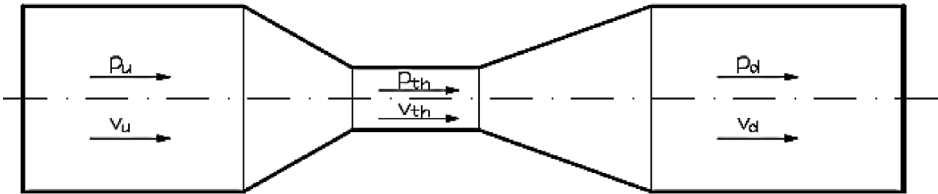


Fig. 1. Schematic of a Venturi: p_u – upstream pressure [Pa], v_u – upstream velocity [m/s], p_{th} – pressure in the throat [Pa], v_{th} – velocity in the throat [m/s], p_d – downstream pressure [Pa] and v_d – downstream velocity [m/s]

The history of the experimental investigations of cavitating Venturis dates back to the 1960s. In this time, RANDALL (1952) presented his pioneering works concerning construction and principles of operation of cavitating Venturis in rocket applications. After a long pause, scientists came back to the topic in 1990s. UNGAR et al. (1994) investigated Venturis under low inlet sub-cooling. Based on their research, it is known that in these devices during work at unchoked mode a decrease of downstream pressure can lead to overflow. Ungar in cooperation with MAL (1994) presented work which aimed to investigate the influence of alternative geometries of Venturis on the overflow conditions. LIOU et al. (1998) continued research on the topic of the small cavitating Venturis under low inlet sub-cooling. Simultaneously began the first numerical simulations of the flow in Venturis. NAVICKAS and CHEN (1993), among others, are pioneers of computer calculation in this field. They concentrated their research on the flow characteristic. The results of their numerical calculations were an irrefutable proof of the usefulness of this method to obtain significant parameters of the Venturis. XU et al. (2002) continued numerical investigation of cavitating Venturis using a homogeneous flow model. The scientists validated the results of simulations e.g. mass flow rate and oscillation frequency with the data obtained in experiments. HARADA et al. (2006) presented results of experimental investigations of the flow in a Venturi channel using the PIV method. GHASEMMI and FASIH (2011) examined small sized cavitating Venturis in three ways: under different upstream and constant

downstream conditions, under constant upstream and different downstream conditions Venturi and under variable downstream conditions. The newest works consider the accuracy of the numerical simulations of small-sized cavitating Venturis (ASHRAFIZADEH, GHASEMMI 2015) or insert image analysis to show vapour formation during the cavitating process (ABDULAZIZ 2014). Abdulaziz proposed a new model to predict vapour void fraction and validated it using the results of the image analysis.

The work presented in this article is a continuation of the prior works, especially the experimental measurements presented in the work of (NIED-ZWIEDZKA, SOBIESKI 2016). Results of experimental measurements of three types of Venturis with different angles of converging and diverging section and constant throat diameter are presented. The results of experimental measurements are subjected to further analysis and as a result characteristics of Venturis performance are developed. The main aim of the investigations was to analyse the degree of compliance of the obtained characteristics with the characteristics reported in the literature (ABDULAZIZ 2014, ASHRAFIZADEH, GHASEMMI 2015, GHASEMMI, FASIH 2011). The additional aim was estimating the range in which it is possible to make characteristics of Venturis performance using the test rig.

It should be added, that the investigations are not only an interpretation of the obtained experimental data, but firstly a material for numerical simulations which will be the topic of the future works. Development of numerical models of flows with cavitation is the main aim of the authors' research project.

Theoretical background

The construction of a Venturi tube assumes a division into three parts: converging section, throat and diverging section. According to the continuity equation (Eq. 2) and Bernoulli's equation (Eq. 3), the change of the cross section area of a fluid flux (here described by the diameters) is closely connected to the changes in pressure at the inlet and outlet of the Venturi (GHASEMMI, FASIH 2011). The relationship between the values of these pressures, e.g. pressure ratio (see eq. (10)), is decided about the character of mass flow rate (see eq. 1). If the pressure ratio is smaller than 0.8, the mass flow rate is constant and also independent from the downstream pressure. Additionally, at these conditions cavitation appears. This operation mode can be determined as „choked”. When the pressure ratio exceeds 0.8, cavitation does not occur, in the Venturi the phenomenon of overflow can be observed and the mass flow rate decreases. It means, the actual mass flow rate is smaller than expected constant value. The relationship between the actual and expected mass flow

rate is called mass flow ratio. This mode of operation is determined as „unchoked” or „all-liquid” mode. The relationship between mass flow ratio and pressure ratio (measurements under different downstream pressure conditions) is shown in Figure 2. The general principle, which describes the conditions necessary for the occurrence of cavitation phenomenon, refers to the relationship between the actual and the saturation pressure of the analysed fluid. According to this principle, the transition from liquid to vapour phase in the throat comes when the static pressure drops below the saturated liquid pressure. The reduction of the static pressure in the throat is a consequence of the acceleration process in the converging section (ASHRAFIZADEH, GHASEMMI 2015).

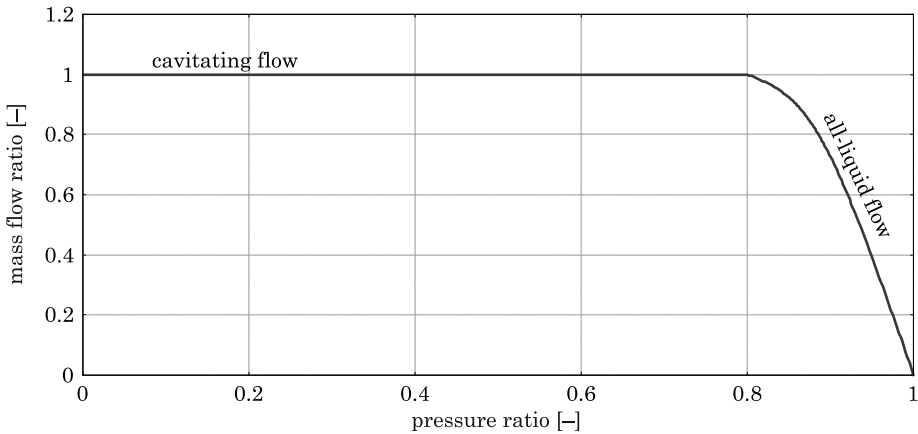


Fig. 2. Characterization curve of cavitating Venturi

Mass flow rate through a Venturi

The mass flow rate through a Venturi is given as

$$\dot{m} = A_{th}\rho_l v_{th} \quad (1)$$

where:

\dot{m} – mass flow rate [kg/s],

A_{th} – cross section area of the throat [m²],

ρ_l – liquid density [kg/m³],

v_{th} – fluid velocity in the throat [m/s], is accounted for basis of two equations.

The first is the continuity equation

$$\dot{V} = A_u v_u = A_{th} v_{th} \quad (2)$$

where:

\dot{V} – volume flow rate [m³/s],

A_u – cross section area of the inlet pipe [m²],

A_{th} – cross section area of the throat [m²].

The second equation is the Bernoulli's equation (ABDULAZIZ 2014)

$$\frac{v_u^2}{2g} + \frac{p_u}{\rho_l g} + h = \frac{v_{th}^2}{2g} + \frac{p_{th}}{\rho_l g} + h \quad (3)$$

where:

g – acceleration [m²/s],

h – elevation of the point above a reference plane [m].

Both equations (2 and 3) are valid for steady and incompressible flows. This assumption is also applied in the current description.

The development of the mass model for cavitating flow should be preceded by appropriate and necessary assumptions. According to the first assumptions, the flow in the converging part is isentropic. The second assumption concerns the density of the fluid, which should be constant and equal to the liquid density at the analysed operating temperature (ABDULAZIZ 2014).

The Bernoulli's equation (Eq. 3) will be used to obtain the dependence on the velocity in the throat. The formula for the upstream velocity will be added to this equation

$$v_u = \frac{A_{th}}{A_u} v_{th} \quad (4)$$

It is derived from the continuity equation (Eq. 2). The third term of the Bernoulli's equation (Eq. 3), the elevation of the point above a reference plane, can be omitted here, because in the experiment all parts of the Venturi are in the same height. Accordingly, accelerations in the both sides of the equation reduce. By substituting Eq. 4 in Eq. 3 the following formula is achieved:

$$\frac{\left(\frac{A_{th}}{A_u} v_{th}\right)^2}{2} + \frac{p_u}{\rho_l} = \frac{v_{th}^2}{2} + \frac{p_{th}}{\rho_l} \quad (5)$$

Then, moving all the terms containing v_{th} to the left side and the remaining terms to the right side

$$v_{th}^2 - \left(\frac{A_{th} v_{th}}{A_u} \right)^2 = \frac{2(p_u - p_{th})}{\rho_l} \quad (6)$$

The final form of the dependence on the velocity in the throat has the form:

$$v_{th} = \sqrt{\frac{1}{\left(1 - \frac{A_{th}^2}{A_u^2}\right)} \cdot \frac{2(p_u - p_{th})}{\rho_l}} \quad (7)$$

By substituting v_{th} from Eq. 7 in Eq. 1, the final form of the mass flow rate formula for the Venturi is achieved:

$$\dot{m} = A_{th} \rho_l v_{th} = \frac{\pi d_{th}^2}{4} \sqrt{\frac{1}{\left(1 - \frac{A_{th}^2}{A_u^2}\right)} \cdot 2\rho_l (p_u - p_{th})} \quad (8)$$

The presented mass flow rate in the throat (Eq. 8) is only theoretical and should be used for the unchoked mode. To account for the actual value of the mass flow rate

$$\dot{m}_\alpha = C_d \frac{\pi d_{th}^2}{4} \sqrt{\frac{1}{\left(1 - \frac{A_{th}^2}{A_u^2}\right)} \cdot 2\rho_l (p_u - p_{th})} \quad (9)$$

the discharge coefficient C_d should be considered. For Venturis with a converging angle, at a setting higher than 10° the discharge coefficient takes value 0.99 (READER-HARRIS et al. 2001).

Pressure ratio, cavitation number and Reynolds number

Occurrence of cavitation phenomenon is closely connected to many values, which describe the character of the flow. To these values belong e.g. cavitation number, Reynolds number and Weber number. Two of them are considered in the paper, namely cavitation number and Reynolds number. Additionally, pressure ratio is analysed.

Pressure ratio

$$p_r = \frac{p_d}{p_u} \quad (10)$$

is a relationship between the downstream and upstream pressure, respectively p_d and p_u . This relationship is an important indicator for Venturis. The critical pressure ratio p_{rc} gives the information about the value which, if exceeded, leads to loss of the cavitating character. The literature gives that this value should be about 0.8 (ABDULAZIZ 2014). Cavitation number is:

$$\sigma = \frac{p_d - p_{\text{sat}}}{\frac{1}{2} \rho_l v_{th}^2} \quad (11)$$

where:

σ – cavitation number [-],

p_{sat} – saturation pressure [Pa],

is a dimensionless quantity, which is an useful instrument to the analysis of the occurrence and development conditions of cavitation phenomenon. Its formula (Eq. 11) is close to the Euler number, which is used for determination of the similarity of dynamic flows (BAGIEŃSKI 1998). For Venturis, cavitation number expresses the relationship between the difference of a downstream pressure from a saturation pressure at the corresponding temperature and the kinetic energy per volume. The expression for kinetic energy per volume consists of the dependence between liquid density ρ_l and velocity of the fluid in the throat v_{th} . Cavitation inception is possible when the cavitation number is equal to 1. Decreasing of the value is connected with the intensification of the phenomenon (ABDULAZIZ 2014, BAGIEŃSKI 1998).

In case of Venturis, cavitation number and pressure ratio take similar values. This can be explained through a mathematical analysis (ABDULAZIZ 2014). The starting point of this analysis is Eq. 11. After modification through simultaneously applying multiplication and division by upstream pressure, the following formula is obtained:

$$\sigma = \frac{p_u}{\frac{1}{2} \rho_l v_{th}^2} \left(\frac{p_d}{p_u} - \frac{p_{\text{sat}}}{p_u} \right) \quad (12)$$

Because of the very small value of the relationship of saturation pressure p_{sat} to upstream pressure p_u , it can be omitted. The modified form of the equation of the cavitation number (Eq. 12) is as follow:

$$\sigma = \frac{p_u}{\frac{1}{2} \rho_l v_{th}^2} \left(\frac{p_d}{p_u} \right) = \frac{p_d}{\frac{1}{2} \rho_l v_{th}^2} \quad (13)$$

After comparison of the equation (1) and (9) following expression is obtained

$$\rho_l A_{th} v_{th} = \rho_l \frac{\pi d_{th}^2}{4} v_{th} = C_d \frac{\pi d_{th}^2}{4} \sqrt{\frac{1}{\left(1 - \frac{A_{th}^2}{A_u^2}\right)} \cdot 2\rho_l (p_u - p_{th})} \quad (14)$$

The formula, after dividing by the throat area A_{th} and multiplying by liquid density ρ_l , velocity in the throat v_{th} and discharge coefficient C_d , translates into:

$$\rho_l^2 v_{th}^2 = C_d^2 \frac{1}{\left(1 - \frac{A_{th}^2}{A_u^2}\right)} 2\rho_l (p_u - p_{th}) \quad (15)$$

Through dividing both sides by 2 and liquid density ρ_l , the expression takes the following form:

$$\frac{1}{2} \rho_l v_{th}^2 = C_d^2 \frac{1}{\left(1 - \frac{A_{th}^2}{A_u^2}\right)} (p_u - p_{th}) \quad (16)$$

After substituting of Eq. 16 into Eq. 13 the cavitation number is expressed as follow:

$$\sigma = \frac{\left(1 - \frac{A_{th}^2}{A_u^2}\right) p_d}{C_d^2 (p_u - p_{th})} \quad (17)$$

Due to the low value of the throat pressure p_{th} with respect to the upstream pressure p_u and the low value of the rest of part of Eq. 16, the cavitation number can be approximated to the form

$$\sigma \cong \frac{p_d}{p_u} \quad (18)$$

Reynolds number

$$\text{Re} = \frac{v_u l}{\nu} \quad (19)$$

This represents a relationship between upstream velocity v_u , characteristic linear dimension l and kinematic viscosity ν . Reynolds number is a criterion for estimating the stability of fluid motion. Based on Reynolds number, the character of the flow, laminar or turbulent, can be specified.

Experimental setup and methods

The diagram of the test rig is presented in the Figure 3. The test rig is constructed from acid-proof profiles and pipes with diameters of 60 mm and 50 mm. The main parts of the test rig belong to water tank, motor, and water pump as well as cavitation chamber. The water tank has the capacity of 70 l. The used pump self-priming up to 10 bars is suitable for liquids with the temperature not exceeding 110°C, density not exceeding 1,300 kg/m³ and viscosity not exceeding 150 mm²/s. A motor having a power of 5.5 kW is used as a drive to the self-priming pump. The test rig is equipped with seven sensors that can work with temperature below 100°C and humidity below 50%. The

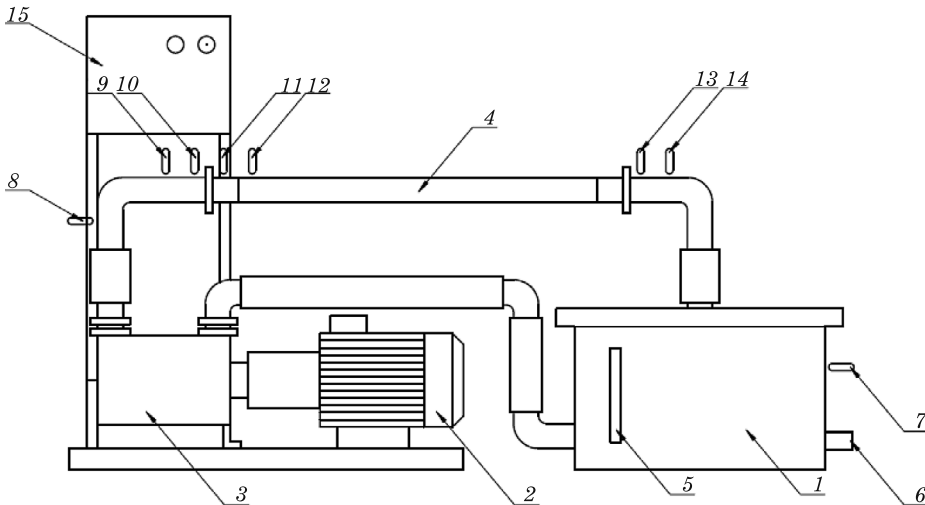


Fig. 3. The diagram of the test rig: 1 – water tank, 2 – motor, 3 – water pump, 4 – cavitation chamber, 5 – water indicator, 6 – heater, 7 – sensor of water level, 8 – velocity inlet sensor, 9 – pressure inlet sensor, 10 – temperature inlet sensor, 11 – proximity sensor of the chamber, 12 – additional proximity sensor, 13 – pressure outlet sensor, 14 – temperature outlet sensor, 15 – control panel
Source: NIEDŹWIEDZKA, SOBIESKI (2016).

seven sensors are: a water level sensor, a sensor for determining of flow velocity at the inlet, sensors of temperature and pressure at the inlet and outlet of the cavitation chamber, a proximity sensor which aims to counteract the switching of the hydraulic system in case of lack of the cavitation chamber and an additional proximity sensor. The other details of the test rig are in the work (NIEDŹWIEDZKA, SOBIESKI 2016).

Three types of Venturis, with throat diameter of 3 mm and angles of converging and diverging sections for the first type ($v1$) 45° and 45° (Fig. 4a), for the second type ($v2$) 60° and 30° (Fig. 4b) and for the third type ($v3$) 30° and 60° (Fig. 4c), were designed and built. The throat length is 6 mm and the outside diameter of the Venturi is 50 mm.

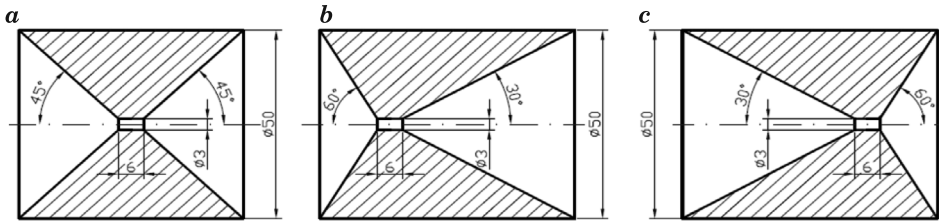


Fig. 4. Dimensions of the Venturi tubes

Source: NIEDŹWIEDZKA, SOBIESKI (2016).

In the experiment the mass flow rate was examined only under different upstream pressure conditions. Using the data obtained in the experiment it is possible to determine mass flow rate, pressure ratio, cavitation number and Reynolds number. Based on this data adequate diagrams can be created, describing relationships between the values.

Results and discussion

In this section performance of the cavitating Venturi has been studied based on the experimental data from the work (NIEDŹWIEDZKA, SOBIESKI 2016). The most attention in discussion is devoted to the mass flow rate, which is the most crucial value for Venturis. The relationships between the mass flow rate and the following values: pressure ratio, cavitation number, Reynolds number and upstream pressure are analysed. Data, which is obligatory for the diagrams, is collected in Tables 1–3.

According to the information from the theoretical background, the low values of the pressure ratio for all Venturi types indicate that the flow is cavitating. The maximum value of pressure ratio for the first type of Venturi is

Table 1

Data for calculating of the diagrams for the first type of Venturi

p_u [Pa]	t_u [°C]	v_{th} [m/s]	p_{th} [Pa]	p_r [-]	σ [-]	Re [-]	m_{th} [kg/s]
481,325	20.2	30.95	2,366	0.211	0.207	5,000	0.217
677,325	20.5	36.74	2,410	0.150	0.147	10,000	0.257
776,325	20.9	39.34	2,470	0.131	0.128	15,000	0.275
846,325	21.1	41.08	2,500	0.120	0.117	20,000	0.287
964,325	21.4	43.86	2,547	0.105	0.103	25,000	0.307

Table 2

Data for calculating of the diagrams for the second type of Venturi

p_u [Pa]	t_u [°C]	v_{th} [m/s]	p_{th} [Pa]	p_r [-]	σ [-]	Re [-]	m_{th} [kg/s]
657,325	31.1	36.13	4,515	0.154	0.148	5,000	0.253
757,325	32.6	38.79	4,915	0.134	0.128	10,000	0.271
1,022,325	35.6	45.09	5,808	0.099	0.094	15,000	0.315

Table 3

Data for calculating of the diagrams for the third type of Venturi

p_u [Pa]	t_u [°C]	v_{th} [m/s]	p_{th} [Pa]	p_r [-]	σ [-]	Re [-]	m_{th} [kg/s]
534,325	24.1	32.60	3000	0.190	0.185	5,000	0.228
719,325	24.7	37.85	3109	0.141	0.137	10,000	0.265
811,325	28	40.19	3778	0.125	0.121	15,000	0.281
980,325	29.7	44.19	4168	0.103	0.100	20,000	0.309
1,099,325	35.8	46.76	5872	0.092	0.087	25,000	0.327

0.211 and the minimum 0.105 (Tab. 1). For the remaining Venturis, the pressure ratio ranges from 0.154 to 0.094 for the second and from 0.190 to 0.092 for the third Venturi type (Tab. 2, 3). The cavitation number takes the similar values in case of all Venturis. It is a proof that these two values can be used interchangeably. This observation is supported by Figure 5, where the relationship between cavitation number and pressure ratio is presented.

The mass flow rate achieves the average value 0.27 kg/s for the first type of Venturi and 0.28 kg/s for the second and third type of Venturi. Applying Venturi as a flow meter supposes that the mass flow rate at invariable upstream pressure and variable downstream pressure conditions is constant for the pressure ratio in the range from 0 to 0.8. Due to the construction of the test rig, it is impossible to make such characteristic for the chosen Venturis.

However, the relationship between the upstream pressure and the mass flow rate can be presented (Fig. 6). These characteristics have a curve form for each of the analysed Venturis. A similar diagram showing a relationship between these variables for other Venturis was presented in work of other scientists (GHASEMMI, FASIH 2011). It confirms that the results of the experimental tests in terms of quality are correct.

Figures 7 and 8 show the relationship between the mass flow rate and the cavitation number and pressure ratio. Their characteristics are summarised by curves with similar shapes. It is a visualization of the possibility of the interchangeable application of pressure ratio and cavitation number. The presented characteristics show that the value of the mass flow rate drops with the increase of the pressure ratio or cavitation number.

The next relationship between the mass flow rate and Reynolds number in the pipe is shown in Figure 9. The Reynolds numbers tested for the analysed

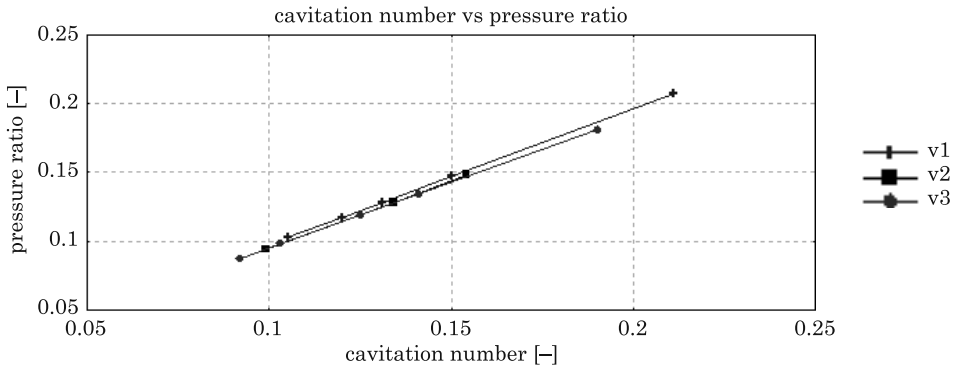


Fig. 5. Cavitation number versus Venturi pressure ratio

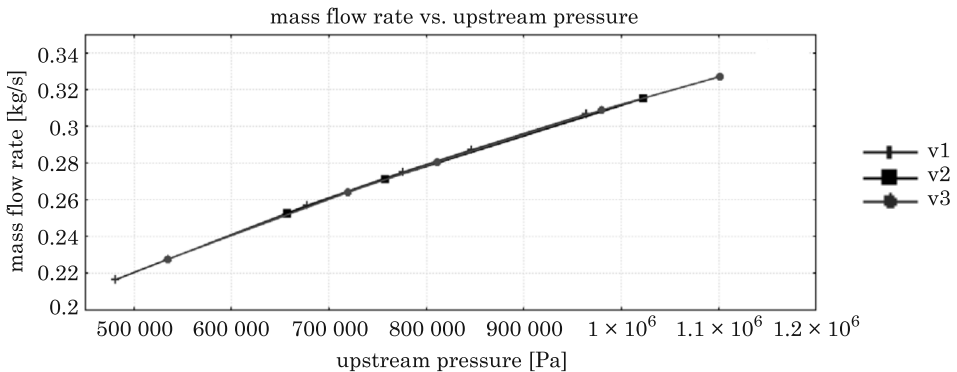


Fig. 6. Mass flow rate versus upstream pressure

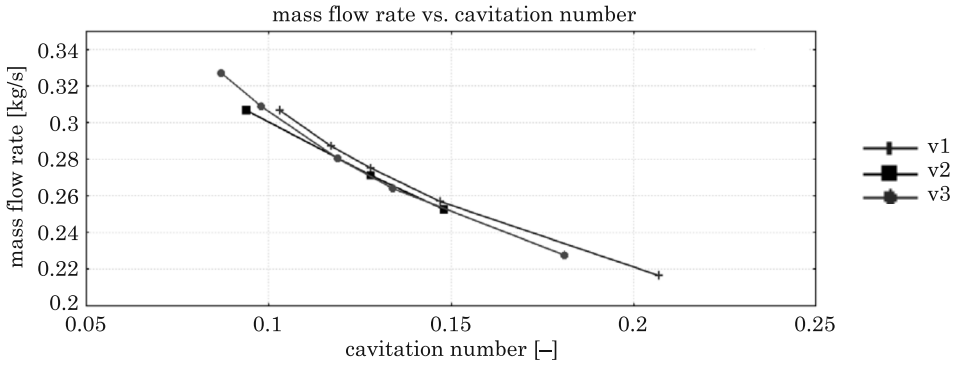


Fig. 7. Mass flow rate versus cavitation number

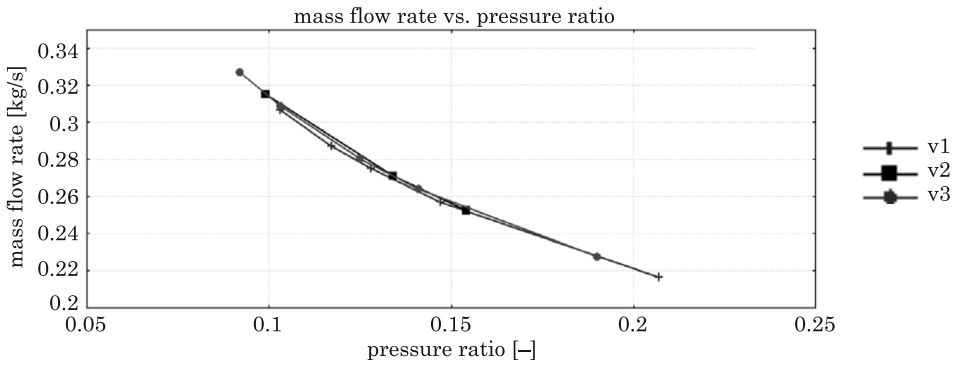


Fig. 8. Mass flow rate versus pressure ratio

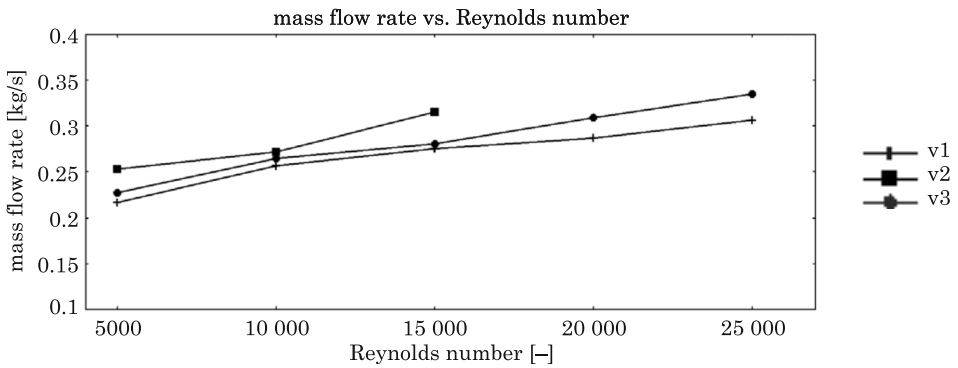


Fig. 9. Mass flow rate versus Reynolds number

flow are in the range from 5,000 to 25,000. The lowest value is higher than the critical Reynolds number for pipes. It shows that the flow in the whole of the experimental measurements has a turbulent character. This information is important in the context of the next step of investigations, i.e. the numerical modelling. The issue of which turbulence models should be used is open.

Conclusions

The article presents results of the examination of the effects of changes in angles of converging and diverging sections of small-sized Venturis on their operating characteristics. Three chosen Venturis have throat diameters of 3 mm and angles of converging and diverging section 45° and 45°, 60° and 30°, 30° and 60°. The Venturis have been examined under different upstream and constant downstream conditions. The following concluding remarks can be made:

- The construction of the test rig in the present configuration prevents carrying out measurements with variable downstream conditions. Because of this restriction, it is not possible anymore to make the most important characterization curve of cavitating Venturi, which describes the usefulness of the device as a flow meter. The critical pressure ratio for the analysed Venturis could not be specified.

- The Venturi in the analysed system works only in „choked” mode. The pressure ratio is in the range from 0.092 to 0.211. It means that the flow inside the Venturi has a cavitating character, what was confirmed during the experiments.

- Cavitation number and pressure ratio can be used for small sized cavitating Venturis interchangeably.

- The simultaneous changes in angles of converging and diverging sections have significant effect on starting point of upstream pressure and Reynolds number of the working Venturi. The decrease of the angle of converging sections results in the drop of the maximum Reynolds number. The shape of the analysed characteristics is similar for all Venturis.

- Characteristics of the upstream pressure and the mass flow rate have a curve form for each of the analysed Venturis. A similar diagram showing a relationship between these variables for other Venturis was presented in work of other scientists (GHASEMMI, FASIH 2011). It confirms that the results of the experimental tests in terms of quality are correct.

- The aims of the future works are simulations of cavitating flow in Venturis. The presented characteristics confirm rightness of the choice of the cavitation inductors.

References

- ABDULAZIZ A.M. 2014. *Performance and image analysis of a cavitating process in a small type Venturi*. Experimental Thermal and Fluid Science, 53: 40–48.
- ASHRAFIZADEH S.M., GHASEMMI H. 2015. *Experimental and numerical investigation on the performance of small-sized cavitating Venturis*. Flow Measurement and Instrumentation, 42: 6–15.
- BAGIEŃSKI J. 1998. *Kawitacja w urządzeniach wodociągowych i ciepłowniczych*. Wydawnictwo Politechniki Poznańskiej, Poznań.
- GHASSEMI H., FASIH H.F. 2011. *Application of small size cavitating Venturi as flow controller and flow meter*. Flow Measurement and Instrumentation, 22: 406–412.
- HARADA K., MURAKAMI M., ISHII T. 2006. *PIV measurements for flow pattern and void fraction in cavitating flows of He II and He I*. Cryogenics, 46: 648–657.
- ISHIMOTO J., KAMIJO K. 2003. *Numerical simulation of cavitating flow of liquid helium in Venturi channel*. Cryogenics, 43: 9–17.
- LIU S.G., CHEN I.Y., SHEU S.J. 1998. *Testing and evaluation of small cavitating Venturis with water at low inlet subcooling*. Space Technology and Applications International Forum, 420: 479–487.
- NAVICKAS J., CHEN L. 1993. *Cavitating Venturi performance characteristics*. ASME Fluids Engineering Division Publication FED, 177: 153–159.
- NIEDŹWIEDZKA A., SOBIESKI W. 2016. *Experimental investigations of cavitating flows in a Venturi tube*. Technical Sciences, 19(2).
- RANDALL L.N. 1952. *Rocket applications of the cavitating Venturi*. J Am Rock Soc., 22: 28–38.
- READER-HARRIS M.J., BRUNTON W.C., GIBSON J.J., HODGES D., NICHOLSON I.G. 2001. *Discharge coefficients of Venturi tubes with standard and non-standard convergent angles*. Flow Measurements and Instrumentation, 12: 135–145.
- SOBIESKI W. 2005. *Stanowisko laboratoryjne do badania zjawiska kawitacji*. V Warsztaty „Modelowanie przepływów wielofazowych w układach termochemicznych. Zaawansowane techniki pomiarowe”, Stawiska.
- UNGAR E.K., DZENTIS J.M., SIFUENTES R.T. 1994. *Cavitating Venturi performance at low inlet subcooling: normal operation, overflow and recovery of overflow*. American Society of Mechanical Engineers, New York, NY (United States).
- UNGAR E.K., MAI T.D. 1994. *Potential cavitating Venturi modifications to improve performance at low inlet subcooling: backward facing steps and threaded throats*. American Society of Mechanical Engineers, New York, NY (United States).
- XU C., HEISTER S.D., FIELD R. 2002. *Modeling cavitating Venturi flows*. Journal of Propulsion and Power, 18: 1227–1234.



THE CAUCHY PROBLEM FOR THE TIME-FRACTIONAL ADVECTION DIFFUSION EQUATION IN A LAYER

Yuriy Povstenko¹, Joanna Klekot²

¹ Institute of Mathematics and Computer Science
Faculty of Mathematics and Natural Sciences
Jan Długosz University in Częstochowa

² Institute of Mathematics
Częstochowa University of Technology

Received 25 March 2016; accepted 10 June 2016; available online 14 June 2016

Key words: porous medium, non-Fickian diffusion, fractional calculus, Mittag-Leffler function.

Abstract

The time-fractional advection-diffusion equation with the Caputo time derivative is studied in a layer. The fundamental solution to the Cauchy problem is obtained using the integral transform technique. The logarithmic singularity term is separated from the solution. Expressions amenable for numerical treatment are obtained. The numerical results are illustrated graphically.

Introduction

The standard advection diffusion equation

$$\frac{\partial c}{\partial t} = a Dc - \mathbf{v} \cdot \text{grad } c, \quad (1)$$

where:

a is the diffusivity coefficient, \mathbf{v} is the given velocity vector, results from the balance equation for mass and the constitutive equation

Correspondence: Yuriy Povstenko, Institute of Mathematics and Computer Science, Jan Długosz University in Częstochowa, al. Armii Krajowej 13/15, 42-200 Częstochowa, e-mail: j.povstenko@ajd.czest.pl

$$\mathbf{j} = -a \operatorname{grad} c + \mathbf{v}c \quad (2)$$

and has several physical interpretations in terms of Brownian motion, diffusion or heat conduction with additional force or with additional velocity field, transport processes in porous media, groundwater hydrology, diffusion of charge in the electric field on comb structures, etc. (FELLER 1971, KAVIANY 1995, NIELD and BEJAN 2006, RISKEN 1989, SCHEIDEGGER 1974, VAN KAMPEN 2007).

In the last few decades, equations with derivatives of fractional order have attracted considerable interest of researchers due to many applications in physics, geophysics, geology, rheology, engineering and bioengineering (GAFIYCHUK and DATSKO 2010, MAGIN 2006, MAINARDI 2010, METZLER and KLAFTER 2000, POVSTENKO 2015b, ROSSIKHIN and SHITIKOVA 1997, UCHAIKIN 2013, WEST et al. 2003).

The time-nonlocal generalizations of the constitutive equation for the matter flux (2) were studied in (POVSTENKO 2015a, 2015b). In the case of the „long-tail” power kernel, we have

$$\mathbf{j} = D_{RL}^{1-\alpha} [-a \operatorname{grad} c + \mathbf{v}c], \quad (3)$$

where:

$D_{RL}^{\alpha}(t)$ is the Riemann-Liouville fractional derivative of the order α (GORENFLO and MAINARDI 1997, KILBAS et al. 2006, PODLUBNY 1999):

$$D_{RL}^{\alpha}(t) = \frac{d^n}{dt^n} \left[\frac{1}{\Gamma(n-\alpha)} \int_0^t (t-\tau)^{n-\alpha-1} c(\tau) d\tau \right], \quad n-1 < \alpha < n. \quad (4)$$

In combination with the balance equation for mass, Eq. (3) leads to the time-fractional advection diffusion equation

$$\frac{\partial^{\alpha} c}{\partial t^{\alpha}} = a Dc - \mathbf{v} \cdot \operatorname{grad} c, \quad (5)$$

with the Caputo fractional derivative of the order α (GORENFLO and MAINARDI 1997, KILBAS et al. 2006, PODLUBNY 1999):

$$\frac{\partial^{\alpha} c}{\partial t^{\alpha}} = \frac{1}{\Gamma(n-\alpha)} \int_0^t (t-\tau)^{n-\alpha-1} \frac{d^n c(\tau)}{d\tau^n} d\tau, \quad n-1 < \alpha < n. \quad (6)$$

In the literature there are only several papers in which the analytical solutions of Eq. (5) were obtained; equation with one spatial variable was considered in (HUANG and LIU 2005, LIU et al. 2003, POVSTENKO and KLEKOT 2014), while equation with two spatial variables was studied in (POVSTENKO 2014, 2015a, 2015b). A comprehensive survey of different approaches to solving the fractional advection diffusion equation as well as of the numerical methods used for its solving can be found in (POVSTENKO 2014). In the present paper, we study Eq. (5) in a layer $0 < x < l$, $-\infty < y < \infty$. The fundamental solution to the Cauchy problem is obtained using the integral transform technique. The logarithmic singularity term is separated from the solution. Expressions amenable for numerical treatment are derived. The numerical results are illustrated graphically.

The paper is organized as follows. In the succeeding section, the initial-boundary-value for the time-fractional advection diffusion equation is formulated and the new sought-for function is introduced to eliminate the gradient term from the equation. Next, the considered problem is solved using the Laplace and Fourier integral transforms. Concluding remarks are presented in the last section.

Statement of the problem

We investigate the time-fractional advection diffusion equation in a layer

$$\frac{\partial^\alpha c}{\partial t^\alpha} = \alpha \left(\frac{\partial^2 c}{\partial x^2} + \frac{\partial^2 c}{\partial y^2} \right) - v \frac{\partial c}{\partial x} - v \frac{\partial c}{\partial y}, \quad x \in (0, l), y \in (-\infty, +\infty), t > 0; \quad (7)$$

with $\alpha > 0$, $v > 0$, $\alpha \in (0,1)$.

Equation (7) is considered under zero Dirichlet boundary conditions at the surfaces of a layer

$$c(0, y, t) = 0, \quad y \in (-\infty, +\infty), t > 0; \quad (8)$$

$$c(l, y, t) = 0, \quad y \in (-\infty, +\infty), t > 0; \quad (9)$$

and the initial condition

$$c(x, y, 0) = f(x, y), \quad (x, y) \in (0, l) \times (-\infty, +\infty). \quad (10)$$

As usually, the zero condition at infinity is also assumed:

$$\lim_{y \rightarrow \pm\infty} c(x, y, t) = 0, \quad x \in [0, l], t > 0. \quad (11)$$

The solution of the considered problem can be written as

$$c(x, y, t) = \iint_{-\infty}^{\infty} f(\zeta, \sigma) G(x, y - \sigma, \zeta, t) d\zeta d\sigma, \quad (12)$$

where:

$G(x, y, \zeta, t)$ is the fundamental solution of (7)–(11) corresponding to the initial condition

$$c(x, y, 0) = G(x, y, \zeta, 0) = p_0 \delta(x - \zeta) \delta(y), \quad 0 < \zeta < l. \quad (13)$$

Here $\delta(x)$ is the Dirac delta function. In Eq. (13), we have introduced the constant multiplier p_0 to obtain the nondimensional quantity displayed in Figures (see Eq. (33)). The initial-boundary-value problem (7)–(11) is well-posed in the Banach space C of continuous functions vanishing at infinity, endowed with the sup norm (HANYGA 2002a, 2002b).

Now we introduce the new sought-for function $u(x, y, \zeta, t)$:

$$G(x, y, \zeta, t) = \exp\left[\frac{v(x+y)}{2a}\right] u(x, y, \zeta, t), \quad (14)$$

which allows us to eliminate the gradient terms from (7) and to reformulate the initial-boundary-value problem (7)–(11) as

$$\frac{\partial^\alpha u}{\partial t^\alpha} = a \left(\frac{\partial^2 u}{\partial x^2} + \frac{\partial^2 u}{\partial y^2} \right) - \frac{v^2}{2a} u, \quad x \in (0, l), y \in (-\infty, +\infty), t > 0; \quad (15)$$

$$u(0, y, \zeta, t) = 0, \quad y \in (-\infty, +\infty), t > 0; \quad (16)$$

$$u(l, y, \zeta, t) = 0, \quad y \in (-\infty, +\infty), t > 0; \quad (17)$$

$$u(x, y, \zeta, t) = p_0 \exp\left(-\frac{v\zeta}{2a}\right) \delta(x - \zeta) \delta(y), \quad (x, y) \in (0, l) \times (-\infty, +\infty); \quad (18)$$

$$\lim_{y \rightarrow \pm\infty} u(x, y, \zeta, t) = 0, \quad x \in [0, l], t > 0. \quad (19)$$

In Eq. (18), we have used the relation $f(x)\delta(x - \zeta) = f(\zeta)\delta(x - \zeta)$ understood in terms of distributions.

Solution of the problem

To solve the problem (15)–(19), the integral transform technique will be used. Recall that the Caputo fractional derivative for the Laplace transform rule requires the knowledge of the initial values of the function and its integer derivatives of the order $k = 1, 2, \dots, n - 1$ (GORENFLO and MAINARDI 1997, KILBAS et al. 2006, PODLUBNY 1999):

$$L \left\{ \frac{d^\alpha f(t)}{dt^\alpha} \right\} = s^\alpha f^*(s) - \sum_{k=0}^{n-1} f^{(k)}(0^+) s^{\alpha-1-k}, \quad n - 1 < \alpha < n, \quad (20)$$

where the asterisk denotes the Laplace transform, s is the transform variable.

The exponential Fourier transform with respect to the spatial coordinate y (denoted by the tilde) has the following form (SNEDDON 1972):

$$F\{f(y)\} = \tilde{f}(\eta) = \frac{1}{\sqrt{2\pi}} \int_{-\infty}^{\infty} f(y)e^{i\eta y} dy, \quad (21)$$

$$F^{-1}\{\tilde{f}(\eta)\} = f(y) = \frac{1}{\sqrt{2\pi}} \int_{-\infty}^{\infty} \tilde{f}(\eta)e^{-i\eta y} d\eta, \quad (22)$$

and

$$F \left\{ \frac{d^2 f(y)}{dy^2} \right\} = -\eta^2 \tilde{f}(\eta) \quad (23)$$

The finite sin-Fourier transform with respect to the spatial coordinate is marked by the hat and is expressed as (SNEDDON 1972).

$$F\{f(x)\} = \hat{f}(\xi_k) = \int_0^L f(x) \sin(x\xi_k) dx, \quad (24)$$

$$\mathbb{F}^{-1}\{\hat{f}(\xi_k)\} = f(x) = \frac{2}{l} \sum_{k=1}^{\infty} \hat{f}(\xi_k) \sin(x\xi_k), \quad (25)$$

where

$$\xi_k = \frac{k\pi}{l}, \quad k = 1, 2, 3, \dots \quad (26)$$

This transform is used in the case of the Dirichlet boundary conditions as for the second derivative of a function we have

$$\mathbb{F} \left\{ \frac{d^2 f(x)}{dx^2} \right\} = -\xi_k^2 \hat{f}(\xi_k) + \xi_k [f(0) - (-1)^k f(l)]. \quad (27)$$

Applying the integral transforms to Eqs. (15)–(19), we get

$$\hat{u}^*(\xi_k, \eta, \zeta, s) = \frac{p_0}{\sqrt{2\pi}} \exp\left(-\frac{v\zeta}{2a}\right) \sin(\zeta\xi_k) \frac{s^{\alpha-1}}{s^\alpha + a(\xi_k^2 + \eta^2) + \frac{v^2}{2a}} \quad (28)$$

The inverse integral transforms give

$$\begin{aligned} u(x, y, \zeta, t) &= \frac{p_0}{\pi l} \exp\left(-\frac{v\zeta}{2a}\right) \sum_{k=1}^{\infty} \sin(x\xi_k) \sin(\zeta\xi_k) \\ &\times \int_{-\infty}^{\infty} E_\alpha \left[-a \left(\xi_k^2 + \eta^2 + \frac{v^2}{2a^2} \right) t^\alpha \right] \cos(y\eta) d\eta, \end{aligned} \quad (29)$$

where $E_\alpha(z)$ is the Mittag-Leffler function in one parameter α (GORENFLO et al. 2014)

$$E_\alpha(z) = \sum_{n=0}^{\infty} \frac{z^n}{\Gamma(\alpha n + 1)}, \quad \alpha > 0, z \in C, \quad (30)$$

and the following formula

$$\mathbb{L}^{-1} \left\{ \frac{s^{\alpha-1}}{s^\alpha + b} \right\} = E_\alpha(-bt^\alpha) \quad (31)$$

has been used.

Hence, for the fundamental solution $G(x,y,\zeta,t)$ we have the expression:

$$G(x,y,\zeta,t) = \frac{p_0}{\pi L} \exp \left[\frac{v(x + y - \zeta)}{2a} \right] \sum_{k=1}^{\infty} \sin(x\xi_k) \sin(\zeta\xi_k) \times \int_{-\infty}^{\infty} E_{\alpha} \left[-a \left(\xi_k^2 + \eta^2 + \frac{v^2}{2a^2} \right) t^{\alpha} \right] \cos(y\eta) d\eta. \tag{32}$$

For $v = 0$, the fundamental solution (32) coincides with the corresponding solution to the time-fractional diffusion-wave equation obtained in (POVSTENKO 2015c).

In calculations we will use the following nondimensional quantities

$$\bar{c} = \frac{\sqrt{a} t^{\alpha/2} l}{p_0} G, \quad \bar{x} = \frac{x}{l}, \quad \bar{y} = \frac{y}{l}, \quad \bar{\zeta} = \frac{\zeta}{l}, \quad \bar{v} = \frac{lv}{a}, \quad \tau = \frac{at^{\alpha}}{l^2}. \tag{33}$$

In the case of the standard advection diffusion equation corresponding to $\alpha = 1$, taking into account that $E_1(z) = e^z$ and evaluating the following integral (PRUDNIKOV et al. 1986a)

$$\int_0^{\infty} e^{-p^2x^2} \cos(qx) dx = \frac{\sqrt{\pi}}{2p} \exp\left(-\frac{q^2}{4p^2}\right), \quad p > 0, \tag{34}$$

we get

$$G(x,y,\zeta,t) = \frac{p_0}{\sqrt{\pi at} l} \exp \left[\frac{v}{2a} \left(x - \zeta - \frac{vt}{2} \right) \right] \exp \left[-\frac{(y - vt)^2}{4at} \right] \times \sum_{k=1}^{\infty} \sin(x\xi_k) \sin(\zeta\xi_k) \exp(-at\xi_k^2). \tag{35}$$

The solution (35) is shown in Fig. 1 and Fig. 2 for different values of the drift parameter \bar{v} .

Unfortunately, for $\alpha \neq 1$ Eq. (32) is not amenable for numerical treatment as it has singularity at the point $x = \zeta, y = 0$. The type of singularity is the same as in the case of an infinite plane, and for numerical calculations it is convenient to separate the singularity term from Eq. (32). For this purpose, we recall the fundamental solution (POVSTENKO 2014) to the Cauchy problem for the time-fractional advection diffusion equation in a plane:

$$\frac{\partial^\alpha G_\infty}{\partial t^\alpha} = a \left(\frac{\partial^2 G_\infty}{\partial x^2} + \frac{\partial^2 G_\infty}{\partial y^2} \right) - v \frac{\partial G_\infty}{\partial x} - \bar{v} \frac{\partial G_\infty}{\partial y}, \quad x \in (-\infty, +\infty), y \in (-\infty, +\infty), t > 0; \tag{36}$$

$$G_\infty(x, y, \zeta, 0) = p_0 \delta(x - \zeta) \delta(y), \quad x \in (-\infty, +\infty), y \in (-\infty, +\infty) \tag{37}$$

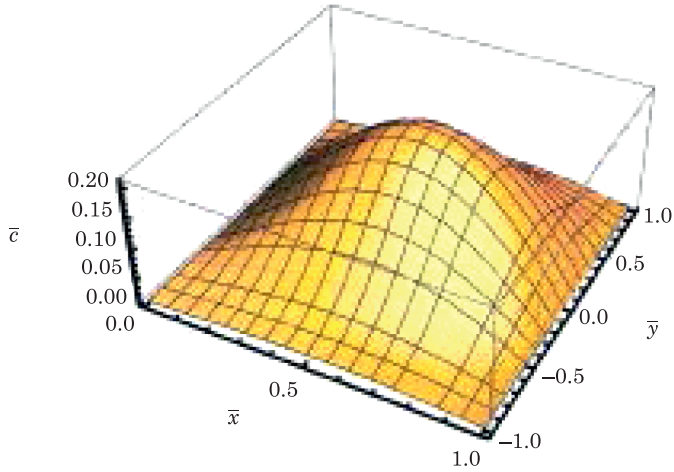


Fig. 1. Fundamental solution to the advection diffusion equation; $\alpha = 1, \tau = 0.1, \bar{\zeta} = 1/2, \bar{v} = 1$

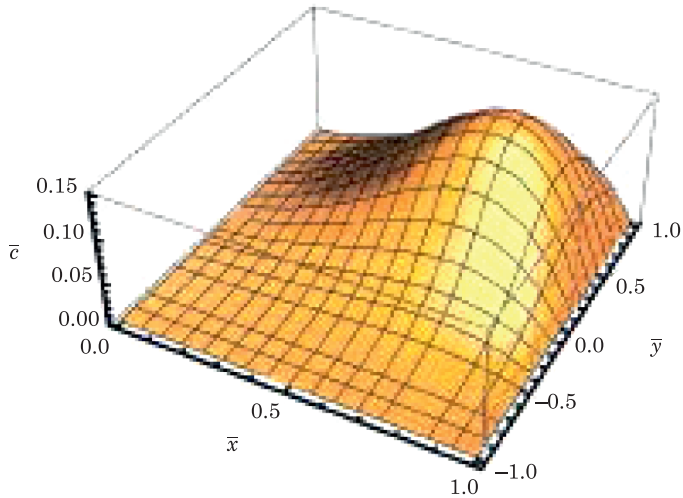


Fig. 2. Fundamental solution to the advection diffusion equation $\alpha = 1, \tau = 0.1, \bar{\zeta} = 1/2, \bar{v} = 5$

For the auxiliary function $u_\infty(x, y, \zeta, t)$ (14) after applying the Laplace transform with respect to the time t and the double exponential Fourier transform with respect to the spatial coordinates x and y we obtain

$$\tilde{u}_\infty^*(\xi, \eta, \zeta, s) = \frac{p_0}{2\pi} \exp\left(-\frac{v\zeta}{2a}\right) \exp(i\zeta\xi) \frac{s^{\alpha-1}}{s^\alpha + a(\xi^2 + \eta^2) + \frac{v^2}{2a}} \quad (38)$$

and

$$\tilde{u}_\infty^*(x, \eta, \zeta, s) = \frac{p_0}{(2\pi)^{3/2}} \exp\left(-\frac{v\zeta}{2a}\right) \int_{-\infty}^{\infty} \frac{\cos[(x - \zeta)\xi] s^{\alpha-1}}{s^\alpha + a(\xi^2 + \eta^2) + \frac{v^2}{2a}} d\xi, \quad (39)$$

$$u_\infty(x, \eta, \zeta, t) = \frac{p_0}{(2\pi)^2} \exp\left(-\frac{v\zeta}{2a}\right) \int_{-\infty}^{\infty} \int_{-\infty}^{\infty} \cos[(x - \zeta)\xi] \cos(y\eta), \quad (40)$$

$$\times E_\alpha\left[-a\left(\xi^2 + \eta^2 + \frac{v^2}{2a^2}\right)t^\alpha\right] d\xi d\eta.$$

After introducing the polar coordinates in the (ξ, η) -plane, we get (for details, see (POVSTENKO 2014)):

$$G_\infty(x, y, \zeta, t) = \frac{p_0}{2\pi} \exp\left[\frac{v(x + y - \zeta)}{2a}\right] \int_0^\infty E_\alpha\left[-\left(ar^2 + \frac{v^2}{2a}\right)t^\alpha\right] J_0[\rho\sqrt{(x - \zeta)^2 + y^2}] \rho d\rho, \quad (41)$$

where $J_0(r)$ is the Bessel function.

For large values of the negative argument, the Mittag-Leffler function $E_\alpha(-x)$ has the asymptotic

$$E_\alpha(-x) \sim \frac{1}{\Gamma(1 - \alpha)x}, \quad (42)$$

and for $\alpha \neq 1$ the integral in (41) is divergent at the point $x = \zeta, y = 0$. To separate the singularity, we rewrite (41) as

$$G_{\infty}(x,y,\zeta,t) = \frac{p_0}{2\pi} \exp\left[\frac{v(x+y-\zeta)}{2a}\right] \left\{ \int_0^{\infty} E_{\alpha}\left[-\left(ar^2 + \frac{v^2}{2a}\right)t^{\alpha}\right] - \frac{1}{\Gamma(1-\alpha)\left[1 + \left(ar^2 + \frac{v^2}{2a}\right)t^{\alpha}\right]} \right. \\ \left. \times J_0[\rho\sqrt{(x-\zeta)^2 + y^2}] \rho d\rho + \int_0^{\infty} \frac{J_0[\rho\sqrt{(x-\zeta)^2 + y^2}]}{\Gamma(1-\alpha)\left[1 + \left(a\rho^2 + \frac{v^2}{2a}\right)t^{\alpha}\right]} \rho d\rho \right\}. \tag{43}$$

The first integral in (43) has no singularity, the second one can be evaluated analytically taking that (PRUDNIKOV et al. 1986b)

$$\int_0^{\infty} \frac{x}{x^2 + p^2} J_0(qx) dx = K_0(pq), \quad p > 0, q > 0, \tag{44}$$

where $K_0(x)$ is the modified Bessel function having the logarithmic singularity at the origin. Hence

$$G_{\infty}(x,y,\zeta,t) = (\text{regular term}) + \\ + \frac{p_0}{2\pi\Gamma(1-\alpha)at^{\alpha}} \exp\left[\frac{v(x+y-\zeta)}{2a}\right] K_0\left[\sqrt{1 + \frac{v^2t^{\alpha}}{2a}} \sqrt{\frac{(x-\zeta)^2 + y^2}{at^{\alpha}}}\right]. \tag{45}$$

Now we reformulate the considered problem for a layer $0 < x < l, -\infty < y < \infty$. Let

$$u(x,y,\zeta,t) = u_{\infty}(x,y,\zeta,t) + g(x,y,\zeta,t), \tag{46}$$

and

$$G(x,y,\zeta,t) = G_{\infty}(x,y,\zeta,t) + \exp\left[\frac{v(x+y)}{2a}\right] g(x,y,\zeta,t) \tag{47}$$

where G_{∞} is the solution of the corresponding Cauchy problem in an infinite plane. In such a way, we get

$$\frac{\partial^{\alpha}g}{\partial t^{\alpha}} = a \left(\frac{\partial^2g}{\partial x^2} + \frac{\partial^2g}{\partial y^2} \right) - \frac{v^2}{2a} g, \quad x \in (0,l), y \in (-\infty, +\infty), t > 0; \tag{48}$$

$$g(0,y,\zeta,t) = -u_{\infty}(0,y,\zeta,t), \quad y \in (-\infty, +\infty), t > 0; \tag{49}$$

$$g(l,y,\zeta,t) = -u_\infty(l,y,\zeta,t), y \in (-\infty, +\infty), t > 0; \tag{50}$$

$$g(x,y,\zeta,0) = 0, x \in (0,l), y \in (-\infty, +\infty). \tag{51}$$

From (48)–(51), we have

$$\hat{g}^*(\xi_k, \eta, \zeta, s) = -\frac{\alpha \xi_k [\tilde{u}_\infty^*(0, \eta, \zeta, s) - (-1)^k \tilde{u}_\infty^*(l, \eta, \zeta, s)]}{s^\alpha + a(\xi_k^2 + \eta^2) + \frac{v^2}{2a}} \tag{52}$$

The values $\tilde{u}_\infty^*(0, \eta, \zeta, s)$ and $\tilde{u}_\infty^*(l, \eta, \zeta, s)$ can be found from (39). Hence,

$$\hat{g}^*(\xi_k, \eta, \zeta, s) = -\frac{\alpha p_0 \xi_k}{(2\pi)^{3/2}} \exp\left(-\frac{v\zeta}{2a}\right) s^{\alpha-1} \int_{-\infty}^{\infty} \frac{\cos(\zeta\xi) - (-1)^k \cos[(l-\zeta)\xi]}{\Delta(\xi, \xi_k, \eta, s)} d\xi, \tag{53}$$

where

$$\Delta(\xi, \xi_k, \eta, s) = \left[s^\alpha + a(\xi_k^2 + \eta^2) + \frac{v^2}{2a} \right] \left[s^\alpha + a(\xi^2 + \eta^2) + \frac{v^2}{2a} \right]. \tag{54}$$

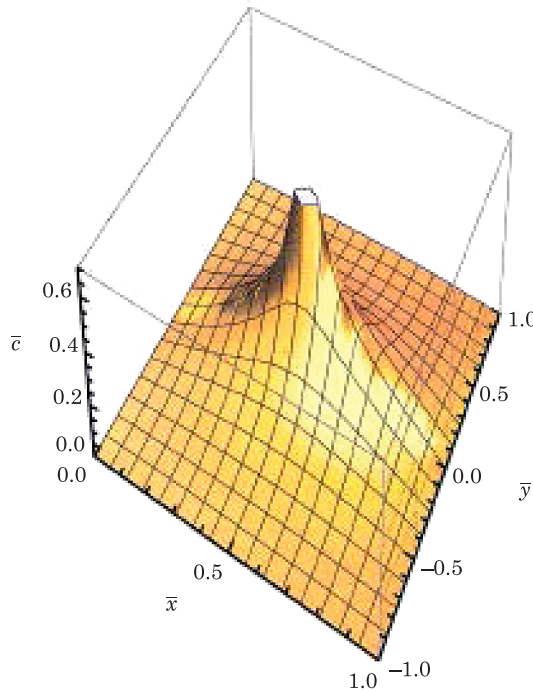


Fig. 3. Fundamental solution to the time-fractional advection diffusion equation; $\alpha = 0.5, \tau = 0.1, \zeta = 1/2, \bar{v} = 1$

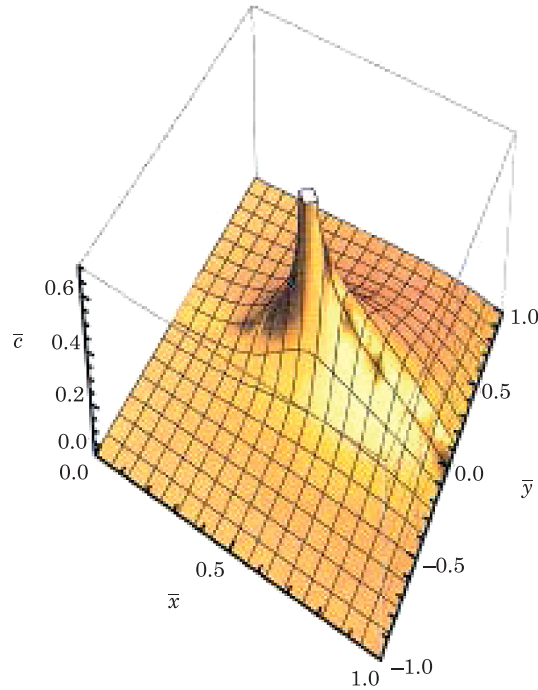


Fig. 4. Fundamental solution to the time-fractional advection diffusion equation; $\alpha = 0.5, \tau = 0.1, \zeta = 1/2, \bar{v} = 5$

After decomposition of $1/\Delta(\xi, \xi_k, \eta, s)$ into partial fractions we obtain

$$\hat{g}^* (\xi_k, \eta, \zeta, s) = -\frac{p_0 \xi_k}{(2\pi)^{3/2}} \exp\left(-\frac{v\zeta}{2a}\right) \int_{-\infty}^{\infty} \frac{\cos(\zeta\xi) - (-1)^k \cos[(l - \zeta)\xi]}{\xi^2 - \xi_k^2} d\xi, \tag{55}$$

$$\times \left[\frac{s^{\alpha-1}}{s^\alpha + a(\xi_k^2 + \eta^2) + \frac{v^2}{2a}} - \frac{s^{\alpha-1}}{s^\alpha + a(\xi^2 + \eta^2) + \frac{v^2}{2a}} \right] d\xi.$$

The inversion of all the integral transforms gives the final result:

$$\begin{aligned}
 G(x,y,\zeta,t) &= G_\infty(x,y,\zeta,t) + \frac{p_0}{2\pi^2 l} \exp\left[\frac{v(x+y-\zeta)}{2a}\right] \\
 &\times \sum_{k=1}^\infty \xi_k \sin(x\xi_k) \int_{-\infty}^\infty \int_{-\infty}^\infty \frac{\cos(\zeta\xi) - (-1)^k \cos[(l-\zeta)\xi]}{\xi^2 - \xi_k^2} \cos(y\eta) \\
 &\times \left\{ E_\alpha\left[-a\left(\xi^2 + \eta^2 + \frac{v^2}{2a^2}\right)t^\alpha\right] - E_\alpha\left[-a\left(\xi_k^2 + \eta^2 + \frac{v^2}{2a^2}\right)t^\alpha\right] \right\} d\xi d\eta.
 \end{aligned}
 \tag{56}$$

Figs. 3 and 4 show the fundamental solution to the Cauchy problem to the time-fractional advection diffusion equation $\bar{c} = \sqrt{at^{\alpha/2}}lp_0^{-1}G$ for $\alpha = 0.5$ and different values of the drift quantity \bar{v} .

Conclusions

We have considered the time-fractional advection diffusion equation with the Caputo fractional derivative in a domain $0 < x < l, -\infty < y < \infty$. The Laplace transform with respect to time t , the finite sin-Fourier transform with respect to the spatial coordinate x , and the exponential Fourier transform with respect to the spatial coordinate y have been used. The fundamental solution to the Cauchy problem has been obtained. The results of numerical calculations are displayed in Figures for different values of the nondimensional spatial variables \bar{x} and \bar{y} , the drift parameter \bar{v} , and the order of the time-fractional derivative α . To evaluate the Mittag-Leffler function $E_\alpha(-x)$ we have used the algorithm suggested in (GORENFLO et al. 2002).

In the case of the standard diffusion equation with the order of time derivative $\alpha = 1$, the fundamental solution has no singularity, and the increase in the quantity \bar{v} causes a drift of the maximum value of the solution and a decrease in this value (see Figs. 1 and 2). In the case of time-fractional advection diffusion equation with the order of time derivative $0 < \alpha < 1$, the fundamental solution to the Cauchy problem has no singularity only in the case of one spatial variable, whereas in the case of two spatial variables the fundamental solution has the logarithmic singularity, and the influence of the drift parameter \bar{v} is less noticeable (Figs. 3 and 4). Increase in the drift parameter \bar{v} only presses the plot to the singularity point.

References

FELLER W. 1971. *An Introduction to Probability Theory and Its Applications* (2nd ed.). John Wiley & Sons, New York.

- GAFIYCHUK V., DATSKO B. 2010. *Mathematical modeling of different types of instabilities in time fractional reaction-diffusion systems*. *Computers & Mathematics with Applications*, 59(3): 1101–1107.
- GORENFLO R., KILBAS A.A., MAINARDI F., ROGOSIN S.V. 2014. *Mittag-Leffler Functions. Related Topics and Applications*. Springer, New York.
- GORENFLO R., LOUTCHKO J., LUCHKO Yu. 2002. *Computation of the Mittag-Leffler function and its derivatives*. *Fractional Calculus and Applied Analysis*, 5(4): 491–518.
- GORENFLO R., MAINARDI F. 1997. *Fractional calculus: Integral and differential equations of fractional order*. In A. Carpinteri, F. Mainardi (Eds.), *Fractals and Fractional Calculus in Continuum Mechanics* (pp. 223–276). Springer, Wien.
- HANYGA A. 2002a. *Multi-dimensional solutions of space-time-fractional diffusion equations*. *Proceedings of the Royal Society of London A*, 458(2018): 429–450.
- HANYGA A. 2002b. *Multidimensional solutions of time-fractional diffusion-wave equations*. *Proceedings of the Royal Society of London A*, 458(2020): 933–957.
- HUANG F., LIU F. 2005. *The time fractional diffusion equation and the advection-dispersion equation*. *ANZIAM Journal* 46(3): 317–330.
- KAVIANY M. 1995. *Principles of Heat Transfer in Porous Media* (2nd ed.). Springer, New York.
- KILBAS A.A., SRIVASTAVA H.M., TRUJILLO J.J. 2006. *Theory and Applications of Fractional Differential Equations*. Elsevier, Amsterdam.
- LIU F., ANH V., TURNER I., ZHUANG P. 2003. *Time-fractional advection-dispersion equation*. *Journal of Applied Mathematics and Computing*, 13(1-2): 233–245.
- MAGIN R.L. 2006. *Fractional Calculus in Bioengineering*. Begell House Publishers, Inc., Redding.
- MAINARDI F. 2010. *Fractional Calculus and Waves in Linear Viscoelasticity: An Introduction to Mathematical Models*. Imperial College Press, London.
- METZLER R., KLAFTER J. 2000. *The random walk's guide to anomalous diffusion: a fractional dynamics approach*. *Physics Reports*, 339(1): 1–77.
- NIELD D.A., BEJAN A. 2006. *Convection in Porous Media* (3rd ed.). Springer, New York.
- PODLUBNY I. 1999. *Fractional Differential Equations*. Academic Press, New York.
- POVSTENKO Y. 2014. *Fundamental solutions to time-fractional advection diffusion equation in a case of two space variables*. *Mathematical Problems in Engineering* 2014: 705364–1–7.
- POVSTENKO Y. 2015a. *Theory of diffusive stresses based on the fractional advection-diffusion equation*. In R. Abi Zeid Daou, M. Xavier (Eds.), *Fractional Calculus: Applications* (pp. 227–242). NOVA Science Publishers, New York.
- POVSTENKO Y. 2015b. *Fractional Thermoelasticity*. Springer, New York.
- POVSTENKO Y. 2015c. *Linear Fractional Diffusion-Wave Equation for Scientists and Engineers*. Birkhauser, New York.
- POVSTENKO Y., KLEKOT J. 2014. *Fundamental solution to the Cauchy problem for the time-fractional advection diffusion equation*. *Journal of Applied Mathematics and Computational Mechanics*, 13(1): 95–102.
- PRUDNIKOV A.P., BRYCHKOV Yu.A., MARICHEV O.I. 1986a. *Integrals and Series, Vol. 1: Elementary Functions*. Gordon and Breach Science Publishers, Amsterdam.
- PRUDNIKOV A.P., BRYCHKOV Yu.A., MARICHEV O.I. 1986b. *Integrals and Series, Vol. 2: Special Functions*. Gordon and Breach Science Publishers, Amsterdam.
- RISKEN H. 1989. *The Fokker-Planck Equation*. Springer, Berlin.
- ROSSIKHIN Yu.A., SHITIKOVA M.V. 1997. *Applications of fractional calculus to dynamic problems of linear and nonlinear hereditary mechanics of solids*. *Applied Mechanics Reviews*, 50(1): 15–67.
- SCHEIDEGGER A.E. 1974. *The Physics of Flow Through Porous Media* (3rd ed.). University of Toronto Press, Toronto.
- SNEDDON I.N. 1972. *The Use of Integral Transforms*. McGraw-Hill, New York.
- UCHAIKIN V.V. 2013. *Fractional Derivatives for Physics and Engineers. Background and Theory*. Springer, Berlin.
- VAN KAMPEN N.G. 2007. *Stochastic Processes in Physics and Chemistry* (3rd ed.). Elsevier, Amsterdam.
- WEST B.J., BOLOGNA M., GRIGOLINI P. 2003. *Physics of Fractals Operators*. Springer, New York.



Quarterly peer-reviewed scientific journal

ISSN 1505-4675
e-ISSN 2083-4527

TECHNICAL SCIENCES

Homepage: www.uwm.edu.pl/techsci/



DYNAMICS OF ELECTROMECHANICAL DRIVE OF SUSPENDED TIMBERTRANSPORTING ROPE SYSTEM

Lidiya Dzyuba¹, Vasyl Baryliak²

¹ Department of Applied Mathematics and Mechanics, Lviv State University of Life Safety, Ukraine

² Department of Applied Mechanics, Ukrainian National Forestry University, Lviv, Ukraine

Received 17 May 2016; accepted 6 September 2016; available online 27 September 2016

Key words: suspended timbertransporting rope system, rope system drive, dynamic model, dynamic force, torsional stiffness.

Abstract

Dynamic loads of drive of suspended timbertransporting rope system with an electric motor are investigated. Developed a dynamic model of the electromechanical drive considering the changing of the electric motor's moment during start-up and the resistance force moment. The changing of the resistance force moment is expressed through the changes in tension force of the pull-bearing rope systems in various manufacturing operations. In determining the moment of inertia of the drive drum is accounted multi-winding of rope. Research on dynamic load of system elements are made with the taking into account the influence of torsional stiffness of system parts and lifting capacity of the suspended timbertransporting rope system.

Introduction

The suspended timbertransporting rope systems have a number of advantages for the primary transportation of timber in mountainous areas compared with tractor skidding. Such as: much lower amount of roads building, the use in any weather and at any soils, waste reduction at cutting areas, the possibility of exploration of forests in inaccessible places for other equipment, reducing energy costs and protecting the environment (ADAMOVSKY et al. 1997, BELAYA, PROHORENKO 1964, KORZHOV, CUDRA 2010). These systems are equip-

Correspondence: Vasyl Baryliak, Ukrainian National Forestry University, Lviv, Ukraine, e-mail: barylyakw@gmail.com

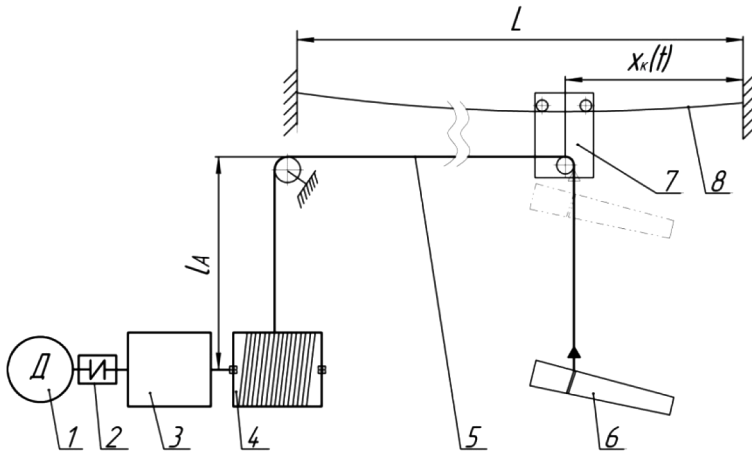


Fig. 1. Schematic diagram of one-drum drive of the timbertransporting rope system: 1 – electric motor; 2 – coupling; 3 – mechanical transmission; 4 – drive drum of power stroke; 5 – pull-hoisting rope; 6 – load; 7 – load carriage; 8 – carrier rope; L – span length of the rope system; $x_c(t)$ – coordinate of load carriage in the span; l_A – length of the reserve rope

ped with electric motor drives or an internal combustion engine (ZANEHYN et al. 2004). The characteristic features of the system drive's work are variable tension force of pull-hoisting rope by various manufacturing operations and multi-winding of rope on the drum. The change of the pull-hoisting rope's tension causes the change of force resistance moment at different stages of the system's process (MALASHHENKO et al. 2013). The multi-winding of the drum drive rope increases its diameter with the wound rope. It causes the changing of the inertia moment of the drive drum. The presence of the drive electric motor causes bigger dynamic loads on system elements when the system is turning on (CZABAN 2008, CZABAN, LIS 2012, KHARCHENKO, SOBKOWSKI 2005). The suspended timbertransporting rope systems are characterized by a low level of unification schemes and constructions. Therefore, the proposed model needs detailing of considering operational and structural features.

The objective is the mathematical modeling of dynamic processes of the suspended timbertransporting rope system's drive with taking into account the changing of the electric motor's moment during start-up and the resistance moment during a steady-state operation mode of the system and studying the impact of structural and operational parameters on the value of dynamic loads in the drive.

To achieve this goal it is necessary to develop a dynamic model of the rope system's drive and take into account, in addition to inertial, elastic and dissipative characteristics of parts, multi-layer winding rope and the real nature of changes in external loads.

Theoretical research

One-drum drive of the timbertransporting rope system is simulated as the equivalent reduced tri-mass dynamic system with three degrees of freedom (Fig. 2). The motor shaft is used as a section of reduction.

Differential equations of drive's motion write down using the principle of d'Alembert in the normal form of Cauchy:

$$\left\{ \begin{array}{l} \frac{d\varphi_1}{dt} = \omega_1 \\ \frac{d\varphi_2}{dt} = \omega_2 \\ \frac{d\varphi_3}{dt} = \omega_3 \\ \frac{d\varphi_1}{dt} = \frac{1}{I_1} \cdot [M_E - v_1(\omega_1 - \omega_2) - c_1(\varphi_1 - \varphi_2)] \\ \frac{d\varphi_2}{dt} = \frac{1}{I_2} \cdot [v_1(\omega_1 + \omega_2) - c_1(\varphi_1 - \varphi_2) - v_2(\omega_2 + \omega_3) - c_2(\varphi_2 - \varphi_3)] \\ \frac{d\varphi_3}{dt} = \frac{1}{I_3(t)} \cdot \left[-M_S(t) - \frac{\omega_3}{2} \frac{d[I_3(t)]}{dt} + v_2(\omega_2 + \omega_3) - c_2(\varphi_2 - \varphi_3) \right] \end{array} \right. \quad (1)$$

where:

$\omega_1, \omega_2, \omega_3$ – angular velocity of corresponding reduced rotating masses, t – time.

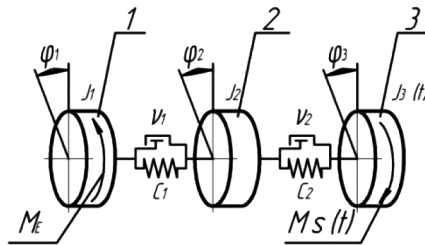


Fig. 2. Estimated diagram of the one-drum drive of the timbertransporting rope system

The notation used on Fig. 2: 1 – rotating mass of motor's rotor and coupling; 2 – reduced rotating mass of drive's mechanical transmission; 3 – reduced rotating mass of drive's drum, pull-hoisting rope and transported load with the load carriage; M_E – electromagnetic moment of motor; $M_S(t)$ – resistance force moment of the drum drive with traction rope reduced to the motor shaft; I_1 – inertia moment of the rotating masses of motor and coupling; I_2 – inertia moment of the drive's mechanical transmission reduced to the motor shaft; $I_3(t)$ – inertia moment of the rotating mass is equivalent to the masses of drive drum, pull-hoisting rope, load with the load carriage and reduced to the motor shaft; c_1, c_2 – reduced coefficients of torsion stiffness of elastic sections; v_1, v_2 – reduced coefficients of elastic sections' viscous resistance; $\varphi_1, \varphi_2, \varphi_3$ – generalized coordinates of drive's rotating masses.

The transient electromagnetic processes in the drive asynchronous electric motor with a shortcircuited rotor (squirrel cage motor) is described briefly based on Park-Gorev equations (PARK 1929, PARK 1933, GOREV 1950). Electromagnetic moment of motor M_E is calculated using the formula (KHARCHENKO, SOBKOWSKI 2005, JOSWIG 2014):

$$M_E = \frac{2}{3} p_0 \frac{1}{\tau} (i_{R_x} i_{S_y} - i_{R_y} i_{S_x}) \quad (2)$$

where:

p_0 – the number of pairs of magnetic poles; $i_{R_x}, i_{S_y}, i_{R_y}, i_{S_x}$ – the projections of currents in the windings of the motor's stator and rotor on the coordinate axes x, y ; τ – the value, which is determined from the magnetization curve. Subscript indicates the value of belonging to the rotor winding, a S – indicates the value of belonging to the stator winding.

The projections of currents $i_{R_x}, i_{S_y}, i_{R_y}, i_{S_x}$ are determined from differential equations of the electromagnetic state of machines (CZABAN 2007, CZABAN, LIS 2012, JOSWIG 2014, KHARCHENKO, SOBKOWSKI 2005), that are written down in matrix form:

$$\begin{aligned} \frac{di_S}{dt} &= A_S(u_S + \Omega_S \psi_S - R_S i_S) + B_S(\Omega_R \psi_R - R_R i_R) \\ \frac{di_R}{dt} &= A_R(\Omega_R \psi_R - R_R i_R) + B_R(u_S + \Omega_S \psi_S - R_S i_S) \end{aligned} \quad (3)$$

where:

i_S, i_R, u_S – matrices column of currents and voltages; A_S, B_S, A_R, B_R – square matrices of communication; Ω_S, Ω_R – frequency rotation matrices; ψ_S, ψ_R – matrices-column of full flows clutches; R_S, R_R – active resistance.

The reduced resistance force moment $M_S(t)$ determine, taking into account the variable of tension force of pull- hoisting rope $S(t)$ and variable radius $r_H(t)$ and variable radius of the drum with wounded rope:

$$M_S(t) = \frac{1}{u} S(t) \cdot r_H(t) \quad (4)$$

where:

u – general gear ratio of drive's mechanical transmission.

To determine the tension force $S(t)$ the technological cycle of work of suspended timbertransporting rope system will be examined. It is divided into the following four stages:

- selection of rope’s weaknesses (characterized by a progressive increase of tension force of the rope to a value equal to the weight of cargo);
- lifting cargo;
- locking cargo with the load carriage;
- transferring cargo with the load carriage along the rope.

The pull-tension power of hoisting rope is determined considering the location coordinates of load carriage, rope system’s process parameters and the duration of each of the stages according to the steps of technological cycle (ADAMOVSKY et al. 1997, ZANEHYN et al. 2004):

$$S(t) = \begin{cases} 0 \leq t \leq \frac{Q[L - x_K(t_0)]}{C_K \cdot v} \Rightarrow S_0(t) = \frac{C_K \cdot v}{L - x_K(t_0)} \cdot t \\ \frac{Q[L - x_K(t_0)]}{C_K \cdot v} < t \leq \frac{1}{v} \left(\frac{Q[L - x_K(t_0)]}{C_K} + H_G \right) \Rightarrow S_1(t) \\ \left[\frac{1}{v} \left(\frac{Q[L - x_K(t_0)]}{C_K} + H_G \right) < t \leq \frac{1}{v} \left(\frac{Q[L - x_K(t_0)]}{C_K} + H_G \right) + t_C \right] \Rightarrow S_2(t) \\ \left. \begin{cases} t > \frac{1}{v} \left(\frac{Q[L - x_K(t_0)]}{C_K} + H_G \right) + t_C \\ t \leq \frac{1}{v} \left(\frac{Q[L - x_K(t_0)]}{C_K} + H_G \right) + \frac{L - x_K(t_0)}{\cos \beta} + \frac{(gq_K)^2 \cdot (L - x_K(t_0))^3}{24 \cdot H^2} \cos \beta \end{cases} \right\} \Rightarrow S_3(t) \end{cases} \quad (5)$$

where:

$S_0(t)$, $S_1(t)$, $S_2(t)$, $S_3(t)$ – pull-tension power of hoisting rope when choosing rope’s weaknesses, lifting cargo, locking cargo with the cargo carriage and transporting of cargo carriage by carrier rope (ADAMOVSKY et al. 1997, ZANEHYN et al. 2004), Q – cargo weight; $x_K(t_0)$ – coordinate of cargo carriage at the initial time t_0 ; H_G – height of lifting cargo; v – velocity of winding of rope on the drum; β – angle between the span’s chord and the horizon; C_K – longitudinal stiffness of pull-hoisting rope; – horizontal component of the tension force of the rope (ADAMOVSKY et al. 1997, BELAYA, PROHORENKO 1964, ZANEHYN et al. 2004); t_C – time of cargo’s locking (ADAMOVSKY et al. 1997); q_K – mass per unit length of the rope.

The expression for determining the radius of the drum with wounded rope in the random time moment writes down as follows:

$$r_H(t) = \frac{d_{B3}}{2} + d_K \cdot (n'(t) - 0,5), \quad (6)$$

where:

d_{B3} – diameter of the drum without a rope, d_K – rope’s diameter, $n'(t)$ – the number of wound rope’s layers.

To determine $n'(t)$, express estimated number of wound rope's layers through the angular rotation velocity of the drum drive:

$$n(t) = n_0 + \frac{\omega_{B3}(t) \cdot d_K \cdot t}{2\pi L_{B3}}, \quad (7)$$

where:

$n(t)$ – angular velocity of the drum drive with rope; n_0 – the number of wound rope's layers at the initial time moment t_0 ; L_{B3} – length of the working surface of the drum. To get the value of $n'(t)$ round the value of $n(t)$ to the upper whole number.

To determine the value of n_0 is used known dependency for the length of wound rope on the drum (GOROKHOVSKI, LIVSHITS 1991):

$$l_0 = \pi \cdot \frac{L_{B3}}{d_K} \cdot n_0 \cdot [d_{B3} + C_y d_K \cdot (n_0 - 1)] \quad (8)$$

where:

C_y – the ratio of wound rope's density.

The length of wound rope at the initial time moment is determined because total capacity of the rope of the drum drive and coordinate's placement of cargo carriage in flight are set. Taking into account the rope's sagging by a parabola (ADAMOVSKY et al. 1997, BELAYA, PROHORENKO 1964) and the available rope's reserve (GOROKHOVSKI, LIVSHITS 1991, KORZHOV, CUDRA, 2010) this length is equal to:

$$l_0 = l_A + \frac{x_K(t_0)}{\cos\beta} + \frac{q_K^2 \cdot x_K(t_0)^3}{24H^2} \cos\beta \quad (9)$$

Equating (8) and (9), we obtain an expression for determining the number of wound rope's layers at the initial time t_0 :

$$n_0 = \frac{C_y d_K - d_{B3} + \sqrt{(d_{B3} - C_y d_K)^2 + \frac{4C_y d_K^2 l_0}{\pi \cdot L_{B3}}}}{2C_y d_K} \quad (10)$$

Thus, the radius of the drum with wounded rope at a random moment of time is calculated by the relation (6) using (7) – (10).

To determine the variable reduced moment of $I_3(t)$ specified stages of the rope system's cycle of work must be taken into account. The inertia moment of of the drive drum, the mass of cargo and area of rolling rope are forming factors for $I_3(t)$ at the stage of lifting and locking loads. The expression for determining the reduced moment of inertia at this stage is:

$$I_3(t) = \frac{1}{u^2} \left(I_{B3}(t) + \frac{q_K}{3} \left(\frac{L - x_K(t_0)}{\cos\beta} + \frac{q_K^2 \cdot (L - x_K(t_0))^3}{24H^2} \cos\beta \right) r_H^2(t) + \frac{Q}{g} r_H^2(t) \right) \quad (11)$$

where:

u – general gear ratio of drive's transmissions; I_{B3} – inertia moment of the drive of the drum.

To determine the reduced moment $I_3(t)$ the moving mass of cargo carriage is taken to account at the stage of displacement:

$$I_3(t) = \frac{1}{u^2} \left(I_{B3}(t) + \frac{q_K}{3} \left(\frac{L - x_K(t_0)}{\cos\beta} + \frac{q_K^2 \cdot (L - x_K(t_0))^3}{24H^2} \cos\beta \right) r_H^2(t) + \frac{Q + G}{g} r_H^2(t) \right) \quad (12)$$

where:

G – weight of cargo carriage.

The drive drum's moment of inertia depends on the drum's weight with the wound rope and the distribution of mass in the drum (ADAMOVSKY et al. 1997, MALASHHENKO et al. 2013):

$$I_{B3}(t) = k_M \cdot [m_{B3} + l_T(t) \cdot q_K] \cdot r_H^2(t), \quad (13)$$

where:

k_M – coefficient of mass distribution in the drum ($k_M = 0,7$); m_B – mass of drive drum without a rope; $m_K(t)$, $l_T(t)$ – mass and length of wound rope.

The length of wound rope at the initial time moment is is determined by taking into account (7):

$$l_T(t) = \pi \cdot \frac{L_{B3}}{d_K} \cdot n_0 + \frac{\omega_{B3}(t) \cdot d_K \cdot t}{2\pi L_{B3}} \cdot \left[d_{B3} + C_y \cdot d_K \cdot \left(n_0 + \frac{\omega_{B3}(t) \cdot d_K \cdot t}{2\pi L_{B3}} - 1 \right) \right]. \quad (14)$$

Taking into account (13), (14) the expression (11), (12) can calculate a reduced moment of inertia $I_3(t)$.

Results and discussion

Since all the drum's elements are fixed at the time of motor's start-up, all the angles of rotation φ_i and angular velocity ω_i of reduced masses are equal to zero.

The value of the currents in the windings of the motor at the initial start-up time are equal to zero, and therefore the projection of these currents on the coordinate axes are also equal to zero. Thus, there are zero initial conditions at the initial time t_0 :

$$t_0 = 0, i_{Sx}(t_0) = 0, i_{Sy}(t_0) = 0, i_{Rx}(t_0) = 0, i_{Ry}(t_0) = 0, \varphi_1(t_0) = 0, \varphi_2(t_0) = 0, \varphi_3(t_0) = 0, \\ \omega_1(t_0) = 0, \omega_2(t_0) = 0, \omega_3(t_0) = 0.$$

The differential equations (1) and (3) with given initial conditions form a closed system that describes the dynamic state of the electromechanical drive. It is solved by Euler's numerical method with recalculation. At each step, common numerical integration of differential equations (1) and (3) determine the drive's variables:

- electromagnetic moment of the motor M_E ;
- reduced moment of the force resistance on the drive drum $M_S(t)$;
- increasing of the dynamic moment due to increasing the moment of inertia of the drum drive $\frac{d[I_3(t)]}{dt}$.

The solution of systems of differential equations (1) and (3) allows determining the parameters of the motion of drive's mechanical part such as rotating angles and angular velocities of reduced rotating masses. In addition to the motion parameters of the mechanical part, you can also define the electromagnetic moment and angular velocity of the motor's rotor. The time dependencies of reduced dynamic moments in the parts of drive's dynamic model can be build using determined motion parameters.

The reduced dynamic moments in the drive's coupling and mechanical transmissions are calculated as follows:

- the reduced dynamic moments in the drive's coupling:

$$M_{d1} = c_1[\varphi_1 - \varphi_2] + v_1[\omega_1 - \omega_2] \quad (15)$$

- the reduced dynamic moments in the drive's mechanical transmissions:

$$M_{d2} = c_2[\varphi_2 - \varphi_3] + v_1[\omega_2 - \omega_3] \quad (16)$$

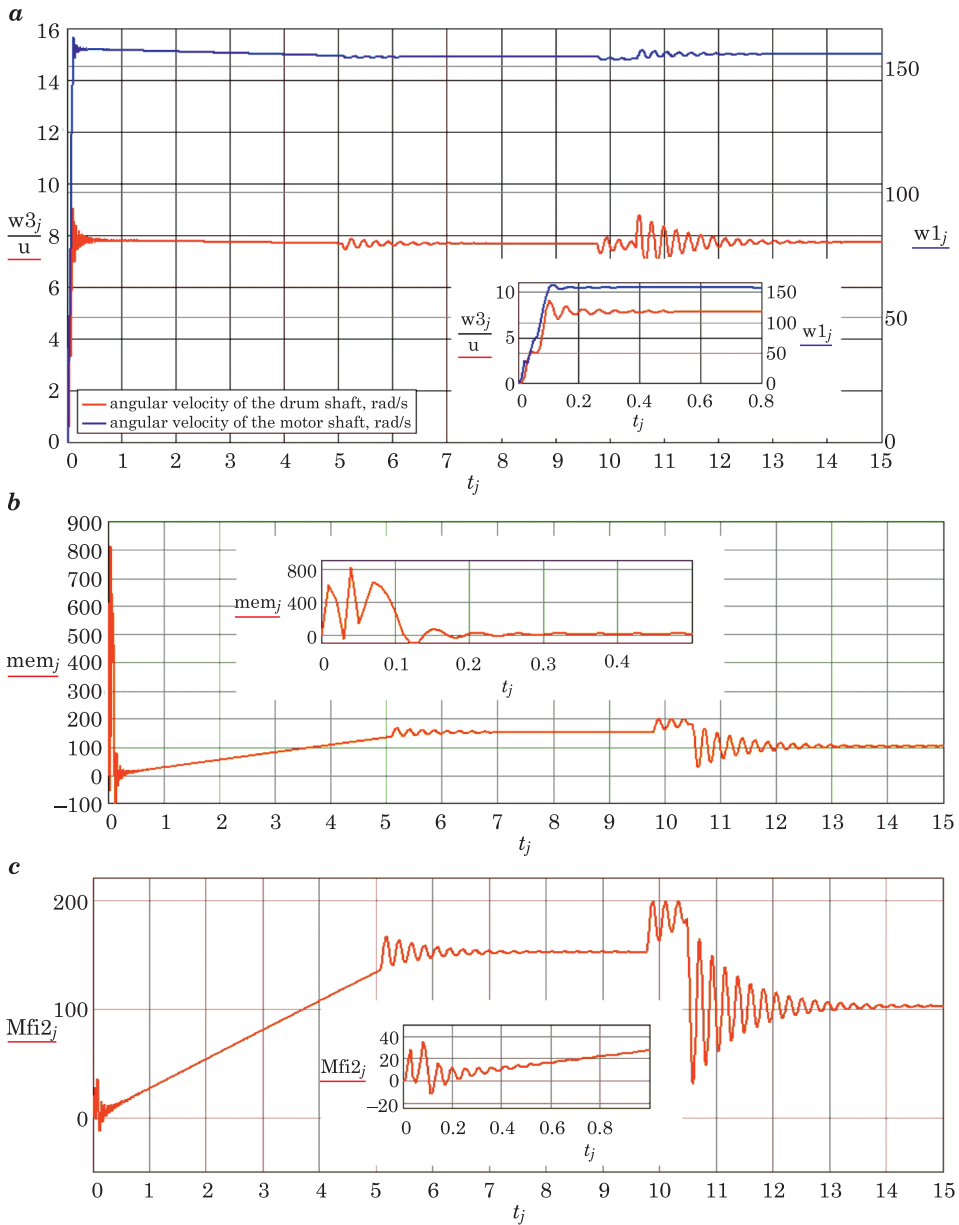


Fig. 3. The time dependence of the angular velocity drive's shaft (a) of the electric motor's moment (b) and reduced dynamic moment in drive's transmissions (c).

The example of calculating the angular velocity and dynamic moments in one-drum drive equipped with an electric motor and elastic coupling shown in Fig. 3-4 in graphs. The calculation is performed using the following inputs:

electric motor 4A180M4 ($R_S = 0,134 \text{ Ohm}$; $R_R = 0,117 \text{ Ohm}$; $L_S = 0,8 \cdot 10^{-3} \text{ H}$; $L_R = 0,82 \cdot 10^{-3} \text{ H}$; $L_m = 4,9 \cdot 10^{-2} \text{ H}$; $U_m = 310,5 \text{ W}$; $\alpha_1 = 4,714 \cdot 10^{-2} \text{ Wb/A}$; $\alpha^2 = -2,094 \cdot 10^{-5} \text{ Wb/A}^3$; $\alpha_3 = 6,003 \cdot 10^{-9} \text{ Wb/A}^5$; $i_{mk} = 15,0 \text{ A}$; $\omega_0 = 157 \text{ rad/s}$; $p_0 = 2$); $J_1 = 23,5 \text{ kg/m}^2$; $J_2 = 0,02 \text{ kg/m}^2$; $c_1 = 35 \cdot 10^3 \text{ N}^* \text{m/rad}$; $c_t = 40 \cdot 10^3 \text{ N}^* \text{m/rad}$; $\nu_1 = 15 \text{ N}^* \text{m}^* \text{s/rad}$; $\nu_2 = 2,96 \cdot 10^{-3} \text{ N}^* \text{m}^* \text{s/rad}$; $L = 400 \text{ m}$; $x_K(t) = 80 \text{ m}$; $Q = 16 \text{ kHz}$; $G = 240 \text{ N}$; $u = 20$; $H_G = 4 \text{ m}$; $m_{B3} = 30 \text{ kg}$; $L_{B3} = 0,6 \text{ m}$; $d_{B3} = 0,3 \text{ m}$; $d_K = 9,7 \cdot 10^{-3} \text{ m}$; $\beta = 30^\circ$.

The analysis of graphs has shown that acceleration of drive system is less than 0.2 s (Fig. 3a). The initial phase of acceleration accompanied by intense electromagnetic fluctuations of the electric motor (800) with a frequency of power line 50 Hz (Fig. 3b). This small acceleration time due to the lack of technological load at the time of start and a gradual linear increase of tension force of pull- hoisting rope at the initial of the technological cycle from zero to a value of . The amplitude and intensity fluctuations of reduced dynamic moment in transferring (Fig 3c) during start-up is much lower (up to 40N*m). Low values of amplitude and intensity fluctuations of dynamic moments in transmissions drive during acceleration is also due to the linear nature of the increasing process of load and reducing the influence of fluctuations of the electric motor to the transmission due to the elastic properties of the coupling.

During the separation of load bearing surface (5.5–6.5 second of work) and docking with the cargo load carriage (9.5 seconds of work) observed synchronous oscillation of angular velocities of the drive shaft of the electric motor and the drive drum (Fig. 3a). The amplitude of oscillation of the angular velocity of the motor shaft is higher than during start-up. The dynamic moment in the line of drive's transmissions (Fig. 3b) also reaches maximum values (up to 230) during the separation of load bearing surface and with locking the cargo freight carriage.

Therefore, the start-up and acceleration stage of transmissions drive are less dangerous compared to locking cargo and cargo separation from the bearing surface.

To evaluate the dynamic loads of the drive the coefficient of dynamics k_d is used:

$$k_d = \frac{M_{d \max}}{M_n} \quad (17)$$

where:

$M_{d \max}$ – maximum value of reduced dynamic moment in mechanical transmissions drive, calculated by the formula (16); M_n – elevated moment at the nominal load. The value of cargo is used as the nominal load. Reduced to the motor shaft moment from the nominal load is calculated as follows:

$$M_n = \frac{Q \cdot r_H'(t)}{u} \quad (18)$$

where:

$r_H'(t)$ – radius of the drive drum with wound rope at the time of action of maximum dynamic load in the transmissions drive.

The reduced coefficient of torsion stiffness is an important generalized indicator that considers both the geometric dimensions and mechanical characteristics of the material of the drive parts and kinematic characteristics (the gear ratio of drive mechanical transmission). Therefore, the limits for the selection of values of reduced torsion stiffness coefficient, when the dynamic load factor will be of the smallest values are substantiated in the article. The calculation of dynamic coefficient performed for different values of cargo weight and reduced torsion stiffness coefficients of drive's units (Fig. 4).

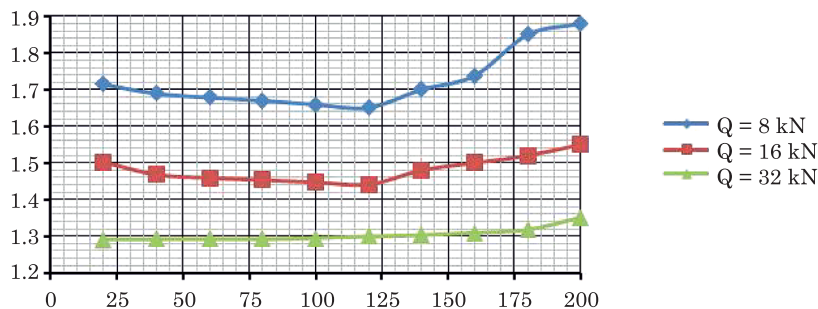


Fig. 4. Graphs of the dependence of dynamic coefficient on reduced coefficient of torsion stiffness transmissions of the one-drum drive of the timbertransporting rope system.

Conclusions

1. Studies have shown the most potentially dangerous operating modes of timbertransporting rope system are periods of separation of cargo's bearing surface and locking of cargo with cargo carriage. At higher values of cargo weight ($Q = 32..64$ kN) the more dangerous mode is a time of separation of cargo from bearing surface, and at lower values of cargo weight ($Q = 8..16$ kN) – the process of locking cargo with cargo carriage.

2. The dynamic load is minimal and close to a constant value in the range of reduced coefficients of the torsion stiffness of transmissions of 100 ... 125 N^*m/rad . Therefore, geometric and kinematic parameters of mechanical transmissions and shaft drive of timbertransporting rope systems are recommended to have its reduced torsional stiffness transmissions coefficient between indicated limits.

References

- ADAMOVSKY M., MARTYNTSIV M., BADERA J. 1997. *Suspended cable timbertransporting plants*, IZMN, Kyiv.
- BARYLIAK V. 2015. *Justification of the parameters of the drives of timber transporting rope systems*. Dissertation for the degree of the Candidate of engineering science (comparable to the academic degree of Ph.D.), Lviv.
- BELAYA N., PROHORENKO A. 1964. *Cable timbertransporting plants*, Forest Industry, Moscow.
- CZABAN A. 2007. *Mathematical modeling of processes oscillating electromechanical systems*, T. Soroki, Lviv.
- CZABAN A., LIS M. 2012. *Mathematical modelling of transient states in a drive system with a long elastic element*. *Electrical Review*. R. 88, nr 12b, (pp. 167–170), Sigma-Not, Warsaw.
- GOREV A.A. 1950. *The transient processes of synchronous machine*. Moscow.
- GOROKHOVSKI K., LIVSHITS N. 1991. *Machines and equipment for logging and forest storage works*. Ecology, Moscow.
- JOSWIG Fr. 2014. *The electro-mechanical coupling as the cause of torsional oscillations and their effects on shafting*. Dissertation for the academic degree Doctor of Engineering. Dortmund.
- KHARCHENKO YE., SOBKOWSKI S. 2005. *Mathematical modelling of transients in drives of building elevating devices*, *Diagnostyka*. Quarterly published by the Polish Society of Technical Diagnostics. Vol. 35, (pp. 37–42), Warsaw.
- KORZHOV V., CUDRA V. 2010. *Constructive-technological features of mobile cable timbertransporting plants of built up type*. *Industrial hydraulics and automation*. Vol. 3.29, (pp. 18–20). Lviv.
- MALASHHENKO V., MARTYNCIV M., BARYLIAK V. 2013. *Research of work of cable timber transporting plants drives with regard multilayer winding rope*. *Lifting and conveying equipment*. 2, (pp. 29–38), Dnipropetrovsk.
- PARK R.H. 1929. *Two-reaction theory of synchronous machines generalized method of analysis-part I*. *Transactions of the American Institute of Electrical Engineers*. Vol. 48, (pp. 716–727), (republished NAPS, University of Waterloo, Canada. 2000), Waterloo.
- PARK R.H. 1933. *Two-reaction theory of synchronous machines -part II*. *Transactions of the American Institute of Electrical Engineers*. Vol. 52, (pp. 352–354).
- ZANEHYN L., VOSKOBONIKOV I., YEREMEEV N. 2004. *Machines and Mechanisms for cable logging*. MHUL, Moscow.



STRUCTURE STUDIES OF POROUS OXIDE LAYERS FORMED ON 13CrMo4-5 STEELS LONG-TERM OPERATED IN THE POWER INDUSTRY

Monika Gwoździk

Faculty of Production Engineering and Materials Technology,
Institute of Materials Engineering
Czestochowa University of Technology

Received 1 June 2016; accepted 6 September 2016; available online 27 September 2016

Key words: 13CrMo4-5 steel, oxide layer, porosity.

Abstract

The paper contains results of studies on the formation of oxide layers on 13CrMo4-5 steel long-term operated at an elevated temperature. The material studied comprised specimens of 13CrMo4-5 steel operated at the temperature of 455°C during 130,000 hours (steel 1) and 540°C during 120,000 hours (steel 2). The oxide layer was studied on a surface and a cross-section at the outer surface of the tube wall. The paper contains results of studies of porosity in the oxide layer. The oxide layer formed on the studied steel 1 is ~146 μm thick, while on the steel 2 ~248 μm. It has been found that steel 2 has higher porosity.

Introduction

At present the huge development in materials engineering has taken place, especially in surface engineering (JAGIELSKA-WIADEREK 2012, KULESZA and BRAMOWICZ 2014, LABISZ 2014, PRISS et al. 2014, SZAFARSKA and IWASZKO 2012). In the previous years a lot of articles were devoted to the topic of steel oxidation (BISCHOFF et al. 2013, CHABIČOVSKÝ et al. 2015, FRANGINI et al. 2014, GRUBER et al. 2015), especially the steel used in power industry. The subject area is connected with oxidation and steel corrosion used in power industry.

This topic is widely discussed by a lot of scientific centers in our country and in the world. The research is carried out i.e. on steel such as: 13CrMo4-5, 10CrMo9-10, 16Mo3 and X10CrMoVNb9-1 (ABANG et al. 2011, BANKIEWICZ et al. 2013, GRUBER et al. 2015, GWOŹDZIK 2015, PRISS et al. 2014). The problem of this corrosion, so-called high temperature corrosion is still up to date, i.e. because of modernization and prolonging operation time of existing energetic units. The growth of the oxide layer is accompanied by the growth of numerous defects such as: pores, fissures, flaking. Abang and others in paper (ABANG et al. 2011) conducted the examination i.e. connected with steel oxidation: 16Mo3, 13CrMo4-5 and 10CrMo9-10 during 1100 hours. The researchers showed that dominating oxides are hematite (Fe_2O_3) and magnetite (Fe_3O_4) for these three steels. The researches showed that the created oxide layer is characterized by porosity for these three steels. However, depending on oxidation conditions (air or oxyfuel) and also from oxidation side, porosity is less or more intensified.

Chemical compounds in the flue gas have a strong influence on the formed oxide layers. The service life of components operating in the power industry is highly affected by aggressive components of the flue gases and ashes. Such components cause corrosion of external surfaces of tubes and their corrosion damage. Under normal conditions oxide layers form on the steel surface at the presence of oxygen, making a natural passive layer of steel and a barrier to other gaseous components of the flue gas. However, the situation changes drastically under conditions of oxygen deficiency and at the moment of accumulation of thick deposit layers on the tube surface. This happens because physicochemical parameters under the deposits substantially differ from those existing in the flowing flue gas stream and then – depending on the chemical composition of the formed deposits and on their morphology – to a varying extent they can aggressively influence the steel and protective layers. The high-temperature corrosion threat may be higher or smaller, depending on the fuel type. Acc. to authors (GAWRON and KLEPACKI 2012) the high-temperature corrosion threat to boiler heatable surfaces increases under conditions of low-emission combustion with a share of alternative fuels.

The aim of the paper was conducting the examination connected with the structure studies of porous oxide layers created on 13CrMo4-5 steel operated in different temperature-time conditions.

Material and Experimental Methods

The material studied comprised specimens of 13CrMo4-5 (15HM) steels long-term operated at an elevated temperature:

- steel 1, $T = 455^{\circ}\text{C}$, $t = 130,000$ h,
- steel 2, $T = 540^{\circ}\text{C}$, $t = 120,000$ h.

The oxide layer was studied on a surface and a cross-section at the outer surface of the tube wall (Fig. 1).

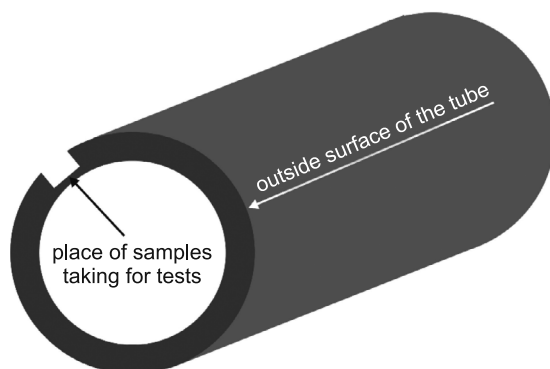


Fig. 1. Place of samples taking for tests

Thorough examinations of the oxide layer carried out on the outer surface wall of tube wall comprised:

- the analysis of steel chemical composition was carried out using spark emission spectroscopy on a Spectro spectrometer (Table 1),
- macroscopic and microscopic examinations of the oxide layer were performed using an Olympus SZ61, GX41 optical microscope and Jeol JSM-6610LV scanning electron microscope (SEM),
- thickness measurements of formed oxide layers,
- chemical composition analysis of deposits/oxides using a Jeol JSM-6610LV scanning electron microscope (SEM) working with an Oxford EDS electron microprobe X-ray analyser,
- X-ray (XRD) measurements; the layer was subject to measurements using a Seifert 3003T/T X-ray diffractometer and the radiation originating from a tube with a cobalt anode ($\lambda_{\text{Co}} = 0.17902$ nm). A computer software and the DHN PDS, PDF4+2009 crystallographic database were used for the phase identification.

Table 1

Chemical composition of examined steel, wt %

Acc.	Chemical composition, wt %						
	C	Si	Mn	P	S	Cr	Mo
Analysis (steel 1)	0.16	0.30	0.57	0.019	0.009	0.90	0.54
Analysis (steel 2)	0.09	0.31	0.47	0.014	0.007	0.91	0.52
PN-EN 10028-2	0.08-0.18	max.0.35	0.40-1.00	max.0.025	max.0.010	0.70-1.15	0.40-0.60

Results of examinations

Steels 1 and 2 have the same structure, which is ferrite, perlite and bainite (Fig. 2). For steel 1 it was observed that the size of the grain is diversified and the elements of the structure are unequally placed. In addition, in this steel there are sporadic sulphide precipitates which occur both inside and on the grain boundaries (Fig. 2a). The structure of steel 2 is characterized by a large amount of carbide precipitates both inside and on the grain boundaries. The carbides which occur on the grain boundaries create so-called “chains” (Fig. 2b).

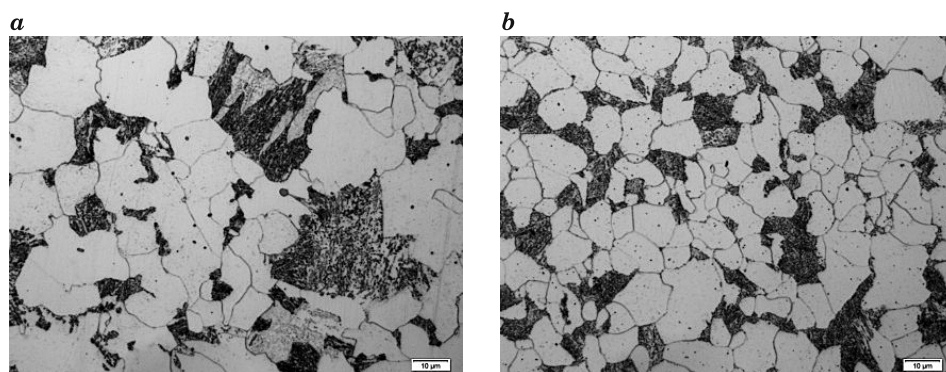


Fig. 2. Microstructure of 13CrMo4-5 steel, LM, 1000x: *a* – steel 1, *b* – steel 2

The macroscopic observation of the examined surfaces (Fig. 3) showed that in both cases the significant development level of the surfaces and the outer layer damages occur.

Observations of the oxide layer surface by means of scanning electron microscopy have shown that in the case of steel 1 there are oxide areas without damage, presented in Fig. 4a. In turn, Fig. 4b presents a damaged oxide layer from the same steel. Damaged areas of the layer, which are crystalline in nature, are visible. Figs. 4c and d present the oxide surface formed on steel 2. A significant surface development may be observed on this steel. Also deposits exist, apart from the oxide layer, confirmed by the EDS analysis (Fig. 5).

Performed XRD measurements (Fig. 6) have shown that in both cases (steel 1 and 2) the oxide layer is built of hematite (Fe_2O_3) and magnetite (Fe_3O_4). Moreover, the EDS analysis in both cases have shown the existence of Si and additionally – for steel 2 – of Al. These elements form such compounds as SiO_2 and Al_2O_3 , which are components of hard coal ashes.

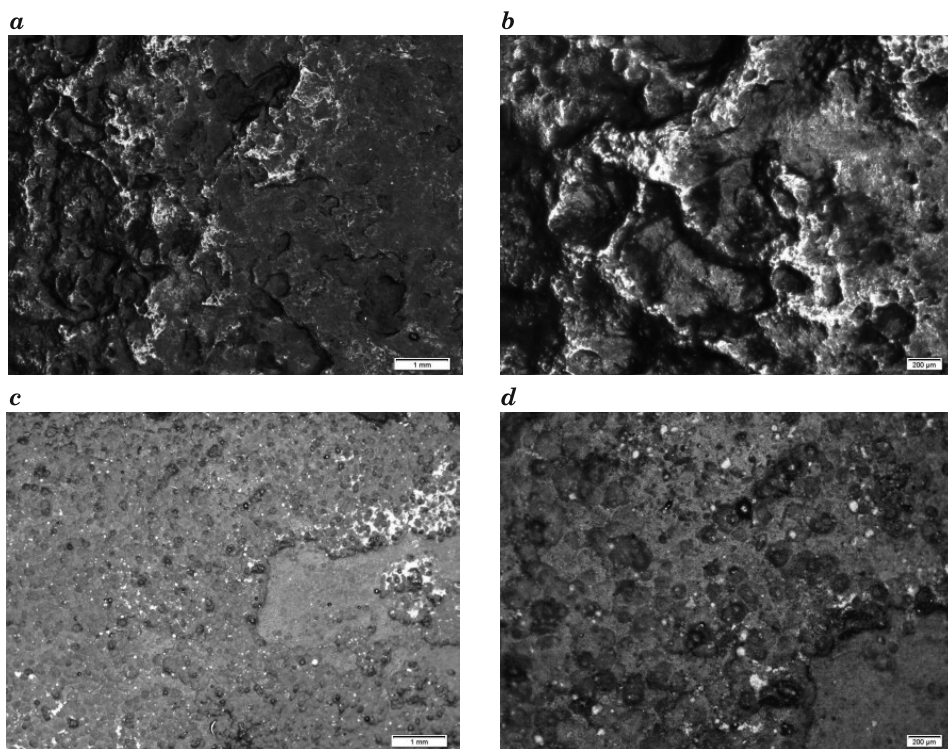


Fig. 3. Oxides formed on 13CrMo4-5 steel, outer surface, LM: *a* – steel 1, 15x, *b* – steel 1, 45x, *c* – steel 2, 15x, *d* – steel 2, 45x

Observations of metallographic microsections made on a cross-section have shown that for steel 1 the oxide layer was $\sim 146 \mu\text{m}$ thick (Fig. 7a), while for steel 2 it was $100 \mu\text{m}$ thicker and was $\sim 248 \mu\text{m}$ (Fig. 7b).

In the case of steel 1 (Fig. 8) the amount of defects in the formed layer is much smaller than for steel 2 (Fig. 9). The oxide layer formed on steel 1 shows local damage in the form of numerous cracks, which locally create a network on the entire layer cross-section (Fig. 8a, b). Large fissures originate in places and fine porosity exists locally. In turn steel 2 features a great degradation (Fig. 9). In some places the oxide layer is entirely separated from the substrate, which is shown in Fig. 9a. Also huge fissures occur, reaching the depth of $70 \mu\text{m}$ (Fig. 9b). The oxide layer on steel 2 is mostly torn off and cracked (Fig. 9c). In addition, in steel 2 directly on the steel side there is major corrosion along grain boundaries, reaching the depth of $15 \mu\text{m}$ (Fig. 10). Abang and others in paper (ABANG et al. 2011) showed that, under both operating conditions the surface layer was characterised by loosely attached formations of ash that were partially flaked. The outer layer of corrosion was covered with many tiny pores. Apart from the tiny pores under oxyfuel conditions, the inner layer of corrosion also had a few large pores.

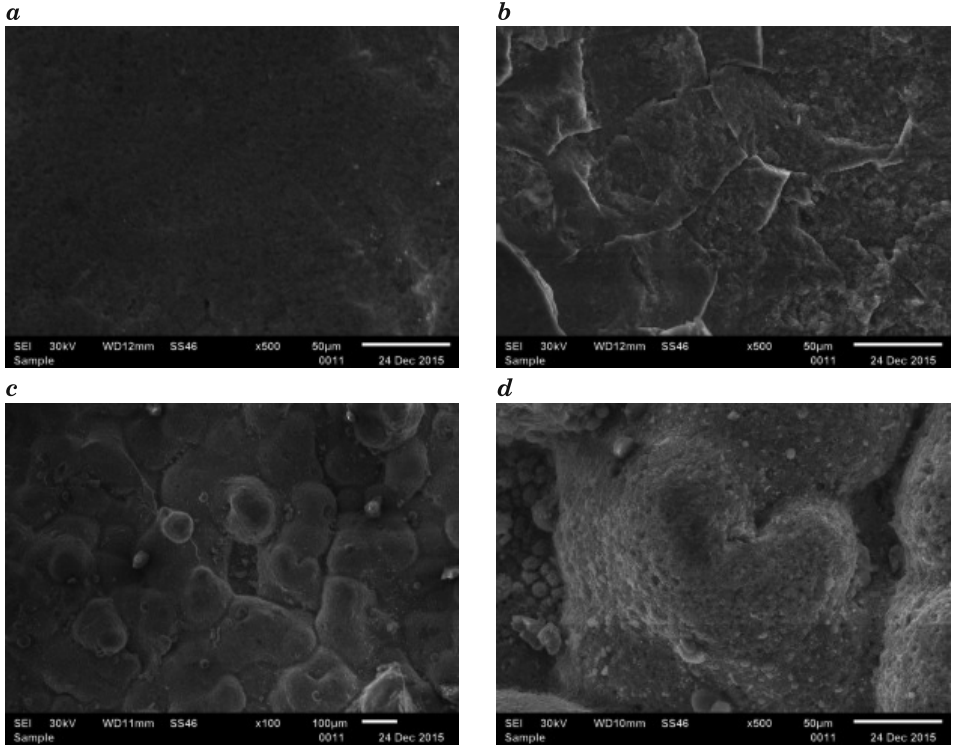


Fig. 4. Oxides formed on 13CrMo4-5 steel, outer surface, SEM: *a, b* – steel 1, 500x, *c* – steel 2, 100x, *d* – steel 2, 500x

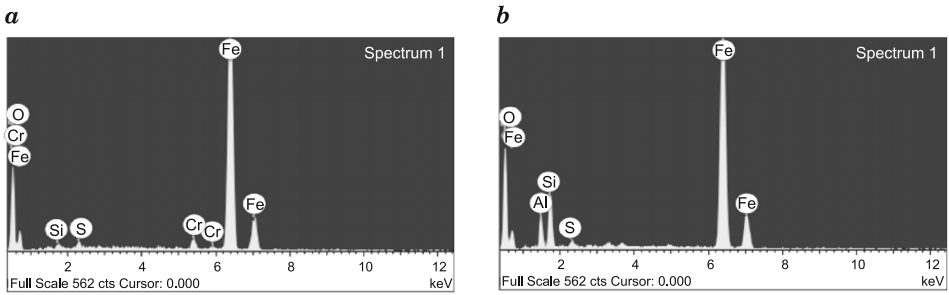


Fig. 5. SEM / EDS: *a* – steel 1, *b* – steel 2

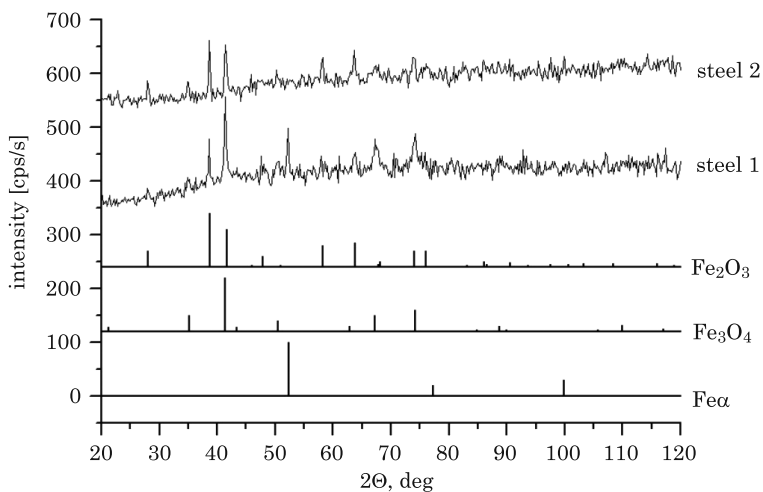


Fig. 6. X-ray diffraction patterns from the oxides layer obtained by means of XRD technique

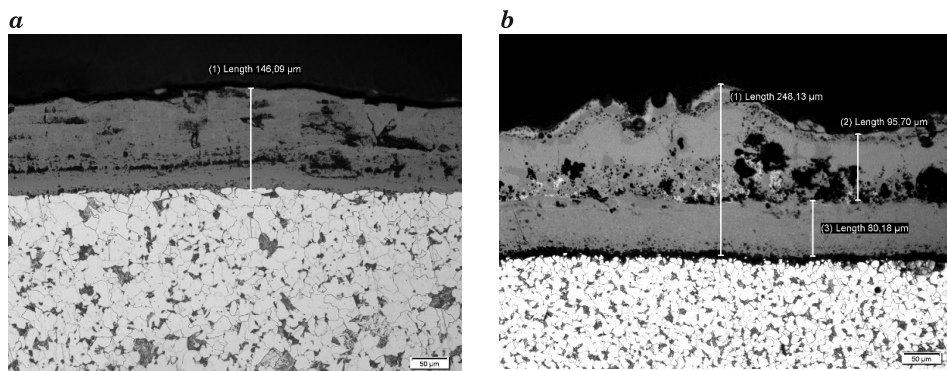


Fig. 7. The thickness of oxide layer formed on the steel examined, LM, 200x: *a* – steel 1, *b* – steel 2

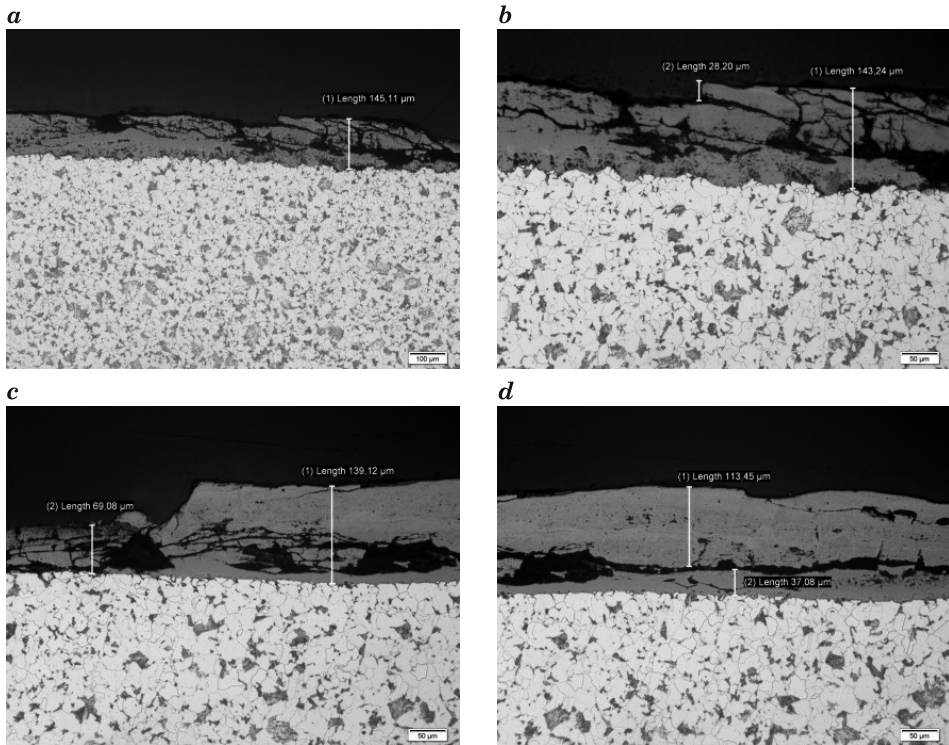


Fig. 8. Defects of oxides layer existing on steel 1

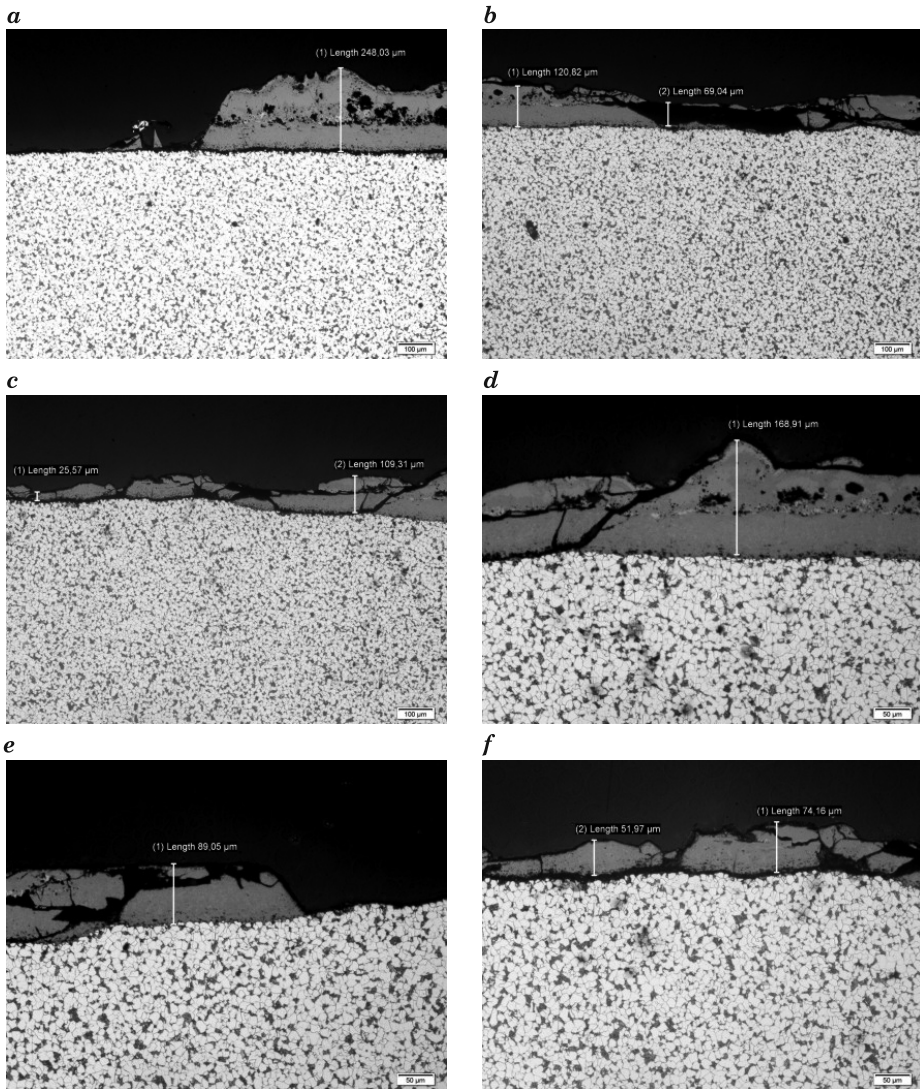


Fig. 9. Defects of oxides layer existing on steel 2

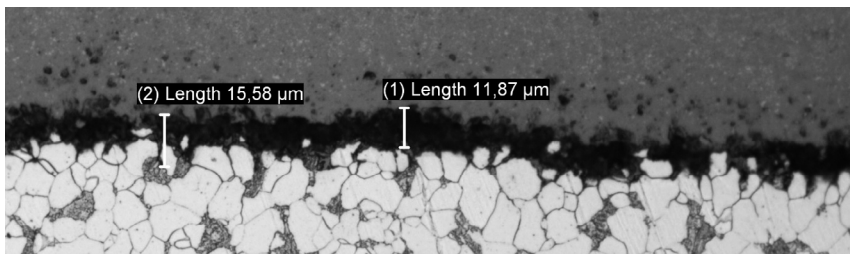


Fig. 10. Corrosion on the grain boundaries at the outside surface, 500x

Summary

The obtained results of studies have shown that porosity exists in the oxide layer formed on both steels. When observing a continuous oxide layer (without spalling) it is possible to notice that the porosity is situated mainly on the flue gas inflow side. Much larger pores were observed for steel 2 than for steel 1, which is visible in Fig. 7. Instead, photographs of areas covered by major degradation show numerous cracks and spalling cases of the oxide layer, resulting from such defects of the structure as numerous pores, which then transform into fissures. Areas of spalling covering in places the entire cross-section of the oxide layer thickness were observed for steel 2. The results of studies for steel 13CrMo4-5 have shown that during a component operation at a higher temperature the oxide layer is degraded to a greater degree.

References

- ABANG R., FINDEISEN A., KRAUTZ H.J. 2011. *Corrosion behaviour of selected power plant materials under oxyfuel combustion conditions*. *Górnictwo i Geoinżynieria*, 35(3/1): 23–42.
- BANKIEWICZ D., YRJAS P., LINDBERG D., HUPA M. 2013. *Determination of the corrosivity of Pb-containing salt mixtures*. *Corrosion Science*, 66: 225–232.
- BISCHOFF J., MOTTA A.T., EICHFELD C., COMSTOCK R.J., CAO G., ALLEN T.R. 2013. *Corrosion of ferritic-martensitic steels in steam and supercritical water*. *Journal of Nuclear Materials*, 441: 604–611.
- CHABIČOVSKÝ M., HNÍZDIL M., TSENG A.A., RAUDENSKÝ M. 2015. *Effects of oxide layer on Leidenfrost temperature during spray cooling of steel at high temperatures*. *International Journal of Heat and Mass Transfer*, 88: 236–246.
- EN 10028-2:2009: *Flat products made of steels for pressure purposes – Part 2: Non-alloy and alloy steels with specified elevated temperature properties*.
- FRANGINI S., MASCI A., MCPHAIL S.J., SOCCIO T., ZAZA F. 2014. *Degradation behavior of a commercial 13Cr ferritic stainless steel (SS405) exposed to an ambient air atmosphere for IT-SOFC interconnect applications*. *Materials Chemistry and Physics*, 144: 491–497.
- GAWRON P., KLEPACKI F. 2012. *Trwałość wybranych elementów kotłów w warunkach współspalania biomasy*. *Energetyka*, 6(696): 293–303.
- GRUBER T., SCHARLER R., OBERNBERGER I. 2015. *Application of an empirical model in CFD simulations to predict the local high temperature corrosion potential in biomass fired boilers*. *Biomass and Bioenergy*, 79: 145–154.
- GWOŹDZIK M. 2015. *Characterization of Oxide Layers Formed on 13CrMo4-5 Steel Operated for a Long Time at an Elevated Temperature*. *Archives of Metallurgy and Materials*, 60(3A): 1783–1788.
- JAGIELSKA-WIADEREK K. 2012. *Depth-profiles of corrosion properties of carbonitrided AISI 405 steel*. *Archives of Metallurgy and Materials*, 57(2): 637–642.
- KULESZA S., BRAMOWICZ M. 2014. *A comparative study of correlation methods for determination of fractal parameters in surface characterization*. *Applied Surface Science*, 293: 196–201.
- LABISZ K. 2014. *Microstructure and mechanical properties of high power diode laser (HPDL) treated cast aluminium alloys*. *Mat.-wiss. U. Werkstofftech*, 45(4): 314–324.
- PRISS J., ROJACZ H., KLEVTSOV I., DEDOV A., WINKELMANN H., BADISCH E. 2014. *High temperature corrosion of boiler steels in hydrochloric atmosphere under oil shale ashes*. *Corrosion Science*, 82: 36–44.
- SZAFARSKA M., IWASZKO J. 2012. *Laser remelting treatment of plasma-sprayed Cr₂O₃ oxide coatings*. *Archives of Metallurgy and Materials*, 57(1): 215–221.



MODELLING OF THE HYDRODYNAMICS OF CONCURRENT GAS AND LIQUID FLOW THROUGH PACKED BED

Daniel Janecki¹, Grażyna Bartelmus², Andrzej Burghardt²

¹ Department of Process Engineering
University of Opole

² Institute of Chemical Engineering, Polish Academy of Sciences

Received 7 June 2016; accepted 20 October 2016; available online 21 October 2016

Key words: trickle-bed reactors, CFD, hydrodynamics, packed bed

Abstract

The aim of the present study is to simulate concurrent gas and liquid flow through packed bed in the gas continuous flow regime (GCF) and continuity shock waves regime (CSW) using computational fluid dynamics (CFD). The application of multiple gas-liquid-solid model requires the knowledge of relationships determining interactions between phases. The exchange coefficients of these forces were defined by means of equations suggested by ATTOU et al. (1999). As a result of the computational simulation the following data were obtained: gas pressure drop in the bed, volume fraction distribution of a given phase (liquid and gas holdups) along the packing and its mean value in the reactor. The comparison of the values of the hydrodynamic parameters, both calculated and obtained experimentally in a column packed with 3 mm glass spheres, indicates that CFD model can be applied to model the hydrodynamics of concurrent gas and liquid flows through a packed bed because a good compatibility of the compared parameters was obtained.

Symbols

$d_{\min} = \left(\frac{\sqrt{3}}{\pi} - \frac{1}{2} \right) d_p$ – minimum equivalent diameter of the area [m]

d_p – particle diameter [m]

E_1, E_2 – Ergun constants

f – wetting efficiency of the bed

F_{jk} – momentum exchange coefficients between phases j and k [$\text{kgm}^{-3}\text{s}^{-1}$]

g – acceleration due to gravity [ms^{-2}]

J_0 – zero th order Bessel function

K_k – drag between phases j and k [Nm^{-3}]

Correspondence: Daniel Janecki, Samodzielna Katedra Inżynierii Procesowej, Uniwersytet Opolski, ul. Dmowskiego 7-9, 45-365 Opole, phone: 48 77 401 67 00, e-mail: zecjan@uni.opole.pl

P	– pressure [Pa]
r	– radial coordinate [m]
R	– radius of column [m]
t	– time [s]
\bar{u}	– interstitial velocity [ms^{-1}]
w	– superficial velocity [ms^{-1}]

Greek letters

α	– volume fraction
ε	– porosity of the bed
e_L	– liquid holdup
η	– dynamic viscosity [Pas]
ρ	– density [kg m^{-3}]
σ	– surface tension [Nm^{-1}]
τ	– stress tensor [Nm^{-2}]

Subscripts

av	– denotes average
b	– denotes base
c	– denotes capillary
d	– denotes dynamic
g	– denotes gas phase
ip	– denotes impulse
j	– denotes phase other than k
k	– denotes k^{th} phase
L	– denotes liquid phase
S	– denotes solid phase
α	– L, g

Introduction

Three-phase reactors in which the liquid and gas phases flow down a fixed catalytic bed are termed trickle-bed reactors (TBR). This type of reactor is employed on an industrial scale in the processes of selective hydrogenation of various petroleum fractions, as well as in the oxidation of organic pollutants in waste waters and flue gases via reactions occurring over a bed of immobilized bacteria. Depending on the flow rates of the two phases, their physicochemical properties and geometry and size of the packing, various flow patterns can be observed of which two are of considerable industrial importance: the gas – continuous flow regime (GCF) and the pulsing flow regime (PF). The pulsing flow regime is especially attractive in the processes of mass and heat transfer as the experimental values of the transfer coefficients are by far larger than those in the GCF regime; moreover, perfect wetting of the packing is observed. However, carrying out the processes in the PF regime requires supplying the reactor with large streams of gas and liquid which results in a very short residence times of reagents in a bed and this, in turn, has an unfavourable influence on their conversion. Taking the above into consider-

ation, the idea of carrying out processes in TBRs at periodically changing feeding the bed with liquid was created (BELHOUWER et al. (1999)). Unsteady state (periodic) operations can be realized either by means of temporary stopping the stream of liquid (ON-OFF method) or by periodic change in the liquid velocity between low, but not equal zero, and high value of this parameter (BASE-IMPULSE method). Taking into account the liquid velocity in an impulse, the process can be carried out as continuity shock wave flow (CSW) or liquid induced pulsing flow (LIPF).

Periodic operations can be also grouped with respect to the criterion of duration of particular liquid cycles. Thus the processes can be carried out by means of slow or fast changing cycles of liquid modulation (SLOW MODE or FAST MODE).

In the present study, the subject of analysis is the hydrodynamics of TBR operating at GCF and CSW regimes. The key hydrodynamic parameters are pressure drop and liquid holdup. These parameters are inseparable connected and occur simultaneously in balance equations of both fluids. In the literature, a large number of papers can be found, that present, for various experimental systems, the results of experiments in which mentioned above parameters have been determined (CLEMENTS and SCHMIDT (1980), ELLMAN et al. (1990), LARACHI et al. (1991), MIDOUX et al. (1976), RAO et al. (1983), RAO and DRINKENBURG (1983), SAI and VARMA (1987), SPECCHIA and BALDI (1977), WAMMES i wsp. (1991)). The analysis of correlation equations which were developed on the basis of experimental data showed considerable differences between calculated values. Therefore, it was necessary to formulate a mathematical model describing the hydrodynamics of TBRs. A few one-dimensional models describing concurrent gas and liquid flow through packed bed of TBR operating in GCF regime can be found in literature. They are both phenomenological microscopic models (single canals in packing are taking into account) (AL-DAHAN et al. (1998), HOLUB et al. (1992, 1993), ILIUTA and LARACHI (1999), ILIUTA et al. (2000)) and macroscopic models by SAEZ and CARBONELL (1985), GROSSER et al. (1988) or ATTOU et al. (1999), based on volume averaged balances of mass and momentum of both phases flowing concurrently through packing. Unfortunately, in the empirical equations and models uniform porosity and velocity of fluids in the bed has been assumed and the phenomena concerning complex flow, mixing and wetting of the bed are usually expressed jointly by some empirical parameters. Therefore, recently fast development of the Computational Fluid Dynamic (CFD) model, which is a quantitative formulation of the momentum balance (Navier-Stokes equations) caused a more frequent application of the CFD to simulate the dynamic phenomena in the TBR. The application of the CFD method to simulate the operation of trickle-bed reactors is much more difficult than to simulate the

processes in two-phase systems (KHAN et al. (2014), KEIR and JEGATHEESAN (2014), KUIPERS and VAN SWAAIJ (1997), SAJJADI et al. (2012), SHAIKH and AL-DAHMAN (2013), WANG et al. (2007), WANG et al. (2010)) which, among others, is due to difficulties connected with a proper description of the structure of the bed of solid particles, interaction forces between the flowing phases and the wetting efficiency of the surface of the packing (JAWORSKI (2005), JIANG et al. (2001), WANG et al. (2013)).

The aim of the present study was the simulation of concurrent flow of gas and liquid through a packed bed in GCF and CSW regimes using the CFD model. The simulations were carried out using commercial FLUENT 6.1.22 software. As the pressure gradient and average holdup are two main hydrodynamic parameters, these quantities have been chosen for comparison. The mean relative error and standard deviation of experimental and computed values of the parameters mentioned above were used as the validation criteria of the model.

Mathematical model

The Eulerian multi-fluid model was used to simulate the fluid flow through the bed of solid particles. The model treats each phase as continuous fluid having various velocities, volume fractions and physicochemical properties. The volume averaged equations of mass and momentum balances expressed by means of volume fractions occupied by each phase and their local velocities can be written as:

$$\frac{\partial}{\partial t}(\alpha_k \rho_k) + \nabla \cdot (\alpha_k \rho_k \vec{u}_k) = 0; \quad k = L, g \quad (1)$$

$$\frac{\partial}{\partial t}(\alpha_k \rho_k \vec{u}_k) + \nabla \cdot (\alpha_k \rho_k \vec{u}_k \vec{u}_k) = -\alpha_k \nabla P + \nabla \cdot \bar{\bar{\tau}}_k + \alpha_k \rho_k \vec{g}_k + \vec{K}_k; \quad k = L, g \quad (2)$$

where the viscous stress tensor is expressed by the dependency:

$$\bar{\bar{\tau}}_k = \alpha_k \eta_k (\nabla \vec{u} + \nabla \vec{u}^T) \quad (3)$$

The effect of pre-wetting of packing was also taken into consideration in the model. JIANG et al. (2002a) introduced the empirical coefficient f , characterizing the wetting efficiency of the bed, into the capillary pressure relation:

$$P_g - P_L = (1 - f)P_c \quad (4)$$

For pre-wetted bed f is set equal to one implying a zero capillary pressure and for non-wetted bed f is set to zero. Capillary pressure was described by means a function suggested in the work of ATTOU and FERSCHNEIDER (2000):

$$P_g - P_L = 2\sigma \left(\frac{\alpha_s}{1 - \alpha_g} \right)^{0.333} \left(\frac{1}{d_p} + \frac{1}{d_{\min}} \right) \left(1 + 8.1 \frac{\rho_g}{\rho_L} \right) \quad (5)$$

Capillary pressure gradient, described by relationship (5), should be introduced into the balance equation of the liquid phase in case of an incomplete wetting of the bed by means of the User Defined Function (UDF).

The application of the multiple gas-liquid-solid model requires a knowledge of relationships determining the interactions between phases. It is very significant element of uncertainty in the modelling of the processes in TBR. These forces are considerable and dominate in the momentum balance equations. The last term of this equation (2), \vec{K}_k , represents interaction forces between phases in the form of:

$$\vec{K}_k = \sum_{j=1}^n F_{jk} (\vec{u}_j - \vec{u}_k) \quad (6)$$

Since $u_s = 0$ and $F_{jk} = F_{kj}$ (FLUENT (2006)), then the above relationship is reduced to the form of:

– for the gas phase:

$$\vec{K}_g = -F_{gL}(\vec{u}_g - \vec{u}_L) - F_{gS}\vec{u}_g \quad (7)$$

– for the liquid phase:

$$\vec{K}_L = F_{gL}(\vec{u}_g - \vec{u}_L) - F_{LS}\vec{u}_L \quad (8)$$

The coefficients of momentum exchange between phases (F_{jk}) occurring in these equations were analysed in the work by JANECKI et al. (2016). They can be derived from one-dimensional models (slit model of HOLUB et al. (1992), permeability model of SAEZ and CARBONELL (1985)) as well as from two-phase model of interphase actions of ATTOU et al. (1999). The first two models neglect interaction forces between the gas and liquid phases due to their decay in the GCF regime (SOUADNIA et al. (2005)). However, experimental research (AL-DAHMAN and DUDUKOVIC (1994), AL-DAHMAN et al. (1997), LARACHI et al. (1991a)) shows that gas flow has a significant influence on the hydrodynamics of TBRs, especially at elevated pressure. The exchange coefficients F_{jk} descri-

bing interactions between phases in a three-phase system (gas-liquid-solid) can be derived only from the ATTOU et al. (1999) model. They have the form similar to the Ergun relations:

– for gas-liquid momentum exchange coefficient:

$$F_{gL} = A_g \left(\frac{\alpha_S}{1 - \alpha_g} \right)^{2/3} + B_g \left(\frac{\alpha_S}{1 - \alpha_g} \right)^{1/3} |u_g - u_L| \quad (9)$$

– for gas-solid momentum exchange coefficient :

$$F_{gS} = A_g \left(\frac{\alpha_S}{1 - \alpha_g} \right)^{2/3} + B_g \left(\frac{\alpha_S}{1 - \alpha_g} \right)^{1/3} |u_g| \quad (10)$$

– for liquid-solid momentum exchange coefficient:

$$F_{LS} = (1 - \alpha_S)(A_L + B_L|u_L|) \quad (11)$$

Coefficients A_g , A_L , B_g i B_L present in the above equations are expressed by the following formulas:

$$A_g = E_1 \mu_g \frac{(1 - \alpha_g)^2}{\alpha_g d_p^2} \quad (12)$$

$$B_g = E_2 \rho_g \frac{1 - \alpha_g}{d_p} \quad (13)$$

$$A_L = E_1 \mu_L \frac{\alpha_S^2}{\alpha_L d_p} \quad (14)$$

$$B_L = E_2 \rho_L \frac{\alpha_S}{\alpha_L d_p} \quad (15)$$

In the presented relationships there are parameters which determine the values of interaction forces. They are Ergun's constants (E_1 and E_2). Since by changing the values of E_1 and E_2 one can control the values the interaction forces, doubts keep appearing which values of Ergun's constants to use in the calculations. The values determined experimentally or suggested by

MACDONALD et al. (1979) ($E_1= 180$; $E_2= 1.8$) are most commonly applied in literature.

Description of the fixed bed structure in trickle-bed reactors

Numerous experiments showed (BENENATI and BROSILOW (1962), GOODLING et al. (1983), MUELLER (1992)) that randomly packed beds exhibit greater porosity in the vicinity of the column wall (in the region equaling to the width of 4–6 diameters of solid particles). In this region porosity exhibit strong fluctuations which are attenuated at greater distances from the wall. It makes the radial profile of bed porosity at the wall undergo strong changes which may significantly influence mean liquid holdup and gas pressure drop in the bed, especially in a reactor whose ratio of the column diameter to the particle diameter is low (laboratory reactors). Porosity values in the core of the bed show significantly lower differences and reach values close to the mean values of the parameter.

A proper description of a bed structure in a reactor should include the following elements (GUNJAL et al. (2005), JIANG et al. (2002a), LI et al. (2006)):

- the overall mean porosity,
- the axial porosity profile,
- the axially averaged radial porosity profile.

In literature one can find various correlation equations describing porosity distribution along the radius of the apparatus. Those that can be applied to model TBR were set in works by WANG et al. (2013) and VAN ANTWERPEN et al. (2010). These relationships can be divided into two groups. The first one is represented by the oscillatory correlations (MARTIN (1978), COHEN and METZNER (1981), MUELLER (1992), BEY and EINGENBERGER (1997), DE KLERK (2003)) and the other one is represented by the exponential correlations (VORTMEYER and SHUSTER (1983), HUNT and TIEN (1990) and SUN et al. (2000)). The chosen relationships describing the radial porosity profiles were analysed in detail in the work by JANECKI et al. (2014).

Experimental set-up and procedure

The experiments, being the comparative base for computational simulations, were carried out in an installation which main part was cylindrical column of 0.057 m I.D. packed with 3 mm glass spheres ($\epsilon = 0.38$, $a = 1240 \text{ m}^{-1}$) to a height of 1.35 m. The column operated at concurrent down-flow of gas (nitrogen) and liquid phases. In order to investigate the influence of the

physicochemical properties of the liquid phase on the experimental results water, two aqueous solutions of glycerol (with the viscosity of $2.5 \cdot 10^{-3}$ and $3 \cdot 10^{-3}$ Pas) and methanol solution with viscosity of $1.64 \cdot 10^{-3}$ Pas and surface tension $45.8 \cdot 10^{-3}$ Nm⁻¹ have been used.

The experiments were carried out at constant temperature and pressure (30°C, $\sim 10^5$ Pa) for a wide range of flow rates of both phases (fully in GCF and CSW regimes). The operation of the system both in GCF and CSW regimes was discussed in detail elsewhere (BARTELMUS and JANECKI (2003), BARTELMUS et al. (2006)).

The electrochemical method was used to measure the liquid hold-up. The basic value determined during the experiments were the variations in conductivity of the two-phase gas-liquid mixture flowing through the void volume of the bed. The conductance cells placed in the bed were used to measure the conductivity of the solution; the changes in conductivity reflect the changes in the amount of gas and liquid in the mixture. Detailed description of the experimental procedure was presented elsewhere (BARTELMUS, JANECKI (2003)).

Gas pressure drop in the packing was measured by means of piezoelectric gauges (Cole-Palmer); the pressure signal, converted into electric signal, was fed into computer memory. The values of pressure drop used in calculations are the values averaged in time.

The results of experiments are discussed in detail in the earlier studies (BARTELMUS, JANECKI (2003), GANCARCZYK et al. (2014)).

Computational calculations

In order to obtain reliable results of numerical computations it is essential to select optimum grid in the system considered. It was selected as a result of numerical simulations in which the number and sizes of the cells were changed both in the core of the bed and in the layer at the wall. The way of the selection of the optimum grid was presented in detail in the work by JANECKI et al. (2014). The optimum grid, finally used in the computations, was composed of 7700 cells, out of which 4400 cells were the size of 3mm x 5mm (the core of the bed) and 3300 cells forming the layer at the wall were the size of 1mm x 5 mm. The grid was created by means of GAMBIT preprocessor.

The following boundary conditions were attributed to the generated grid: in the axis of the reactor – symmetry, at the wall – lack of slip, at the inlet – flat velocity profile, at the outlet – zero velocity gradient.

As it has been mentioned earlier, a proper description of bed structure should include: overall mean porosity, variance of porosity in axial direction

and axially averaged radial porosity distribution. In the present study the overall mean porosity of bed was determined experimentally and it was 0.38.

The algorithm of generating random numbers of the normal distribution, for a given mean value and standard deviation (5%) was used to determine the changes in porosity in the axial direction. Experimentally determined value of bed porosity ($\varepsilon = 0.38$) was used as a mean value of the parameter.

The relationships describing momentum exchange coefficients (F_{jk}), occurring in interaction forces between phases (Eqns 9–11), were implemented into a commercial Fluent software by means of the User Definition Function (UDF) and were used to calculate gas pressure drop in bed and mean liquid holdup.

To qualify the procedure of computational calculations and at the same time decrease the differences between calculated and experimental values the parametric sensitivity of CFD model was checked in the study by JANECKI et al. (2014). The following parameters, which have the greatest influence on the computed values, were analysed: relations defining the interphase momentum exchange coefficients and different radial porosity profiles.

In the present study, as a result of parametric sensitivity analysis, the classical equations of ATTOU et al. (1999) defining the friction factors (F_{jk}), with Ergun's constants calculated from neuron nets (ILIUTA et al. (1998)) ($E_1 = 235.53$; $E_2 = 1.59$) were applied in the CFD model. The radial porosity profiles were calculated from MARTIN'S (1978) correlations:

$$\varepsilon(x) = \varepsilon_{\min} + (1 - \varepsilon_{\min})x^2 \quad \text{for } -1 \leq x \leq 0 \quad (16)$$

$$\varepsilon(x) = \varepsilon + (\varepsilon_{\min} - \varepsilon) \exp\left(\frac{-x}{4}\right) \cos\left(\frac{\pi x}{0.876}\right) \quad \text{for } x \geq 0 \quad (17)$$

where:

$$x = 2 \frac{R - r}{d_p} - 1; \quad \varepsilon_{\min} = 0.2$$

A flat velocity profiles of the liquid phase was assumed at the inlet into the column because a distributor of liquid, distributing liquid evenly on the surface of the bed, was used during the experiments. The following initial conditions were used for a reactor operating in the GCF regime: experimental values of gas (w_g) and liquid (w_L) velocities as well as mean volume fraction of the liquid phase (α_L).

However, the initial conditions for a reactor operating in the CSW regime were the following: experimental values of liquid holdup (ε_L), gas velocity (w_g),

liquid velocity in the base (w_{Lb}) and in the impulse (w_{Lip}), base and impulse durations (t_b and t_{ip} , respectively). Velocity of the solid phase was assumed to be zero. A unsteady state simulations with a time step of $t = 0.01$ s was used in the calculations.

Findings of the simulations

As a result of the computational simulations one can obtain gas pressure drop in bed, volume fraction distribution of a given phase (liquid holdup and gas holdup) along the bed and its mean value in the reactor. The comparative base for the simulations was our own data base obtained in experiments carrying out for varying flow rates of both phases and for systems of various physicochemical properties.

Experimental data as well as results of CFD simulations performer for reactor operating at constant feeding the bed with liquid and for GCF regime were illustrated, as an example, in Fig. 1. Good compatibility between calculated and obtained experimentally values of hydrodynamic parameters was obtained; the mean relative error (e_Y) for liquid holdup was 3.95% and for pressure drop was 9.4%.

The results of simulations performed for periodically changing feeding the bed with liquid phase were shown in Figs 2 and 3. They quite faithfully reproduce the changes in both hydrodynamic parameters with the changes in gas phase velocity (Fig. 2), mean liquid phase velocity and duration of base and impulse (Fig. 3). While comparing calculated and experimental values of gas pressure drop in bed and mean values of liquid holdup it has to be stated that the differences between the calculated and measured values of both parameters do not exceed a few per cent.

Fig. 4 shows a computational simulation of changes of liquid holdup in the whole column for nitrogen – 24% methanol solution system. Such result were obtained for fast changing cycles (FAST MODE) and reactor operating in CSW regime. For such low alternate liquid velocities, the impulses seen at the top of the column decay during migration down the bed, forming continuous stream of liquid (GCF regime).

A few impulses can always be seen in the column operating at fast changing cycles, however, for slow changing cycles (SLOW MODE) the duration of base and impulse may be so long that they will not be seen in the column. In such a case, there is a GCF regime in the whole column for a very short time. The results of simulation of a slow changing cycles for a water-nitrogen system and the duration of cycles of $t_b = 20$ s and $t_{ip} = 3$ s are presented, as an example, in Fig. 5. For conventional time of 0 s (the moment of switching the cycle) liquid

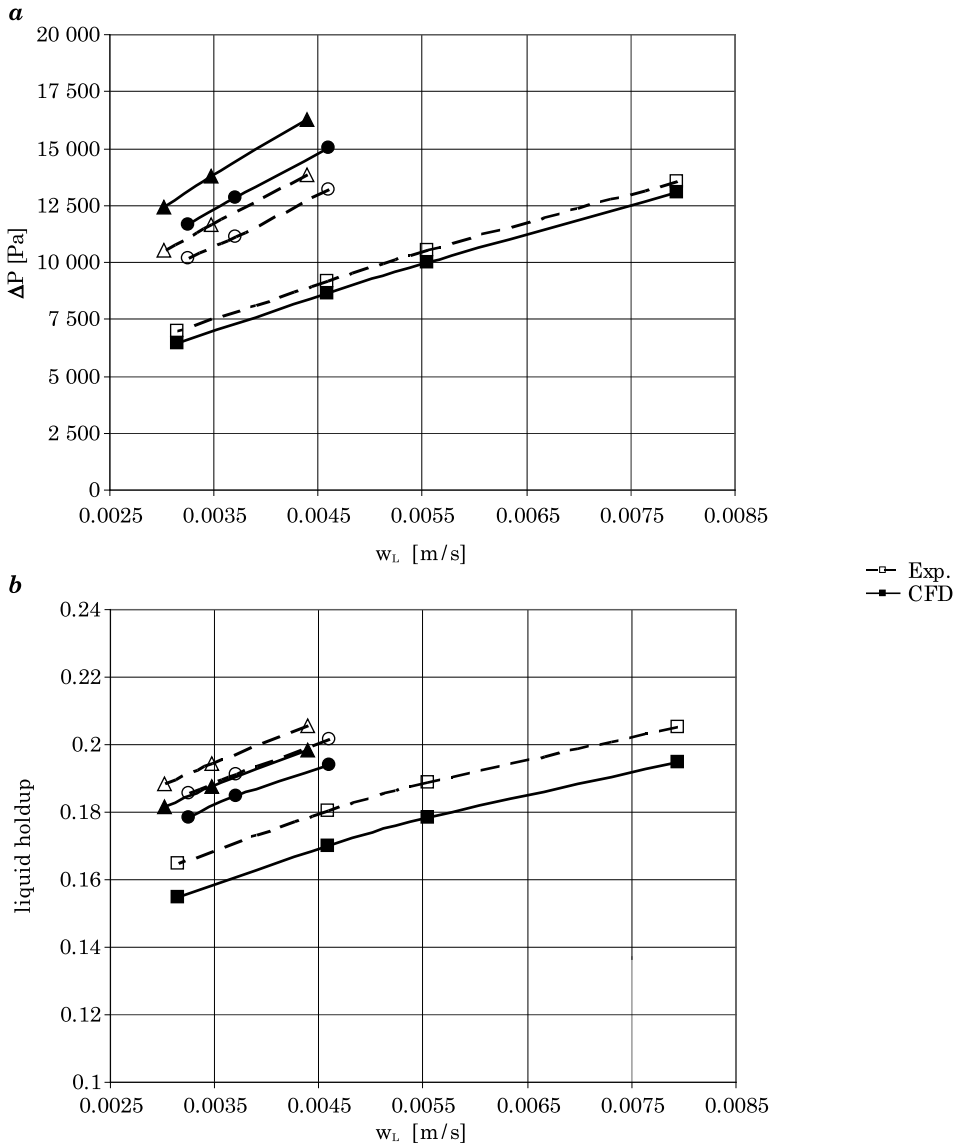


Fig. 1. Dependences of the gas pressure drop ΔP (a) and liquid holdup (b) as function of the liquid velocity w_L and phases' properties (square: water – nitrogen, circle: glycerol solution (30 wt.%) – nitrogen, triangle: glycerol solution (35 wt.%) – nitrogen); $w_g = 0.13$ m/s; GCF regime

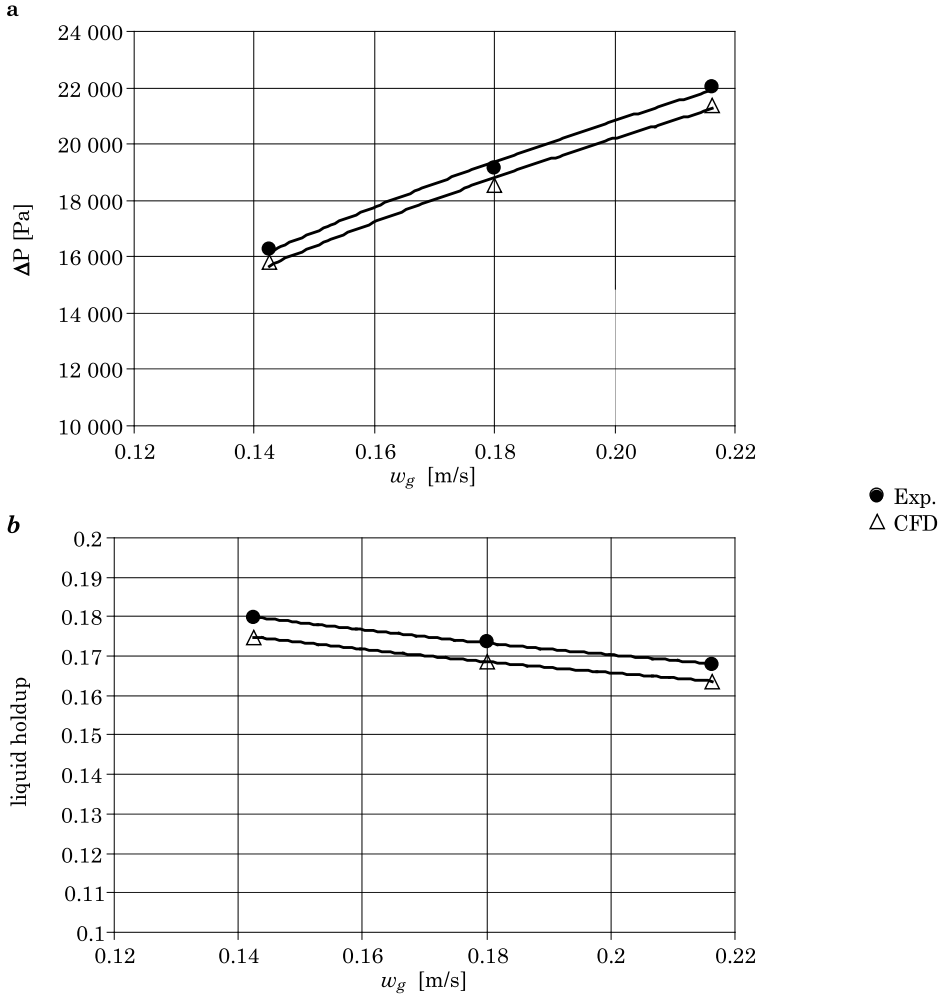


Fig. 2. Dependences of the gas pressure drop ΔP (a) and liquid holdup (b) on the gas velocity w_g ; nitrogen-water system, full symbols – experimental data, open symbols – CFD model; $w_{Lav} = 0.006 \text{ m} \cdot \text{s}^{-1}$, $t_b/t_{ip} = 3/1$; CSW regime

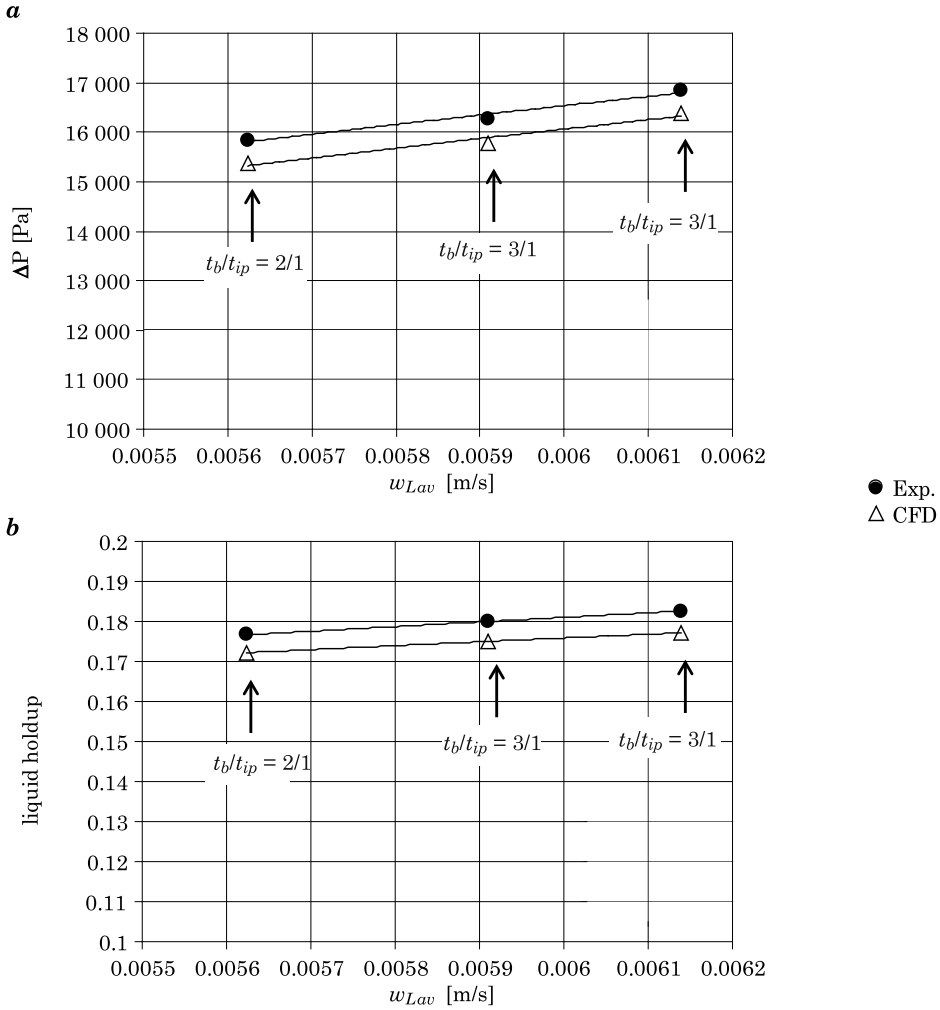


Fig. 3. Dependences of the gas pressure drop ΔP (a) and liquid hold-up (b) on the average liquid velocity w_{Lav} (or duration of the base and impulse) at various Ergun constants, nitrogen-water system, $w_g = 0.143 \text{ m} \cdot \text{s}^{-1}$, $w_{Lb} = 0.0048 \text{ m} \cdot \text{s}^{-1}$; CSW regime

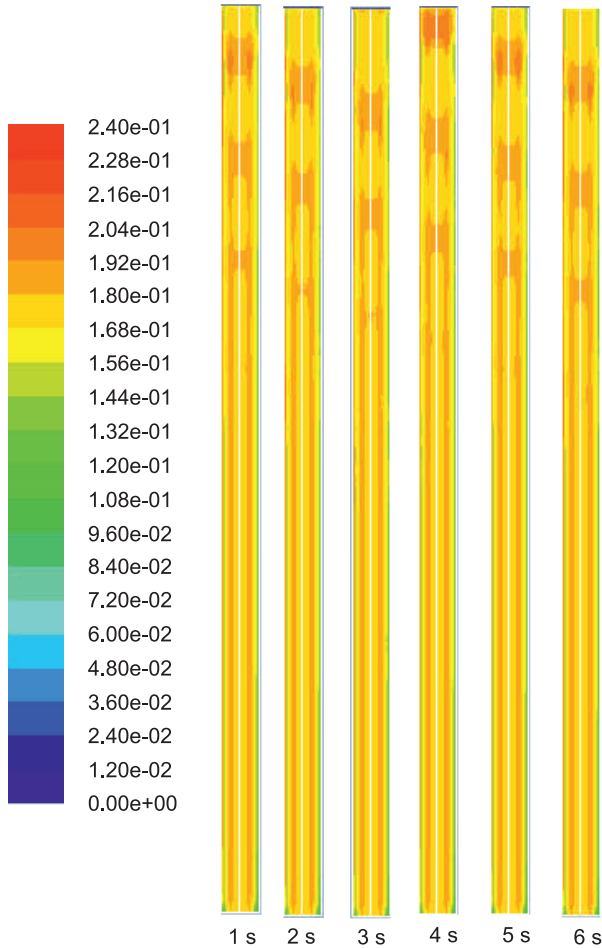


Fig. 4. Time dependences of liquid holdup along the column; nitrogen – 24% methanol solution system, $w_g = 0.1\text{ m/s}$; $w_b = 0.0025\text{ m/s}$, $w_{imp} = 0.0049\text{ m/s}$; $t_b = 3\text{ s}$, $t_{ip} = 1\text{ s}$

flows with a constant velocity (w_{Lb}). The front of impulse, which was created after 4 seconds, reaches the column bottom after about 20 s. After that time the GCF regime is again observed in the column.

Conclusions

A simulation of concurrent flow of gas and liquid through fixed bed of the column operating in GCF and CSW regimes were performed using computational fluid dynamics (CFD) model. As a result of the simulations the following

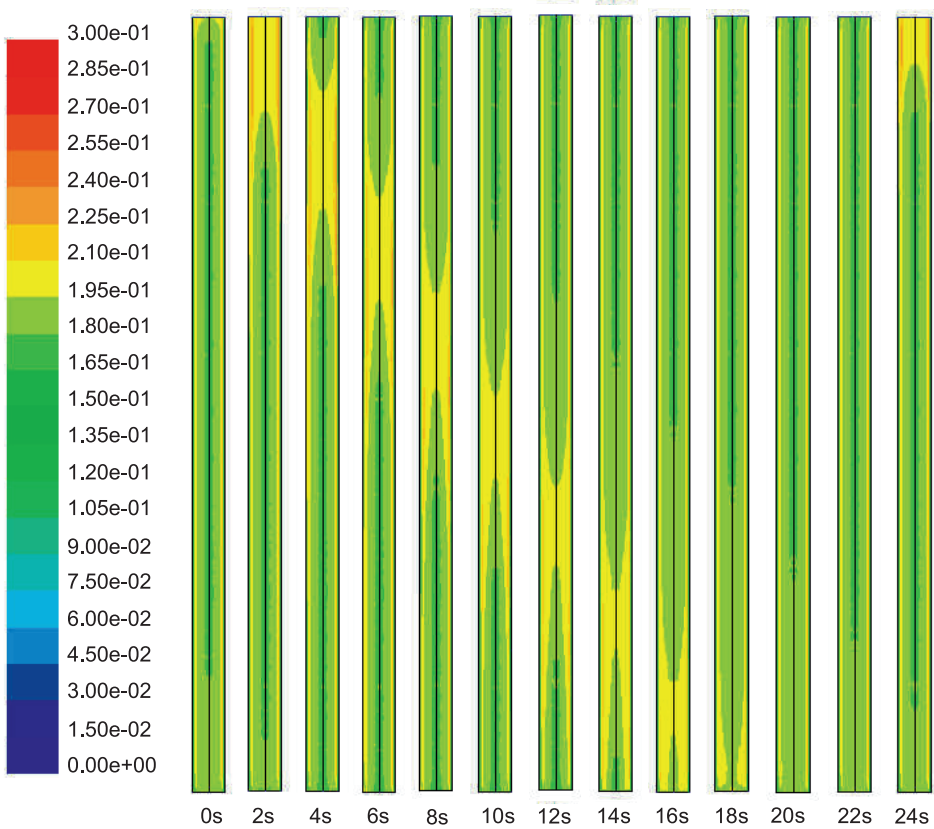


Fig. 5. Liquid hold-up variation with time along the column; nitrogen – water system; $w_g = 0.14$ m/s, $w_b = 0.0048$ m/s, $w_{Lip} = 0.0082$ m/s; $t_b = 20$ s, $t_{ip} = 3$ s

hydrodynamic parameters were obtained: gas pressure drop in the bed, volume fraction distribution of a given phase (liquid holdup and gas holdup) along packing and its mean value in the reactor. The results of the calculations reflect well both quantitative and qualitative changes of hydrodynamic parameters with the changes of: flow rates of both phases, duration of base and impulse and physicochemical properties of the liquid phase. The comparison of liquid holdup values and gas pressure drop in bed calculated and experimentally obtained shows that the CFD model applied in the present study may be used to model the hydrodynamics of concurrent flows of gas and liquid through a fixed bed, since a good compatibility of the compared hydrodynamic parameters was obtained.

References

- AL-DAHMAN M.H., DUDUKOVIC M.P. 1994. *Pressure drop and liquid holdup in high pressure trickle-bed reactors*. Chemical Engineering Science, 49: 5681–5698.
- AL-DAHMAN M.H., KHADILKAR M.R., WU Y., DUDUKOVIĆ M.P. 1998. *Prediction of pressure drop and liquid holdup in high-pressure trickle-bed reactors*. Industrial & Engineering Chemistry Research, 37: 793–798.
- AL-DAHMAN M.H., LARACHI F., DUDUKOVIĆ M.P., LAURENT A. 1997. *High pressure trickle-bed reactors: a review*. Industrial & Engineering Chemistry Research, 36: 3292–3314.
- ATTOU A., BOYER C., FERSCHNEIDER G. 1999. *Modeling of the hydrodynamics of the cocurrent gas-liquid trickle flow through a trickle-bed reactor*. Chemical Engineering Science, 54: 785–802.
- ATTOU A., FERSCHNEIDER G. 2000. *A two-fluid hydrodynamic model for the transition between trickle and pulse flow in cocurrent gas-liquid packed-bed reactor*. Chemical Engineering Science, 55: 491–511.
- BARTELMUS G., JANECKI D. 2003. *Hydrodynamics of a concurrent down-flow of gas and foaming liquid through the packed bed*. Part II. Liquid holdup and gas pressure drop. Chemical Engineering Processing, 42: 993–1005.
- BENENATI R.F., BROSILOW C.B. 1962. *Void fraction distribution in beds of spheres*. AIChE Journal, 8: 359–361.
- BEY O., EINGENBERGER G. 1997. *Fluid flow through catalyst filled tubes*. Chemical Engineering Science, 52: 1365–1375.
- CLEMENTS L.D., SCHMIDT P.C. 1980. *Two-phase pressure drop in cocurrent downflow in packed beds: air-silicone oil systems*. AIChE Journal, 26: 314–317.
- COHEN Y., METZNER A.B. 1981. *Wall effects in laminar-flow of fluids through packed-beds*. AIChE Journal, 27: 705–715.
- DE KLERK A. 2003. *Voidage variation in packed beds at small column to particle diameter ratio*, AIChE Journal, 49: 2022–2029.
- ELLMAN M.J., MIDOUX N., WILD G., LAURENT A., CHARPENTIER J.C. 1990. *A new, improved liquid hold-up correlation for trickle-bed reactors*. Chemical Engineering Science, 45: 1677–1684.
- GANCARCZYK A., JANECKI D., BARTELMUS G., BURGHARDT A. 2014. *Analysis of hydrodynamics of periodically operated trickle bed reactor*. Chemical Engineering Research and Design, 92: 2609–2617.
- GOODLING J.S., VACHON R.I., STELPFUG W.S., YING S.J., KHADER M.S. 1983. *Radial porosity distribution in cylindrical beds packed with spheres*. Powder Technology, 35: 23–29.
- GROSSER K., CARBONELL R.G., SUNDARESAN S. 1988. *Onset of pulsing in two-phase cocurrent downflow through a packed bed*. AIChE Journal, 34: 1850–1860.
- GUNJAL P.R., KASHID M.N., RANADE V.V., CHAUDHARI R.V. 2005. *Hydrodynamics of trickle-bed reactors: Experiments and CFD modelling*. Industrial & Engineering Chemistry Research, 44: 6278–6294.
- HOLUB R.A., DUDUKOVIĆ M.P., RAMACHANDRAN P.A. 1993. *Pressure drop, liquid holdup and flow regime transition in trickle flow*. AIChE Journal, 39: 302–321.
- HOLUB R.A., DUDUKOVIĆ P.A., RAMACHANDRAN P.A. 1992. *A phenomenological model for pressure drop, liquid holdup and flow regime transition in gas-liquid trickle flow*. Chemical Engineering Science, 47: 2343–2348.
- HUNT M.L., TIEN C.L. 1990. *Non-Darcian flow, heat and mass transfer in catalytic packed-bed reactors*. Chemical Engineering Science, 45: 55–63.
- ILIUTA I., LARACHI F. 1999. *The generalized slit model: pressure gradient, liquid holdup & wetting efficiency in gas-liquid trickle flow*. Chemical Engineering Science 54: 5039–5045.
- ILIUTA I., LARACHI F., AL-DAHMAN M.H. 2000. *Double slit model for partially wetted trickle flow hydrodynamics*. AIChE Journal, 46: 597–609.
- JANECKI D., BURGHARDT A., BARTELMUS G. 2014. *Influence of the porosity profile and sets of Ergun constants on the main hydrodynamic parameters in the trickle-bed reactors*, Chemical Engineering Journal, 237: 176–188.
- JANECKI D., BURGHARDT A., BARTELMUS G. 2016. *Parametric sensitivity of a CFD model concerning the hydrodynamics of trickle-bed reactor (TBR)*. Chemical and Process Engineering, 37(1): 97–107.

- JIANG Y., KHADILKAR M.R., AL-DAHMAN M.H., DUDUKOVIC M.P. 2001. *CFD modelling of multiphase flow distribution in catalytic packed bed reactors: scale down issues*. *Catalysis Today*, 66: 209–218.
- JIANG Y., KHADILKAR M.R., AL-DAHMAN M.H., DUDUKOVIC M.P. 2002. *CFD of multiphase flow in packed-bed reactors: I. K-fluid modelling issues*. *AIChE Journal*, 48: 701–715.
- KEIR G., JEGATHEESAN V. 2014. *A review of computational fluid dynamics applications in pressure-driven membrane filtration*. *Reviews in Environmental Science and Bio/Technology*, 13: 183–201.
- KHAN M.J.H., HUSSAIN M.A., MANSOURPOUR Z., MOSTOUFI N., GHASEN N.M., ABDULLAH E.C. 2014. *CFD simulation of fluidized bed reactors for polyolefin production – a review*. *Journal of Industrial and Engineering Chemistry*, 20: 3919–3946.
- KUIPERS J.A.M., VAN SWAALI W.P.M. 1997. *Application of computational fluid dynamics to chemical reaction engineering*. *Reviews in Chemical Engineering*, 13/3: 1–118.
- LARACHI F., LAURENT A., MIDOUX N., WILD G. 1991. *Experimental study of a trickle-bed reactor operating at high pressure: two-phase pressure drop and liquid saturation*. *Chemical Engineering Science*, 46: 1233–1246.
- LI S., DING Y., WEN D., HE Y. 2006. *Modelling of the behavior of gas-solid two-phase mixtures flowing through packed beds*. *Chemical Engineering Science*, 61: 1922–1931.
- MACDONALD L.F., EL-SAYED M.S., MOW K., DULLIEN F.A.L. 1979. *Flow through porous media – the Ergun equation revisited*. *Industrial & Engineering Chemistry Fundamentals*, 18: 199–208.
- MARTIN H. 1978. *Low Peclet number particle to fluid heat and mass transfer in packed beds*. *Chemical Engineering Science*: 33, 913–919.
- MIDOUX N., FAVIER M., CHARPENTIER J.C. 1976. *Flow pattern, pressure loss and liquid holdup data in gas-liquid downflow packed beds with foaming and nonfoaming hydrocarbons*. *Journal Chemical Engineering Japan*, 9: 350–356.
- MUELLER G. 1992. *Radial void fraction distribution in randomly packed fixed beds of uniformly sized spheres in cylindrical containers*. *Powder Technology*, 72: 269–275.
- RAO V.G., ANANTH M.S., VARMA Y.B.G. 1983. *Hydrodynamics of two-phase cocurrent downflow in packed beds*. *AIChE Journal*, 29: 467–483.
- RAO V.G., DRINKENBURG A.A.H. 1983. *Pressure drop and hydrodynamic properties of pulses in two-phase gas-liquid downflow through packed columns*. *Canadian Journal of Chemical Engineering*, 61: 158–167.
- SAEZ A.E., CARBONELL R.G. 1985. *Hydrodynamic parameters for gas-liquid cocurrent flow in packed beds*. *AIChE Journal*, 31: 52–61.
- SAI P.S.T., VARMA Y.B.G. 1987. *Pressure drop in gas-liquid downflow through packed beds*. *AIChE Journal*, 33: 2027–2036.
- SAJJADI B., RAMAN A.A.A., IBRAHIM S., SHAH R.S.S.R.E. 2012. *Review on gas-liquid mixing analysis in multiscale stirred vessel using CFD*. *Reviews in Chemical Engineering*, 28: 171–189.
- SHAIKH A., AL-DAHMAN M. 2013. *Scale-up of bubble column reactors: A review of current state-of-the-art*. *Industrial & Engineering Chemistry Research*, 52: 8091–8108.
- SOUADNIA A., SOLTANA F., LESAGE F., LATIFI M.A. 2005. *Some computational aspects in the simulation of hydrodynamics in a trickle-bed reactor*. *Chemical Engineering and Processing*, 44: 847–854.
- SPECCHIA V., BALDI G. 1977. *Pressure drop and liquid hold-up for two phase cocurrent flow in packed beds*. *Chemical Engineering Science*, 32: 515–523.
- SUN C.G., YIN F.H., AFACAN A., NANDAKUMAR K., CHUANG K.T. 2000. *Modelling and simulation of flow maldistribution in random packed columns with gas-liquid countercurrent flow*. *Chemical Engineering Research and Design*, 78: 378–388.
- VAN ANTWERPEN W., DU TOIT C.G., ROUSSEAU P.G. 2010. *A review of correlations to model the packing structure and effective thermal conductivity in packed beds of mono-sized spherical particles*. *Nuclear Engineering and Design*, 240: 1803–1818.
- VORTMEYER D., SCHUSTER J. 1983. *Evaluation of steady flow profiles in rectangular and circular packed-beds by a variational method*. *Chemical Engineering Science*, 38: 1691–1699.
- WAMMES W.J.A., MIDDELKAMP J., HUISMAN W.J., DEBAAS C.M., WESTERTERP K.R. 1991. *Hydrodynamics in a cocurrent gas-liquid trickle bed at elevated pressures*. *AIChE Journal*, 37: 1849–1862.
- WANG TF., WANG JF., JIN Y. 2007. *Slurry reactors for gas to liquid processes: A review*. *Industrial & Engineering Chemistry Research*, 46: 5824–5847.

- WANG W., LU B.N., ZHANG N., SHI Z.S., LI J.H. 2010. *A review of multiscale CFD for gas-solid CFB modelling*. *International Journal of Multiphase Flow*, 36: 109–118.
- WANG Y., CHEN J., LARACHI F. 2013. *Modelling and simulation of trickle-bed reactors using computational fluid dynamics: A state-of-the-art review*. *Canadian Journal of Chemical Engineering*, 91: 136–180.

Guide for Authors

Introduction

Technical Sciences is a peer-reviewed research Journal published in English by the Publishing House of the University of Warmia and Mazury in Olsztyn (Poland). Journal is published continually since 1998. Until 2010 Journal was published as a yearbook, in 2011 and 2012 it was published semiyearly. From 2013, the Journal is published quarterly in the spring, summer, fall, and winter.

The Journal covers basic and applied researches in the field of engineering and the physical sciences that represent advances in understanding or modeling of the performance of technical and/or biological systems. The Journal covers most branches of engineering science including biosystems engineering, civil engineering, environmental engineering, food engineering, geodesy and cartography, information technology, mechanical engineering, materials science, production engineering etc.

Papers may report the results of experiments, theoretical analyses, design of machines and mechanization systems, processes or processing methods, new materials, new measurements methods or new ideas in information technology.

The submitted manuscripts should have clear science content in methodology, results and discussion. Appropriate scientific and statistically sound experimental designs must be included in methodology and statistics must be employed in analyzing data to discuss the impact of test variables. Moreover there should be clear evidence provided on how the given results advance the area of engineering science. Mere confirmation of existing published data is not acceptable. Manuscripts should present results of completed works.

There are three types of papers: a) research papers (full length articles); b) short communications; c) review papers.

The Journal is published in the printed and electronic version. The electronic version is published on the website ahead of printed version of Technical Sciences.

Technical Sciences does not charge submission or page fees.

Types of paper

The following articles are accepted for publication:

Reviews

Reviews should present a focused aspect on a topic of current interest in the area of biosystems engineering, civil engineering, environmental engineering, food engineering, geodesy and cartography, information technology, mechanical engineering, materials science, production engineering etc. They should include all major findings and bring together reports from a number of sources. These critical reviews should draw out comparisons and conflicts between work, and provide an overview of the 'state of the art'. They should give objective assessments of the topic by citing relevant published work, and not merely present the opinions of individual authors or summarize only work carried out by the authors or by those with whom the authors agree. Undue speculations should also be avoided. Reviews generally should not exceed 6,000 words.

Research Papers

Research Papers are reports of complete, scientifically sound, original research which contributes new knowledge to its field. Papers should not exceed 5,000 words, including figures and tables.

Short Communications

Short Communications are research papers constituting a concise description of a limited investigation. They should be completely documented, both by reference list, and description of the experimental procedures. Short Communications should not occupy more than 2,000 words, including figures and tables.

Letters to the Editor

Letters to the Editor should concern with issues raised by articles recently published in scientific journals or by recent developments in the engineering area.

Contact details for submission

The paper should be sent to the Editorial Office, as a Microsoft Word file, by e-mail: techsci@uwm.edu.pl

Referees

Author/authors should suggest, the names, addresses and e-mail addresses of at least three potential referees. The editor retains the sole right to decide whether or not the suggested reviewers are used.

Submission declaration

After final acceptance of the manuscript, the corresponding author should send to the Editorial Office the author's declaration. Submission of an article implies that the work has not been published previously (except in the form of an abstract or as part of a published lecture or academic thesis or as an electronic preprint), that it is not under consideration for publication elsewhere, that publication is approved by all authors and tacitly or explicitly by the responsible authorities where the work was carried out, and that, if accepted, it will not be published elsewhere in the same form, in English or in any other language.

To prevent cases of ghostwriting and guest authorship, the author/authors of manuscripts is/are obliged to: (i) disclose the input of each author to the text (specifying their affiliations and contributions, i.e. who is the author of the concept, assumptions, methods, protocol, etc. used during the preparation of the text); (ii) disclose information about the funding sources for the article, the contribution of research institutions, associations and other entities.

Language

Authors should prepare the full manuscript i.e. title, abstract and the main text in English (American or British usage is accepted). Polish version of the manuscript is not required.

The file type

Text should be prepared in a word processor and saved in doc or docx file (MS Office).

Article structure

Suggested structure of the manuscript is as follows:

- Title
- Authors and affiliations
- Corresponding author
- Abstract
- Keywords
- Introduction
- Material and Methods
- Results and Discussion
- Conclusions

Acknowledgements (*optional*)
References
Tables
Figures

Subdivision – numbered sections

Text should be organized into clearly defined and numbered sections and subsections (optionally). Sections and subsections should be numbered as 1. 2. 3. then 1.1 1.2 1.3 (then 1.1.1, 1.1.2, ...). The abstract should not be included in numbering section. A brief heading may be given to any subsection. Each heading should appear on its own separate line. A single line should separate paragraphs. Indentation should be used in each paragraph.

Font guidelines are as follows:

- Title: 14 pt. Times New Roman, bold, centered, with caps
- Author names and affiliations: 12 pt. Times New Roman, bold, centered, italic, two blank line above
- Abstract: 10 pt. Times New Roman, full justified, one and a half space. Abstract should begin with the word Abstract immediately following the title block with one blank line in between. The word Abstract: 10 pt. Times New Roman, centered, indentation should be used
- Section Headings: Not numbered, 12 pt. Times New Roman, bold, centered; one blank line above
- Section Sub-headings: Numbered, 12 pt. Times New Roman, bold, italic, centered; one blank line above
- Regular text: 12 pt. Times New Roman, one and a half space, full justified, indentation should be used in each paragraph

Title page information

The following information should be placed at the first page:

Title

Concise and informative. If possible, authors should not use abbreviations and formulae.

Authors and affiliations

Author/authors' names should be presented below the title. The authors' affiliation addresses (department or college; university or company; city, state and zip code, country) should be placed below the names. Authors with the same affiliation must be grouped together on the same line with affiliation information following in a single block. Authors should indicate all affiliations with a lower-case superscript letter immediately after the author's name and in front of the appropriate address.

Corresponding author

It should be clearly indicated who will handle correspondence at all stages of refereeing and publication, also post-publication process. The e-mail address should be provided (footer, first page). Contact details must be kept up to date by the corresponding author.

Abstract

The abstract should have up to 100-150 words in length. A concise abstract is required. The abstract should state briefly the aim of the research, the principal results and major conclusions. Abstract must be able to stand alone. Only abbreviations firmly

established in the field may be eligible. Non-standard or uncommon abbreviations should be avoided, but if essential they must be defined at their first mention in the abstract itself.

Keywords

Immediately after the abstract, author/authors should provide a maximum of 6 keywords avoiding general, plural terms and multiple concepts (avoid, for example, 'and', 'of'). Author/authors should be sparing with abbreviations: only abbreviations firmly established in the field may be eligible.

Abbreviations

Author/authors should define abbreviations that are not standard in this field. Abbreviations must be defined at their first mention there. Author/authors should ensure consistency of abbreviations throughout the article.

Units

All units used in the paper should be consistent with the SI system of measurement. If other units are mentioned, author/authors should give their equivalent in SI.

Introduction

Literature sources should be appropriately selected and cited. A literature review should discuss published information in a particular subject area. Introduction should identify, describe and analyze related research that has already been done and summarize the state of art in the topic area. Author/authors should state clearly the objectives of the work and provide an adequate background.

Material and Methods

Author/authors should provide sufficient details to allow the work to be reproduced by other researchers. Methods already published should be indicated by a reference. A theory should extend, not repeat, the background to the article already dealt within the Introduction and lay the foundation for further work. Calculations should represent a practical development from a theoretical basis.

Results and Discussion

Results should be clear and concise. Discussion should explore the significance of the results of the work, not repeat them. A combined Results and Discussion section is often appropriate.

Conclusions

The main conclusions of the study may be presented in a Conclusions section, which may stand alone or form a subsection of a Results and Discussion section.

Acknowledgements

Author/authors should include acknowledgements in a separate section at the end of the manuscript before the references. Author/authors should not include them on the title page, as a footnote to the title or otherwise. Individuals who provided help during the research study should be listed in this section.

Artwork

General points

- Make sure you use uniform lettering and sizing of your original artwork
- Embed the used fonts if the application provides that option

- Aim to use the following fonts in your illustrations: Arial, Courier, Times New Roman, Symbol
- Number equations, tables and figures according to their sequence in the text
- Size the illustrations close to the desired dimensions of the printed version

Formats

If your electronic artwork is created in a Microsoft Office application (Word, PowerPoint, Excel) then please supply ‘as is’ in the native document format

Regardless of the application used other than Microsoft Office, when your electronic artwork is finalized, please ‘Save as’ or convert the images to one of the following formats (note the resolution requirements given below):

EPS (or PDF): Vector drawings, embed all used fonts

JPEG: Color or grayscale photographs (halftones), keep to a minimum of 300 dpi

JPEG: Bitmapped (pure black & white pixels) line drawings, keep to a minimum of 1000 dpi or combinations bitmapped line/half-tone (color or grayscale), keep to a minimum of 500 dpi

Please **do not**:

- Supply files that are optimized for screen use (e.g., GIF, BMP, PICT, WPG); these typically have a low number of pixels and limited set of colors
- Supply files that are too low in resolution
- Submit graphics that are disproportionately large for the content

Color artwork

Author/authors should make sure that artwork files are in an acceptable format (JPEG, EPS PDF, or MS Office files) and with the correct resolution. If, together with manuscript, author/authors submit color figures then Technical Sciences will ensure that these figures will appear in color on the web as well as in the printed version at no additional charge.

Tables, figures, and equations

Tables, figures, and equations/formulae should be identified and numbered consecutively in accordance with their appearance in the text.

Equations/mathematical and physical formulae should be presented in the main text, while tables and figures should be presented at the end of file (after References section). Mathematical and physical formulae should be presented in the MS Word formula editor.

All types of figures can be black/white or color. Author/authors should ensure that each figure is numbered and has a caption. A caption should be placed below the figure. Figure must be able to stand alone (explanation of all symbols and abbreviations used in figure is required). Units must be always included. It is noted that figure and table numbering should be independent.

Tables should be numbered consecutively in accordance with their appearance in the text. Table caption should be placed above the table. Footnotes to tables should be placed below the table body and indicated with superscript lowercase letters. Vertical rules should be avoided. Author/authors should ensure that the data presented in tables do not duplicate results described in figures, diagrams, schemes, etc. Table must be able to stand alone (explanation of all symbols and abbreviations used in table is required). Units must be always included. As above, figure and table numbering should be independent.

References

References: All publications cited in the text should be presented in a list of references following the text of the manuscript. The manuscript should be carefully checked to ensure that the spelling of authors' names and dates of publications are exactly the same in the text as in the reference list. Authors should ensure that each reference cited in the text is also present in the reference list (and vice versa).

Citations may be made directly (or parenthetically). All citations in the text should refer to:

1. Single author

The author's name (without initials, with caps, unless there is ambiguity) and the year of publication should appear in the text

2. Two authors

Both authors' names (without initials, with caps) and the year of publication should appear in the text

3. Three or more authors

First author's name followed by et al. and the year of publication should appear in the text

Groups of references should be listed first alphabetically, then chronologically.

Examples:

"... have been reported recently (ALLAN, 1996a, 1996b, 1999; ALLAN and JONES, 1995).

KRAMER et al. (2000) have recently shown..."

The list of references should be arranged alphabetically by authors' names, then further sorted chronologically if necessary. More than once reference from the same author(s) in the same year must be identified by the letters "a", "b", "c" etc., placed after the year of publication.

References should be given in the following form:

KUMBHAR B.K., AGARVAL R.S., DAS K. 1981. *Thermal properties of fresh and frozen fish*. International Journal of Refrigeration, 4(3), 143–146.

MACHADO M.F., OLIVEIRA F.A.R., GEKAS V. 1997. *Modelling water uptake and soluble solids losses by puffed breakfast cereal immersed in water or milk*. In Proceedings of the Seventh International Congress on Engineering and Food, Brighton, UK.

NETER J., KUTNER M.H., NACHTSCHEIM C.J., WASSERMAN W. 1966. *Applied linear statistical models* (4th ed., pp. 1289–1293). Irwin, Chicago.

THOMSON F.M. 1984. *Storage of particulate solids*. In M. E. Fayed, L. Otten (Eds.), *Handbook of Powder Science and Technology* (pp. 365–463). Van Nostrand Reinhold, New York.

Citation of a reference as 'in press' implies that the item has been accepted for publication.

Note that the full names of Journals should appear in reference list.

Submission checklist

The following list will be useful during the final checking of an article prior to the submission. Before sending the manuscript to the Journal for review, author/authors should ensure that the following items are present:

- Text is prepared with a word processor and saved in DOC or DOCX file (MS Office). One author has been designated as the corresponding author with contact details: e-mail address

- Manuscript has been 'spell-checked' and 'grammar-checked'

- References are in the correct format for this Journal

- All references mentioned in the Reference list are cited in the text, and vice versa

- Author/authors does/do not supply files that are too low in resolution

- Author/authors does/do not submit graphics that are disproportionately large for the content